

MASSACHUSETTS INSTITUTE OF TECHNOLOGY
ARTIFICIAL INTELLIGENCE LABORATORY

A.I. Memo No. 1504

March, 1995

Passive Dynamics in the Control of Gymnastic Maneuvers

Robert R. Playter

This publication can be retrieved by anonymous ftp to publications.ai.mit.edu.

Abstract

The control of aerial gymnastic maneuvers is challenging because these maneuvers frequently involve complex rotational motion and because the performer has limited control of the maneuver during flight. A performer can influence a maneuver using a sequence of limb movements during flight. However, the same sequence may not produce reliable performances in the presence of off-nominal conditions. How do people compensate for variations in performance to reliably produce aerial maneuvers? In this report I explore the role that passive dynamic stability may play in making the performance of aerial maneuvers simple and reliable.

I present a control strategy comprised of active and passive components for performing robot front somersaults in the laboratory. I show that passive dynamics can neutrally stabilize the layout somersault which involves an “inherently unstable” rotation about the intermediate principal axis. And I show that a strategy that uses open loop joint torques plus passive dynamics leads to more reliable 1 1/2 twisting front somersaults in simulation than a strategy that uses prescribed limb motion.

Results are presented from laboratory experiments on gymnastic robots, from dynamic simulation of humans and robots, and from linear stability analyses of these systems.

Passive Dynamics in the Control of Gymnastic Maneuvers

by

Robert R. Playter

Submitted to the Department of Aeronautics and Astronautics
 on September 1994, in partial fulfillment of the
 requirements for the degree of
 Doctor of Philosophy

Abstract

The control of aerial gymnastic maneuvers is challenging because these maneuvers frequently involve complex rotational motion and because the performer has limited control of the maneuver during flight. While a performer can execute a sequence of limb movements during flight to produce a desired maneuver, the same sequence may not produce reliable performances in the presence of off-nominal conditions. How do people compensate for variations in performance conditions to reliably produce aerial maneuvers? It is possible that people sense errors in performance and actively compute appropriate responses to them to produce reliable maneuvers. However, it is also possible that the maneuver is inherently stable, that the body naturally compensates for variations, and that the athlete does little active computation.

In this thesis I explore the role that passive dynamic stability may play in making the performance of aerial maneuvers simple and reliable. I consider the control of the tucked somersault, the layout somersault, and the 1 1/2 twisting front somersault. I present a control strategy comprised of active and passive components for performing robot front somersaults in the laboratory. I show that passive dynamics can neutrally stabilize the layout somersault which involves an “inherently unstable” rotation about the intermediate principal axis. And I show that a strategy that uses open loop joint torques plus passive dynamics leads to more reliable 1 1/2 twisting front somersaults in simulation than a strategy that uses prescribed limb motion. Results are presented from laboratory experiments on gymnastic robots, from dynamic simulation of humans and robots, and from linear stability analyses of these systems.

Thesis Supervisor: Marc Raibert
 Title: Professor of Electrical Engineering and Computer Science

Thesis Supervisor: Andreas von Flotow
 Title: President, Hood Technology Corporation

Thesis Supervisor: Christopher Atkeson
 Title: Assistant Professor of Computer Science

Acknowledgments

I am grateful to many people and institutions for allowing me the opportunity to pursue this study. I thank Marc Raibert for providing me the opportunity to learn with him in the Leg Lab at MIT and for emphasizing to me the value of curiosity. It was great fun! I thank Andy Von Flotow and Chris Atkeson for their guidance and interest in this project. I thank the other members of the Leg Lab for their invaluable contributions to this project. They helped make the Lab an exciting place to be. I thank the Fergus' for their financial support in the form of the Fergus Award for post graduate study. I thank my close friends Seth and Noah Riskin for their insightful discussions on the nature of gymnastic movement. Finally, I wish to thank my wife, Eftihea Joy, for her lasting support, patience, and love over the course of my studies.

Bibliography

Robert Playter spent the 81-82 academic year in west Texas at Odessa Junior College where he studied engineering science and participated in varsity gymnastics. He transferred to Ohio State University in 1982 where he majored in Aeronautical Engineering and continued his athletics with the varsity men's gymnastics team. Robert won Big Ten Champion Titles on the horizontal bar in 1983 and 1985. In 1984 he became an All-American gymnast on the horizontal bar and in 1985 he and his teammates won the NCAA Division I gymnastic championship for OSU. He earned his bachelor's degree from OSU in 1986. In 1988 he earned his Master's degree from the Department of Aeronautics and Astronautics at the Massachusetts Institute of Technology where he studied automatic control theory. He returned to MIT for doctoral work in 1990. While enrolled in the Department of Aeronautics and Astronautics he performed his research in the Leg Lab of the Artificial Intelligence Lab.

Contents

| | | |
|----------|---|-----------|
| 1 | Introduction | 12 |
| 1.1 | Background | 19 |
| 1.1.1 | Gymnastic Maneuvers | 19 |
| 1.1.2 | Aeronautics, Astronautics and Celestial Mechanics | 23 |
| 1.1.3 | Ballistic Walking | 24 |
| 1.2 | Organization of Thesis | 25 |
| 2 | Rigid Body Rotation | 27 |
| 2.1 | Introduction | 27 |
| 2.2 | Nonlinear Dynamic Model | 27 |
| 2.3 | Linear Analysis | 30 |
| 2.3.1 | Conservative Gyric Systems | 33 |
| 2.3.2 | Rigid Body Inertia Ratios | 34 |
| 2.4 | Rotational Stability of the Rigid Human Body | 39 |
| 2.5 | A Map of Rigid Body Rotation | 42 |
| 2.6 | Dynamic Simulation Environment | 46 |
| 2.7 | Summary | 47 |
| 3 | Robot Tucked Somersaults | 49 |
| 3.1 | Introduction | 49 |
| 3.2 | The Mechanics of the Somersault | 51 |

CONTENTS 6

| | | |
|----------|--|------------|
| 3.3 | Somersault Control Strategies | 53 |
| 3.3.1 | Control of Somersault Angle | 56 |
| 3.3.2 | Accommodating Landing Time Errors | 59 |
| 3.3.3 | Control of Tilt and Twist Angles | 60 |
| 3.4 | Experiments with 3D Biped Somersaults | 61 |
| 3.5 | Summary | 65 |
| 4 | Passively Stable Layout Somersaults | 70 |
| 4.1 | Introduction | 70 |
| 4.2 | Simple Human Model | 72 |
| 4.2.1 | Nonlinear Equations of Motion | 77 |
| 4.2.2 | Linearized Equations of Motion | 78 |
| 4.3 | Stability Analysis | 81 |
| 4.3.1 | Rigid Body | 81 |
| 4.3.2 | Multi-Body | 82 |
| 4.3.3 | Non-Linear Stability via Dynamic Simulation | 91 |
| 4.4 | How Passive Layout Stability Works | 92 |
| 4.4.1 | Stabilization Via Principal Axes Reorientation | 92 |
| 4.4.2 | The Simplest Model | 98 |
| 4.5 | Summary | 105 |
| 5 | Layout Somersault Experiments | 110 |
| 5.1 | Introduction | 110 |
| 5.2 | Experimental Apparatus | 111 |
| 5.2.1 | Human-Like Doll | 111 |
| 5.2.2 | Launching Device | 113 |
| 5.3 | Theoretical Predictions | 117 |
| 5.4 | Description of Experiments | 118 |
| 5.5 | Experimental Results | 120 |

| | | |
|----------|--|------------|
| 5.6 | Summary | 123 |
| 6 | Twisting Somersaults | 124 |
| 6.1 | Introduction | 124 |
| 6.2 | The Tilt of Twisting Somersaults | 125 |
| 6.3 | One and One Half Twisting Front Somersault | 126 |
| 6.3.1 | The Nominal Case | 126 |
| 6.3.2 | Off-Nominal Performance, Prescribed Motion | 127 |
| 6.3.3 | Off-Nominal Performance, Compliant Motion | 128 |
| 6.4 | Twisting Somersault of the 3D Biped | 135 |
| 6.5 | Summary | 137 |
| 7 | Summary and Discussion | 142 |
| 7.1 | Robot Tucked Somersaults | 144 |
| 7.2 | The Layout Somersault | 145 |
| 7.3 | Twisting Somersaults | 146 |
| 7.4 | Do Humans Use Passive Dynamics | 148 |
| 7.5 | A Passive Dynamic Theory of Control Design? | 149 |
| A | Appendix | 151 |
| A.1 | Mathematica Code for Non-linear Equations of Motion | 152 |
| A.2 | Mathematica Code for Linearizing Equations of Motion | 159 |
| A.3 | Parameters of the Five D.O.F. Linear Model | 170 |
| A.4 | Analytic Solution | 175 |

List of Figures

| | | |
|-----|---|----|
| 1-1 | Three types of aerial control movements. | 13 |
| 1-2 | 3D Biped robot | 16 |
| 1-3 | The experimental layout somersault doll | 17 |
| 1-4 | The simulated front somersault with one and a half twists | 18 |
| 2-1 | Somersault, tilt, and twist Euler angles | 29 |
| 2-2 | Inertia ratio diagram | 36 |
| 2-3 | Stability diagram for principal axis spin | 38 |
| 2-4 | Levels of rigid body rotational instability | 39 |
| 2-5 | Tuck, pike, and layout positions for a human. | 40 |
| 2-6 | Inertia ratios of the tuck, pike and layout positions | 41 |
| 2-7 | Rotational map for a human in the layout position | 44 |
| 2-8 | Spherical coordinates of the tilt and twist Euler angles | 46 |
| 3-1 | 3D Biped robot | 50 |
| 3-2 | The 3D Biped somersault | 52 |
| 3-3 | Rotational map of the 3D Biped | 54 |
| 3-4 | Leg inclination angle | 56 |
| 3-5 | 3D Biped somersault data | 66 |
| 3-6 | Tuck servo performance | 67 |
| 3-7 | 3D Biped somersault data, landing time error compensation | 68 |
| 4-1 | Human model for layout somersaults | 71 |

| | | |
|------|---|-----|
| 4-2 | Simulation data: passively stable and unstable layout somersaults | 73 |
| 4-3 | Rotational map for a human in the layout position | 74 |
| 4-4 | Human model with body vectors defined | 76 |
| 4-5 | Layout somersault inertia ratios as a function of arm angle | 83 |
| 4-6 | Root locus for the layout somersault with no damping | 84 |
| 4-7 | Root locus for the layout somersault with damping | 86 |
| 4-8 | Array of root loci as a function of arm angle | 87 |
| 4-9 | Stabilizing shoulder springs, five d.o.f. system | 88 |
| 4-10 | Stabilizing shoulder springs, three d.o.f. subsystem | 89 |
| 4-11 | Stabilizing shoulder springs, two d.o.f. subsystem | 90 |
| 4-12 | Diagrams of non-linear, layout somersault stability | 93 |
| 4-13 | Principal axes tilt | 94 |
| 4-14 | Rotational map for a human, closeup of tilt and twist axes | 96 |
| 4-15 | Passively stable tilt-twist trajectory | 97 |
| 4-16 | The simplest model | 98 |
| 4-17 | Stabilizing shoulder springs that cancel centrifugal forces | 104 |
| 4-18 | Stability diagrams K_{sh} , k_1 , and k_3 | 106 |
| 4-19 | Stability diagrams I_{rel} , k_1 , and k_3 | 107 |
| 4-20 | The effect of arm shape on stability. | 108 |
| 5-1 | The experimental layout somersault doll | 112 |
| 5-2 | Rigid body inertia ratios for the doll and a human | 114 |
| 5-3 | I_{rel} for the doll and a human model | 115 |
| 5-4 | The mechanical doll launcher | 116 |
| 5-5 | Theoretical stabilizing values of K_{sh} for doll. | 117 |
| 5-6 | Photographs of layout somersault experiments | 119 |
| 5-7 | Average number of stable layout somersaults in experiments | 121 |
| 5-8 | Percentage of stable layout dismounts in experiments | 122 |

| | | |
|-----|---|-----|
| 6-1 | Computer graphic images of a 1 1/2 twisting front somersault | 127 |
| 6-2 | Nominal 1 1/2 twisting front somersault accuracy. | 129 |
| 6-3 | Compliant 1 1/2 twisting front somersault accuracy. | 132 |
| 6-4 | 1 1/2 twisting front somersault simulation data, prescribed motion. . | 133 |
| 6-5 | 1 1/2 twisting front somersault simulation data, compliant motion. . | 134 |
| 6-6 | Rotational map of 3D Biped with added weight | 138 |
| 6-7 | Simulated 3D Biped somersault with twist | 139 |
| 6-8 | Simulated 3D Biped Twisting Somersault | 140 |

List of Tables

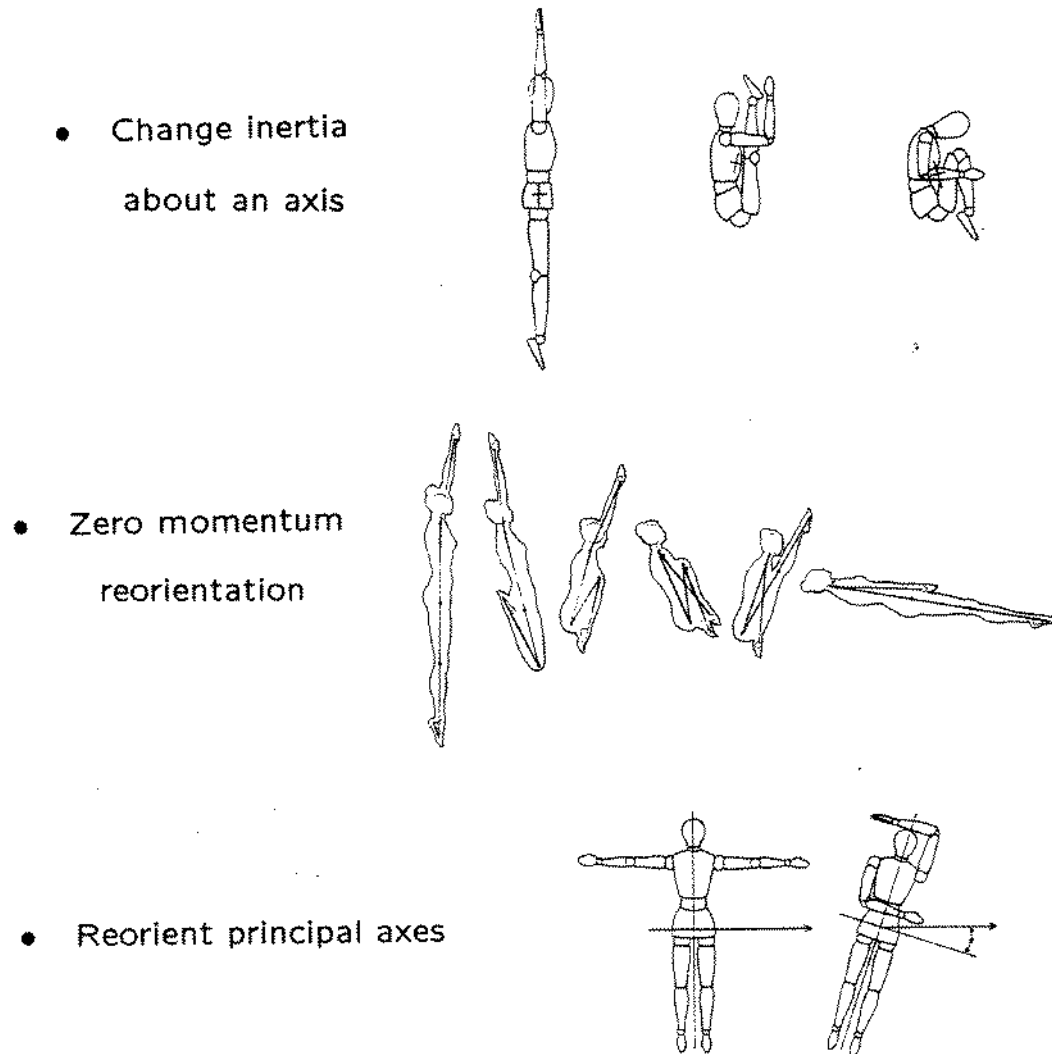
Chapter 1

Introduction

In both the 1992 and 1994 winter Olympics, the final jump performed by the men's champion freestyle skier was a quadruple twisting, triple somersault. In the performance of these 'jumps' the athletes skied off of a ramp from which they soared approximately 45 feet into the air, remained aloft for approximately 3.0 sec, rotated three times about a horizontal axis and four times about their body vertical axis, and finished by landing squarely on their feet so that they could continue skiing down the hill in a controlled fashion. It is incredible that these athletes can perform a maneuver like this with such accuracy. How do they do it?

Two related issues that make these performances challenging are the controllability and stability of aerial maneuvers. Controllability refers to the ability of an athlete to influence the outcome of an aerial maneuver once it has been initiated. An airborne performer can not apply any external forces or torques to the body. So how can a performer control his body orientation? Previous research of this topic has revealed movement techniques that performers can use to produce complicated aerial maneuvers. These techniques involve moving the limbs to reconfigure the body during flight (Figure 1-1). However, while a prescribed set of body configurations can produce a desired aerial maneuver, this sequence may not lead to reliable performances.

The stability of aerial maneuvers concerns their reliable performance in the pres-



From Frohlich 1980.

Figure 1-1: A limited ability to influence the outcome of a ballistic maneuver arises from the relative movement of the limbs and torso during flight. One way to influence the outcome is to change the moment of inertia about an axis in order to change the rotation rate about that axis. The standard being the ice-skater's spin. A second way to influence the outcome is to use momentum-free rotations [Smith 67, Frohlich 79]. This technique allows a structure to be reoriented while maintaining zero angular momentum by performing a sequence of limb movements. A third way is to reconfigure the system so that the principle axes of inertia are reoriented relative to the inertially fixed angular momentum vector. This allows sharing of momentum between principal axes. This procedure is frequently used to introduce or remove twist in somersaults [Batterman 68, Frohlich 79, Yeadon 84]. The existence of these mechanisms makes it possible to actively adjust the outcome of an aerial maneuver once it has been initiated.

ence of off-nominal conditions. Stability is important because the accumulation of even small errors during the relatively long flight times of an aerial maneuver could result in a disastrous outcome. Making a performance reliable requires that the athlete compensate for inaccuracies in movement, variations in equipment, and external disturbances. It is possible that people produce reliable maneuvers by sensing these variations and actively computing appropriate responses to compensate for them. However, the complexity of this feedback control approach would appear to place great demands on the athlete's perceptive and motor control abilities. Is there a more simple approach to producing reliable maneuvers that does not require active compensation by the athlete?

The focus of this thesis is on the use of passive dynamic stability as an alternative or a complement to active control for producing reliable aerial maneuvers. Passive dynamic stability means that a maneuver is inherently stable by virtue of the natural dynamic interaction of the limbs and body. The precise limb movement that a performer makes during a maneuver will depend upon not only his motor activity but also on environmental forces. Is it possible that the passive forces that arise due to off-nominal conditions could provide a built-in correction? If so, passive behavior could automatically compensate for errors in initial conditions, in control movements, or from external disturbances. If this were the case then the demands for active control by the athlete could be dramatically reduced. A passive control strategy is appealing because it could relieve the human performer of sensing small variations in movement and computing control responses fast enough to produce accurate, stable maneuvers. Instead, the athlete may need only to "play back" a pre-recorded set of motor actions. This feed forward command combined with the passive dynamic response of his body may allow the maneuver to "unfold" on its own.

To see if passive dynamic stability could play a role in aerial performances, I consider the control of three gymnastic maneuvers, the tucked front somersault, the back layout somersault, and the front somersault with one and a half twists. I show

that passive dynamics can play a significant role in making these maneuvers reliable. Neutrally stable passive dynamics make the control of the tucked somersault simple since an active controller need only consider rotation about the major principal axis. The layout or straight body somersault is considered to be inherently unstable because it requires rotation about the middle principal axis of inertia, an unstable equilibrium for a rigid body. I show that the layout somersault can passively be made neutrally stable by tuning the compliance of the shoulders of the performer. Finally, I present results that suggest that a passive, compliant model of the human body that uses open loop torque control can produce more reliable 1 1/2 twisting somersaults than a model that uses prescribed limb motion. I obtained these results using simple analytic models, non-linear dynamic simulation, and laboratory robots. Next, I briefly describe the results of experiments on each of these maneuvers.

The somersault is a maneuver in which a performer jumps into the air and rotates once about a side-to-side axis before landing on the ground. The main requirement for the somersault is to land in a balanced manner. This in turn requires the performer to land with a precise body attitude. The tucked somersault exhibits passive directional stability in rotation since it involves rotation about the major principal axis of inertia. This means that imprecise initiation of a somersault will not dramatically affect the orientation of the spin axis during flight. However, avoiding over-rotation or under-rotation of a somersault about the spin axis may require compensation of rotation rate during flight. Active control of the inertia can be used to correct errors in somersault rotation rate. I present results from somersault experiments using a 60 lb, one meter tall laboratory robot that runs on two springy legs (Figure 1-2). The robot was programmed to initiate the somersaults using a pre-programmed pattern of action. To avoid large tilt and twist angles of the 3D Biped during take-off and landing we use a wide double stance of the robot and insure that the feet touch down simultaneously. During flight the robot actively controls rotation rate by “tucking” or “untucking” its legs to manipulate the robots inertia. The robot actively adjusts



Figure 1-2: Photograph of the 3D Biped Robot.

the position of its feet relative to its center of mass just prior to landing. This element was necessary to compensate for errors in the estimated landing time of the robot. On its best day the robot did successful somersaults and continued running on 7 out of 10 attempts.

The layout or straight body somersault is considered to be inherently unstable because it requires rotation about the middle principal axis of inertia, an unstable equilibrium for a rigid body. A rigid body that is somersaulting about the middle principal axis will always exhibit a sequence of half twists about the minor principal axis. Despite this fact, athletes regularly perform this maneuver with apparent ease. Previously, biomechanics researchers have assumed that the athlete senses the instability of the maneuver and actively compensates for it with movements of the arms and body [Nigg 74, Hinrichs 78, Yeadon 90].

I show that the layout somersault can be a passive, neutrally stable maneuver.

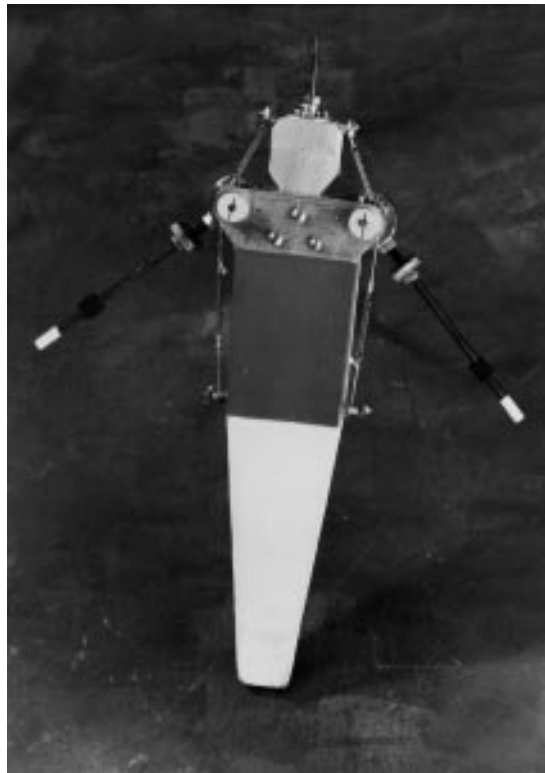


Figure 1-3: Photograph of the mechanical doll used for experiments with layout somersaults. The doll could consistently perform stable, triple layout somersaults.

Passive stabilization of the layout somersault results from the natural dynamic interaction of the limbs and body during movement. Stabilization arises from the inherent tendency of the arms to tilt in response to twisting movement of the body. The arm tilt forces the principal axes of the system to move in a direction that compensates for tilt and twist errors. This built-in correction eliminates the divergent tendency of the system as long as the compliance of the shoulders cancels the unstable centrifugal forces on the arms. I verify this result with linear stability analysis, non-linear dynamic simulation, and experiments on a human-like doll built and tested in the laboratory (Figure 1-3.) The doll has spring-driven arms but has no other control system, sensors, or actuators. The doll routinely exhibits triple somersaults about its middle principal axis without twisting.

While twisting is to be avoided in the layout somersault, it is a feature in other

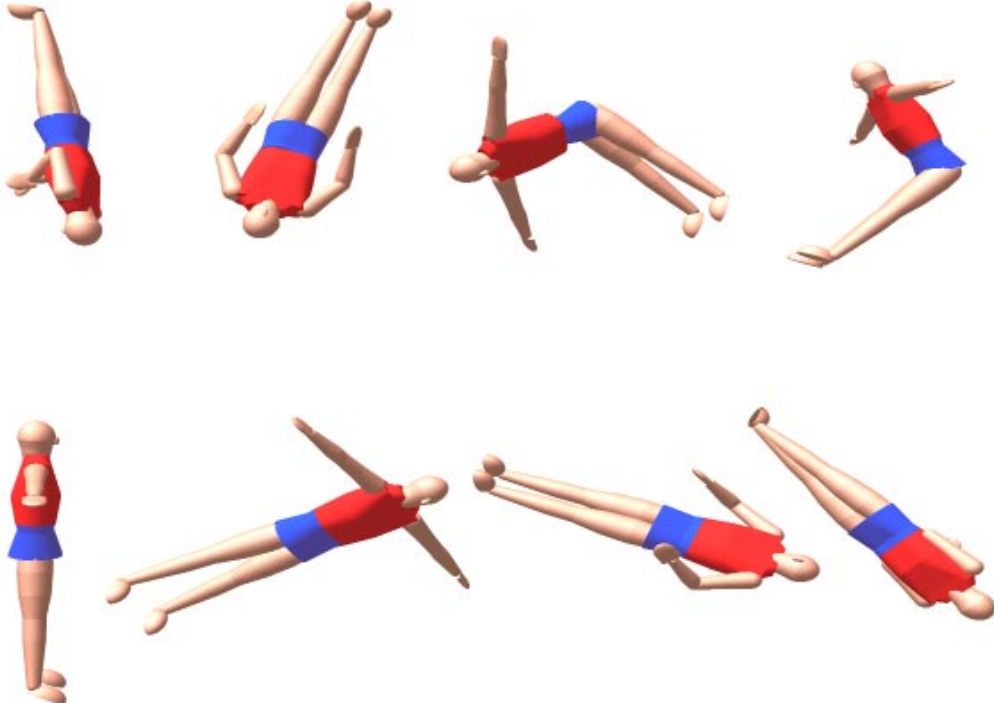


Figure 1-4: Images arranged in **right-to-left, top-to-bottom order** from a dynamic simulation of a 1 1/2 twisting front somersault. We found that open loop torque control of a compliant model led to relatively reliable performances.

tricks. I present results from dynamic simulation of a human performing a front somersault with one and a half twists. The twisting maneuver is started from a front somersault by reconfiguring the body mid-maneuver. While a sequence of prescribed limb movements can be found to produce a twisting maneuver, simulation results show that the performance is sensitive to small variations in initial conditions. If, instead, open loop torque control is used with a compliant, passive dynamic model of the human the maneuver reliability can be significantly improved.

I also present results from dynamic simulation of a front somersault with one half twist performed by the 3D Biped. We found that to make the simulated 3D Biped perform a satisfactory front somersault with one half twist we had to add weight to the robot to make its inertia more like that of a human.

The ultimate goal of this research is to develop a theory of passive dynamic,

aerial maneuvers. By showing that passive dynamics can play a significant role in the performance of reliable aerial maneuvers we argue that they reduce the need for active control from the athlete. The performance of a maneuver may be simplified by relegating some responsibility for control to the natural, mechanical behavior of the body. The appropriate use of passive dynamics may have the added benefit of producing natural looking, coordinated movement. Perhaps athletes and other people use a performance strategy that seeks to maximize passive dynamic behavior. It is difficult to know what control strategies people may or may not use, but in the laboratory we can examine the feasibility of a strategy by testing it in a real or simulated system.

1.1 Background

Relevant background material for the study of gymnastic maneuvers comes from fields such as biomechanics, biology, robotics, aeronautics, and astronautics. Several researchers have explicitly studied the performance of gymnastic maneuvers. These studies have revealed the salient features of known gymnastic techniques for producing maneuvers. Some robotics researchers have studied gymnastic maneuvers using dynamic simulation and/or laboratory robots in order to develop strategies for control. The study of passive dynamic stability has roots in the fields of aeronautics and astronautics. It is common for airplanes and spacecraft to be designed to exhibit passive dynamic stability. The study of human locomotion provides an inspirational example of passive dynamic stability and the rich behavior that it can produce. In the following sections, I briefly discuss background material from each of these fields.

1.1.1 Gymnastic Maneuvers

Most researchers investigating the control of aerial maneuvers have been concerned with explaining the physics of the maneuvers. During the aerial phase of a maneuver

the performer can not produce any external forces on the system so the trajectory of the center of mass and the angular momentum are fixed from the moment of take-off to the moment of landing. Knowing this, early researchers were compelled to find explanations of two aerial maneuvers that at first appeared to violate conservation of angular momentum: 1) a cat when dropped with no net angular momentum will right itself before landing on the ground [Marey, Kane 69] and 2) spring board divers who leave the board with rotation only about a side-to-side (somersault) body axis can subsequently initiate rotation about their head-to-toe (twist) body axis [Batterman 68, Frohlich 79, Yeadon 84]. Where did the extra angular momentum come from? Resolving these apparent discrepancies led researchers to find movement techniques that could be used to perform these and other interesting maneuvers. These techniques involved reconfiguring the body in flight (Figure 1-1).

Takashima [Takashima 90] studied high bar maneuvers. He used the control of rotation rate about the somersault axis to produce a balanced landing of a simulated human dismounting from the horizontal bar. His algorithm could produce accurate tucked, multiple-somersault dismounts. In flight, he used the feedback control of posture to control rotation rate. He used a combination of feed forward and feed back control to execute the landing.

While they appear to be similar maneuvers, the tucked somersault and the layout somersault are dynamically very different. The tucked somersault involves rotation about the major principal axis of inertia, a stable mode of rigid body rotation. Rotation about the major and minor principal axes of inertia exhibits a limited form of stability called directional stability. Directional stability refers to the fact that the spin axis will maintain roughly the same inertial orientation when deviated slightly from that orientation. The layout somersault involves rotation about the intermediate principal axis of inertia, an unstable mode of rigid body rotation [Crandall 68, Hughes 86]. When a rigid body is spun about its intermediate axis, that body axis will exhibit large excursions from its initial orientation. These cyclic excursions are a series of

nearly 180° rotations away from and returning to the initial axis orientation. The different modes of rotation can be easily demonstrated to the reader by spinning a video tape or a book (with a rubber band around it) about each of its axes of symmetry. You will see that when the body is spun about the major and minor principal axes the spin axis roughly maintains its inertial orientation. However, when the body is spun about its middle principal axes it will exhibit a sequence of twists about the long body axis. This rigid body instability has lead researchers to conclude that the layout somersault is inherently unstable.

Nigg recognized that the layout somersault may be unstable since it involved rotation about the middle principal axis [Nigg 74]. Using cinematographic techniques Hinrichs [Hinrichs 78] measured the body configuration of an athlete performing a layout somersault. He confirmed that the layout somersault involved rotation about the middle principal axis of inertia. He hypothesized that the athlete made small corrective movements of the arms and torso in flight to stabilize the somersault.

Yeadon [Yeadon 84] used a combination of cinematography and dynamic simulation to study the control of aerial maneuvers. In his research he developed a mass properties model of the human form that provided an estimate of inertial parameters from anthropometric measurements. He also filmed highly skilled athletes performing complex aerial maneuvers and digitized this data to determine the body attitude, configuration, and angular momentum during flight. Then he used the inertia parameters and digitized configuration and momentum data as input to a dynamic simulation of the human body during flight. This dynamic model computed the gross body attitude during flight as a function of the measured internal configuration and angular momentum. Using this system, Yeadon could numerically study the effect of changes in body configuration on the performance of complex aerial maneuvers.

Yeadon found that by piking or arching (bending at the waist in the sagittal plane) during a layout somersault an athlete can change his or her inertia enough to make the somersault axis an axis of maximum inertia. This in turn implies that

arched/pike somersaults are passively stable. Because many athletes perform layout somersaults with arch, it is possible that this is done to stabilize the maneuver.

However, in Yeadon's analysis of a double layout somersault performed by Carl Furrer, the 1982 World Trampoline Champion, he found that Furrer was in fact rotating about the middle principal axis of inertia during nearly all of the maneuver. Furthermore, dynamic simulation of this layout somersault exhibited the characteristic twist instability of rotation about the middle principal axis while the actual human performance exhibited no such instability. This difference implied that the small digitization errors in translating film configuration data to the simulation were responsible for the change in performance, a fact that would point to an inherently unstable system. These results suggest that the athlete uses some form of stabilization to perform the layout somersault.

Yeadon proposed a specific technique for stabilizing the layout somersault. He realized that asymmetric movement of the arms in the frontal plane could be used to stabilize rotation about the middle principal axis of inertia. He designed a stabilizing feedback controller that used the sensed twist angle as the feedback signal to drive the arm abduction/adduction angular rates. Using a linear model, Yeadon found the athlete would have to respond to a growing twist instability within 0.28 of a somersault ($\approx 200ms$) [Yeadon] in order to maintain stability.

The ballistic nature of many gymnastic performances makes an open-loop (feed forward) component a likely part of any control strategy. An open loop strategy is one in which the performer's control motions are not derived from the current state of motion but are instead produced from a pre-programmed pattern of action. Since important parameters of ballistic motion are fixed from takeoff, an open-loop strategy is required to anticipate the maneuver in order to set up appropriate initial conditions. Raibert and Hodgins programmed a planar biped robot to perform front somersaults in the laboratory using a combination of open loop and feedback control strategies. The biped robot used an open loop strategy for initiation of the somersault and the

majority of flight. A feedback controller was used to accurately place the feet just prior to touch down. Using this combination of feed forward and feedback control, the robot could successfully perform the front somersault followed by balanced running on 90% of the trials.

1.1.2 Aeronautics, Astronautics and Celestial Mechanics

Some modern aircraft are designed to require active control for stabilization. These aircraft use digital computers to manipulate the aircraft control surfaces to render the planes flyable. This inherent instability is tolerated to provide highly maneuverable aircraft. However, passive dynamic stability is commonly built into general aviation aircraft and spacecraft. More precisely, they have an equilibrium condition like flying straight and level for an aircraft, or spinning about the major principal axis for a satellite that is stable so that the craft can tolerate external disturbances without diverging from the stable equilibrium condition. The origin of this topic has its roots in celestial mechanics.

The moon always presents the same face to the Earth. However, it does not do so exactly. Librational stability refers to the stability of the oscillations of the moon about its center of mass as it circles the Earth. Galileo was the first to notice these oscillations. Newton conjectured that a reason for this behavior would be that the moon was elongated towards the Earth. However, it took Louis Lagrange to develop a mathematical theory describing this phenomenon [Lagrange]. Using a linear analysis, Lagrange derived a set of four inequalities involving the inertia of the moon that must be satisfied for the moon to exhibit stable librational motion.

In 1885, Henri Poincaré [Poincare] realized that a linearized analysis could not be conclusive in determining librational stability. This result gave rise to the use of the Hamiltonian as a Lyapunov function candidate in determining Lyapunov stability. This approach established the stability of a satellite configuration called the Lagrange satellite but it could not establish the stability of the Delp satellite which was also

stable according to linear analysis.

The only other example that the author has found of stable rotation about the intermediate axis is from a study of large celestial structures. Duncan and Levison [Duncan 89] simulated the behavior of a self-gravitating system of 2048 bodies in order to determine if it was stable. They found an example of a simple spherical system initially in dynamic equilibrium that experienced an instability producing a final equilibrium state of stable rotation around the intermediate principal axis of inertia of the system of particles. This result was considered noteworthy because it conflicted with the rigid body analogy of unstable rotation about the middle principal axis. No explanation of the source of stability was offered.

1.1.3 Ballistic Walking

While the significance of passive dynamic stability is recognized in studies of celestial structures and in the design of aircraft and spacecraft its relevance to the control of movement in biology and robotics is only beginning to be explored. One possible reason is that these former examples typically involve the stability of an equilibrium configuration, i.e. no accelerations. Animals, people, and robots frequently move with significant accelerations. The stability analysis of non-equilibrium movement is a much more difficult process. Some progress has been made with the analysis of walking.

Mochon and McMahon and later McGeer showed that passive dynamic stability may be important to human locomotion. First proposed by Mochon and McMahon [Mochon 80], a ballistic walker uses only gravity and the dynamic interaction of the swing and stance legs to produce a repetitive walking pattern. The passive pattern accounted for the folding and unfolding of the legs and the positioning of the foot forward. McGeer [McGeer 89] showed the viability of ballistic walking by building passive, planar, anthropomorphic linkages with no sensor or actuators that demonstrated stable walking down an incline.

1.2 Organization of Thesis

The remainder of this thesis is organized as follows.

- Ch. 2 This chapter provides a review of rigid body rotation. Rigid body rotation provides an important simplified model for the analysis of multi-body rotational systems. Analysis and tools introduced here will be used throughout the thesis.
- Ch. 3 In this chapter I discuss somersault experiments with a 3D biped robot. The robot somersault axis is coincident with the major principal axis of inertia so the maneuver exhibits some passive stability properties. The robot actively controls landing attitude by retracting or extending its legs during the maneuver to change somersault rate. The robot has successfully performed front somersaults in the laboratory.
- Ch. 4 In this chapter I present an analysis of the layout somersault. I show that the layout somersault, involving rotation about the middle principal axis of inertia, can be passively stabilized by tuning parameters of a passive dynamic model of the human body. Using the simplest possible model of the layout somersault, I explain the fundamental dynamics of passive stabilization.
- Ch. 5 I describe layout somersault experiments with a human-like doll. These experiments verify that the layout somersault can be consistently stabilized for at least three and one half somersaults.
- Ch. 6 I discuss non-linear dynamic simulation of a 1 1/2 twisting front somersault. Simulation results suggest that maneuvers using prescribed limb motion will not be reliable to off-nominal initial conditions. If instead, a compliant passive model is used with feed forward torques the maneuver can be made more reliable. I also describe twisting somersault experiments with the 3D Biped robot. Using simulation we found that it was important that the robot have an inertia tensor more like that of a human to produce a human-like front somersault with

1/2 twist. Laboratory experiments with 3D Biped robot twisting somersaults were not successful at least in part due to insufficient actuator power.

Ch. 7 Here I summarize the results of the thesis and discuss future work.

Appx. In the Appendix I provide Mathematica code for deriving non-linear equations of motion of a human model, and for analytically linearizing this model. I provide a definition of the parameters used in the linear model. I also provide a derivation of the analytic solution for rigid body rotation.

Chapter 2

Rigid Body Rotation

2.1 Introduction

Humans are multi-body systems and gymnastic maneuvers involve multi-body rotations. We can better understand multi-body rotation by understanding the dynamics and stability of rigid body rotation. In this chapter, I briefly discuss some properties of rigid body rotation. Rigid body rotational stability about a principal axis depends only on the relative magnitude of the principal inertias. This result provides a valuable reference for multi-body rotational stability. A linear analysis of rigid body rotation provides simple stability results, and identifies important non-dimensional parameters that will be useful in multi-body analysis. Visualization tools for rigid body rotation will also prove useful in understanding how to control rotational motion in multi-body systems. Material for this chapter is based on the text of [Hughes 86].

2.2 Nonlinear Dynamic Model

The rotational motion of a free rigid body about its center of mass is governed by Euler's equations.

$$\begin{aligned}
 I_1\dot{\omega}_1 - (I_2 - I_3)\omega_2\omega_3 &= 0 \\
 I_2\dot{\omega}_2 - (I_3 - I_1)\omega_3\omega_1 &= 0 \\
 I_3\dot{\omega}_3 - (I_1 - I_2)\omega_1\omega_2 &= 0
 \end{aligned} \tag{2.1}$$

where I_j refers to the j^{th} principal moment of inertia and ω_j refers to the angular velocity about that principal axis.

The orientation of the rigid body with respect to an inertial coordinate frame is described by a set of three Euler angles. The Euler angles are used to define the 3-by-3 matrix of direction cosines, C_{bi} , that transforms a vector described in inertial coordinates into one described in the body fixed coordinate system. (For the rigid body analyses of this chapter I assume that the principal axis frame is coincident with this body axis frame.) I use a ‘2-1-3’ Euler angle sequence for this purpose. I borrow the names for the three Euler angles, somersault, tilt, and twist, from Yeadon [Yeadon 84]. I use the letters, Φ, Θ, Ψ to refer to the somersault, tilt, and twist angles respectively.

To describe the attitude of the body in inertial space, a coordinate system initially parallel to the inertial reference frame is first rotated through the somersault angle about the inertially fixed ‘2’ axis, then rotated through the tilt angle about the intermediate ‘1’ body axis, and finally rotated through the twist angle about the body fixed ‘3’ axis. Figure 2-1 depicts the Φ, Θ, Ψ Euler angle sequence applied to a rigid human form. The rotation matrix is given by

$$C_{bi} = \begin{bmatrix} C_\Psi C_\Phi + S_\Psi S_\Theta S_\Phi & S_\Psi C_\Theta & -C_\Psi S_\Phi + S_\Psi S_\Theta C_\Phi \\ -S_\Psi C_\Phi + C_\Psi S_\Theta S_\Phi & C_\Psi C_\Theta & S_\Psi S_\Phi + C_\Psi S_\Theta C_\Phi \\ C_\Theta S_\Phi & -S_\Theta & C_\Theta C_\Phi \end{bmatrix} \tag{2.2}$$

The subscript bi refers to the fact that this rotation matrix rotates a vector from the inertial system into the *body* axis system. S and C are the sine and cosine of the

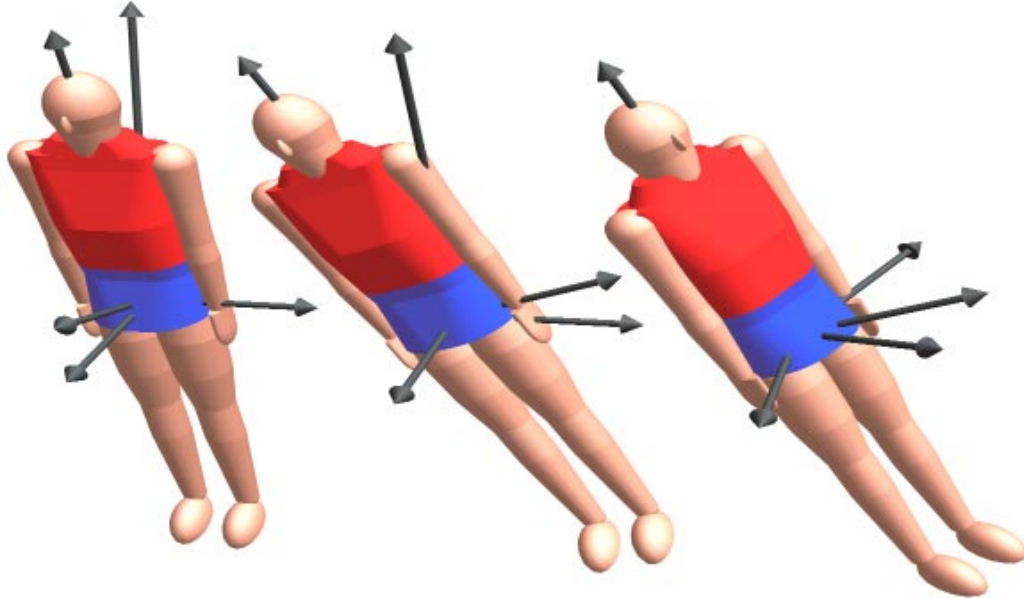


Figure 2-1: Illustration of the somersault (Φ), tilt (Θ), and twist (Ψ) Euler angle sequence used to define body attitude.

respective angle. This Euler angle description of body attitude has a singularity, as do all three parameter descriptions of body attitude. The singularity for this particular sequence occurs at a tilt angle of $\pm\pi/2$. The kinematic equations governing the evolution of the Euler angles are given by

$$\begin{bmatrix} \dot{\Psi} \\ \dot{\Theta} \\ \dot{\Phi} \end{bmatrix} = \begin{bmatrix} S_\Psi S_\Theta C_\Theta & C_\Psi S_\Theta C_\Theta & 1 \\ C_\Psi & -S_\Psi & 0 \\ S_\Psi C_\Theta & C_\Psi C_\Theta & 0 \end{bmatrix} \begin{bmatrix} \omega_1 \\ \omega_2 \\ \omega_3 \end{bmatrix} \quad (2.3)$$

The inverse of the above relationship is also useful. It is given by

$$\begin{bmatrix} \omega_1 \\ \omega_2 \\ \omega_3 \end{bmatrix} = \begin{bmatrix} 0 & C_\Psi & S_\Psi C_\Theta \\ 0 & -S_\Psi & C_\Psi C_\Theta \\ 1 & 0 & -S_\Theta \end{bmatrix} \begin{bmatrix} \dot{\Psi} \\ \dot{\Theta} \\ \dot{\Phi} \end{bmatrix} \quad (2.4)$$

The dynamic equations of motion (2.1) are coupled so that general rotational motion involves all three degrees of freedom. However, three simple solutions exist to these equations. If a rigid body is spinning perfectly around a principal axis such that two of the three angular velocities are zero then the non-linear coupling terms vanish. The body will continue to spin about that axis without coupling to the other degrees of freedom. An analysis of these spin solutions will reveal that for a tri-inertial body, a body with three different principal inertias, only two of the spin solutions are stable while the third is unstable. Here stability means if the spin axis of the system is moved away from the nominal solution the attitude of the spin axis will not diverge radically from its initial orientation. The linear stability analysis provided in the next section reveals the required conditions for stable rotation about a principal axis.

2.3 Linear Analysis

In this section we linearize Euler's equations for the rigid body in order to study the stability of steady rotation about a principal axis. The linear equations govern the motion of the body relative to a reference frame that is rotating steadily about the principal axis of inertia. The resulting equations will be valid for small deviations of the system from the reference frame. This linearization process will be used again when we linearize multi-body rotation about an equilibrium spin condition. The linearizing condition will be steady somersaulting rotation about the '2' axis with angular velocity $\dot{\Phi}$. The angular velocity of the steadily rotating reference coordinate system is $\vec{\omega}_{ra}$.

$$\vec{\omega}_{ra} = \dot{\Phi} \hat{i}_{r2} \quad (2.5)$$

where \hat{i}_{r2} is the unit vector along the '2' axis in the reference coordinate system. The angular velocity of the principal axis system, $\vec{\omega}_{pa}$, is comprised of the angular velocity

relative to the reference coordinate frame, $\vec{\omega}_{pr}$, and $\vec{\omega}_{ra}$,

$$\vec{\omega}_{pa} = \vec{\omega}_{pr} + \vec{\omega}_{ra} \quad (2.6)$$

Let the attitude of the principal axis system relative to the reference frame be described by the 2-1-3 Euler angle sequence of ϕ, θ, ψ . (The lower case notation indicates that these are linearized states. These Euler angles describe the deviations of the body from the rotating reference frame.) We can use Equations 2.2 and 2.4 to express the components of $\vec{\omega}_{pa}$ in terms of ϕ, θ, ψ , their derivatives and $\dot{\Phi}$. First using Equation 2.4

$$\omega_{pr} = \begin{bmatrix} 0 & C_\psi & S_\psi C_\theta \\ 0 & -S_\psi & C_\psi C_\theta \\ 1 & 0 & -S_\theta \end{bmatrix} \begin{bmatrix} \dot{\psi} \\ \dot{\theta} \\ \dot{\phi} \end{bmatrix} \quad (2.7)$$

where ω_{pr} denotes a column whose components are the elements of the vector $\vec{\omega}_{pr}$ when described in the principal axis frame. To form the sum in Equation 2.6, we need to express all the vector components in the same frame. To do this, using Equation 2.2 as a model, form the rotation matrix C_{pr} that rotates a vector from the reference frame into the principal coordinate frame. Then solve for ω_{pa} ,

$$\omega_{pa} = \omega_{pr} + C_{pr}\omega_{ra}$$

When C_{pr} and ω_{pr} are linearized for small ϕ, ψ, θ we get

$$\omega_{pa} = \begin{bmatrix} \dot{\theta} \\ \dot{\phi} \\ \dot{\psi} \end{bmatrix} + \dot{\Phi} \begin{bmatrix} \psi \\ 1 \\ -\theta \end{bmatrix} \quad (2.8)$$

This expression can be differentiated to find the Euler angle expression for angular acceleration.

$$\dot{\omega}_{pa} = \begin{bmatrix} \ddot{\theta} \\ \ddot{\phi} \\ \ddot{\psi} \end{bmatrix} + \dot{\Phi} \begin{bmatrix} \dot{\psi} \\ 0 \\ -\dot{\theta} \end{bmatrix} \quad (2.9)$$

Now, substituting Equations 2.8 and 2.9 into Equation 2.1 and eliminating terms that are second order in θ , ϕ , and ψ results in the following equations

$$\begin{aligned} I_1 \ddot{\theta} - \dot{\Phi} (I_2 - I_3 - I_1) \dot{\psi} - \dot{\Phi}^2 (I_3 - I_2) \theta &= 0 \\ I_2 \ddot{\phi} &= 0 \\ I_3 \ddot{\psi} + \dot{\Phi} (I_2 - I_3 - I_1) \dot{\theta} - \dot{\Phi}^2 (I_1 - I_2) \psi &= 0 \end{aligned} \quad (2.10)$$

These equations govern the behavior of the non-linear system in the vicinity of the pure spin solution. The linear states, θ , ϕ , ψ , describe the deviation of the body axes from the reference coordinate frame.

Examination of Equations 2.10 reveals that the system is unstable in the sense that perturbations in $\dot{\phi}$ will result in unbounded growth in ϕ . Nevertheless, a reduced form of stability called directional stability [Hughes 86] is possible in the subsystem of θ, ψ . Directional stability means that the two attitude variables θ and ψ will not diverge from zero if the system is perturbed slightly from the pure spin solutions. This means that the spin axis will continue to point in roughly the same inertial direction when disturbed from its equilibrium orientation.

The equations for θ and ψ decouple from ϕ . They can be written as

$$M\ddot{x} + \dot{\Phi}G\dot{x} + \dot{\Phi}^2Kx = 0 \quad (2.11)$$

where

$$x = \begin{bmatrix} \theta \\ \psi \end{bmatrix}$$

$$M = \begin{bmatrix} I_1 & 0 \\ 0 & I_3 \end{bmatrix}$$

$$G = \begin{bmatrix} 0 & -(I_2 - I_3 - I_1) \\ I_2 - I_3 - I_1 & 0 \end{bmatrix}$$

$$K = \begin{bmatrix} I_2 - I_3 & 0 \\ 0 & I_2 - I_1 \end{bmatrix}$$

2.3.1 Conservative Gyric Systems

To investigate the stability of the $\theta - \psi$ subsystem, I use the matrix second order stability theory described in [Hughes 86]. Hughes describes a second order system of equations of the form of Equation 2.11 as a *conservative gyric system* when

$$\begin{aligned} M^T &= M > 0 \\ G^T &= -G \\ K^T &= K \end{aligned}$$

The coefficient matrices (M , G and K) are respectively associated with inertial, gyric, and stiffness forces. Conservative refers to the fact that the system energy is conserved, while gyric reflects the fact that these terms often arise in spinning systems. This form of equations will be present in a multi-body analysis of rotating systems.

Hughes proves that asymptotic stability for a conservative gyric system is impossible by showing that if s is a root of the characteristic equation of 2.11 then $-s$ must also be a root. Strictly left half plane poles will always have their right half plane counterparts. Therefore, stability, as opposed to asymptotic stability, is the strongest result possible for a conservative gyric system. A stable system will have all of the roots of its characteristic equation on the imaginary axis.

A sufficient condition for stability of a conservative gyric system is that it be

statically stable, i.e. the stiffness matrix must be positive definite, $K > 0$. The stiffness matrix for the two-by-two system above is positive definite if I_2 is the major principal axis of inertia. That is, rotation about the major axis is directionally stable by virtue of its static stability. However, $K > 0$ is only a sufficient condition for stability. Rotation about the minor principal axis is also stable. Since in this case the stiffness matrix is not positive definite the system is considered gyroically stabilized. To test for gyroic stability we can check the roots of the characteristic equation of the second order system. The system will be considered stable if the roots are purely imaginary.

These results do not preclude the possibility that asymptotic stability could be obtained by adding damping to a conservative gyroic system. However, while damping tends to make statically stable systems become asymptotically stable systems, damping also tends to destabilize gyroically stabilized systems. Hughes proves that statically unstable systems are destabilized if they have a positive definite damping matrix.

2.3.2 Rigid Body Inertia Ratios

Before we solve for the roots of the characteristic equation of Equation 2.11 we should note that we can simplify our analysis by recognizing that only the ratios of inertia are important to the analysis rather than the individual values of inertia. Dividing each equation of Equation 2.11 by the corresponding diagonal term of M results in the following form of M , G and K .

$$M = \begin{bmatrix} 1 & 0 \\ 0 & 1 \end{bmatrix}$$

$$G = \begin{bmatrix} 0 & 1 - k_1 \\ -(1 - k_3) & 0 \end{bmatrix}$$

$$K = \begin{bmatrix} k_1 & 0 \\ 0 & k_3 \end{bmatrix}$$

where

$$k_1 = \frac{I_2 - I_3}{I_1}, \quad k_3 = \frac{I_2 - I_1}{I_3}$$

A physical body can not have arbitrary values of I_1, I_2 and I_3 [Hughes 86]. These constraints are captured by the fact that

$$-1 < k_1 < 1$$

$$-1 < k_3 < 1$$

Therefore, all possible rigid body configurations can be represented on a plot of the parameter space of k_1 and k_3 restricted to the unit square. Figure 2-2 shows how k_1 and k_3 depend upon the relative size of I_1, I_2 , and I_3 . Also included in the figure are schematic drawings of rectangular prisms that would have approximately the correct inertia ratios for selected points around the diagram.

The characteristic equation of this system is formed with the following determinant

$$\det[Ms^2 + \dot{\Phi}Gs + \dot{\Phi}^2K] = 0$$

which results in the following

$$\left(\frac{s}{\dot{\Phi}}\right)^4 + \hat{b}_1 \left(\frac{s}{\dot{\Phi}}\right)^2 + \hat{b}_2 = 0 \quad (2.12)$$

where

$$\begin{aligned} \hat{b}_1 &= 1 + k_1 k_3 \\ \hat{b}_2 &= k_1 k_3 \end{aligned}$$

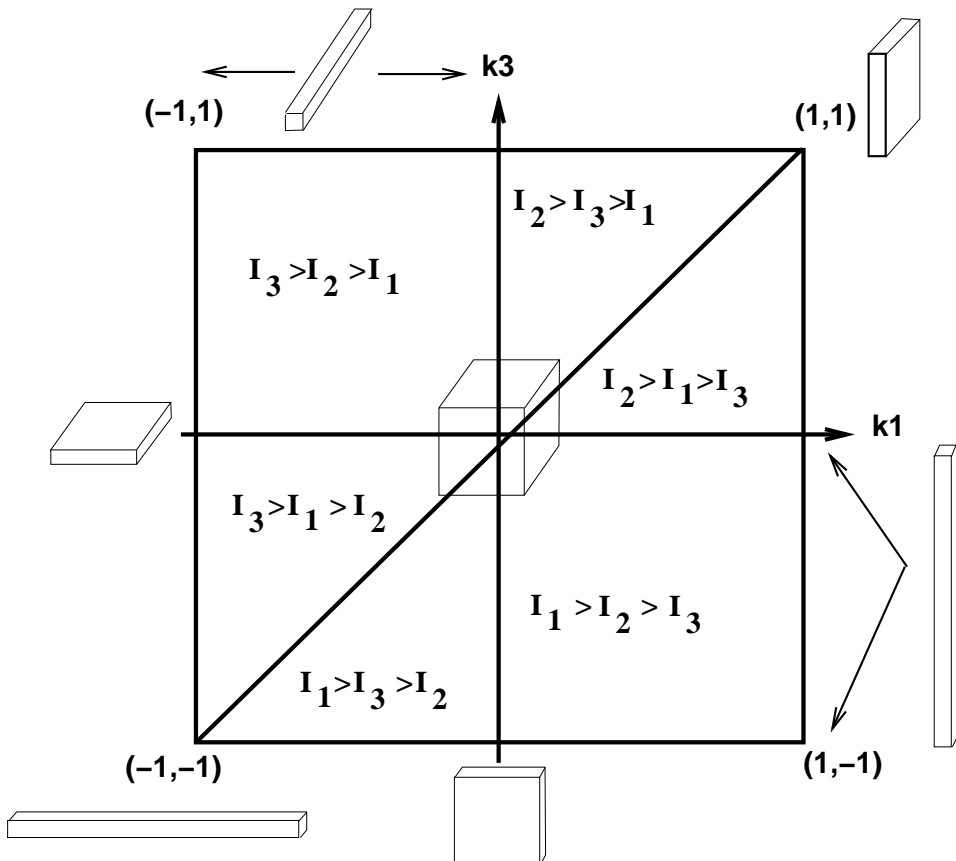


Figure 2-2: The inertia ratio diagram shows how k_1 and k_3 depend upon the relative value of the principal inertias. $k_1 = \frac{I_2 - I_3}{I_1}$, $k_3 = \frac{I_2 - I_1}{I_3}$. The different rectangular prisms located near the axes and corners of the diagram indicate an example shape that would correspond to the local inertia ratios.

For stability we require

1. $\hat{b}_1 = 1 + k_1 k_3 > 0$
2. $\hat{b}_2 = k_1 k_3 > 0$
3. $(\hat{b}_1)^2 - 4\hat{b}_2 = (1 - k_1 k_3)^2 > 0$

The only stability condition not met automatically is $k_1 k_3 > 0$. This requirement specifies that k_1 and k_3 must have the same sign. On a plot of the $\{k_1, k_3\}$ parameter space stability occurs in the first and third quadrants.

Figure 2-3 shows the regions of stability for the simple spin solutions of a rigid body.

Equation 2.12 is simple enough that we can solve for the roots of the characteristic equation in closed form. Two roots are located at $s = \pm j\dot{\Phi}$. This is the stroboscopic mode of rotation. This mode of rotation occurs when the body is still spinning perfectly about the principal axis but this axis is offset from the original orientation. The other two roots are located at $s = \pm\nu$, where

$$\nu = (k_1 k_3)^{1/2} \dot{\Phi}$$

In the first and third quadrants of the inertia ratio diagram, ν is positive and therefore these roots are purely oscillatory. In the second and fourth quadrants of Figure 2-2, ν is imaginary forcing the roots of the characteristic equation to have real positive and negative values. In these quadrants, the unstable mode of motion is governed by the following equation

$$x = x_0 e^s \text{ where } s = (-k_1 k_3)^{1/2} \dot{\Phi} t \quad (2.13)$$

To get an idea of how unstable the system is we compute the change in the nominal somersault angle, Φ , required for the the unstable rotational mode to grow by a factor

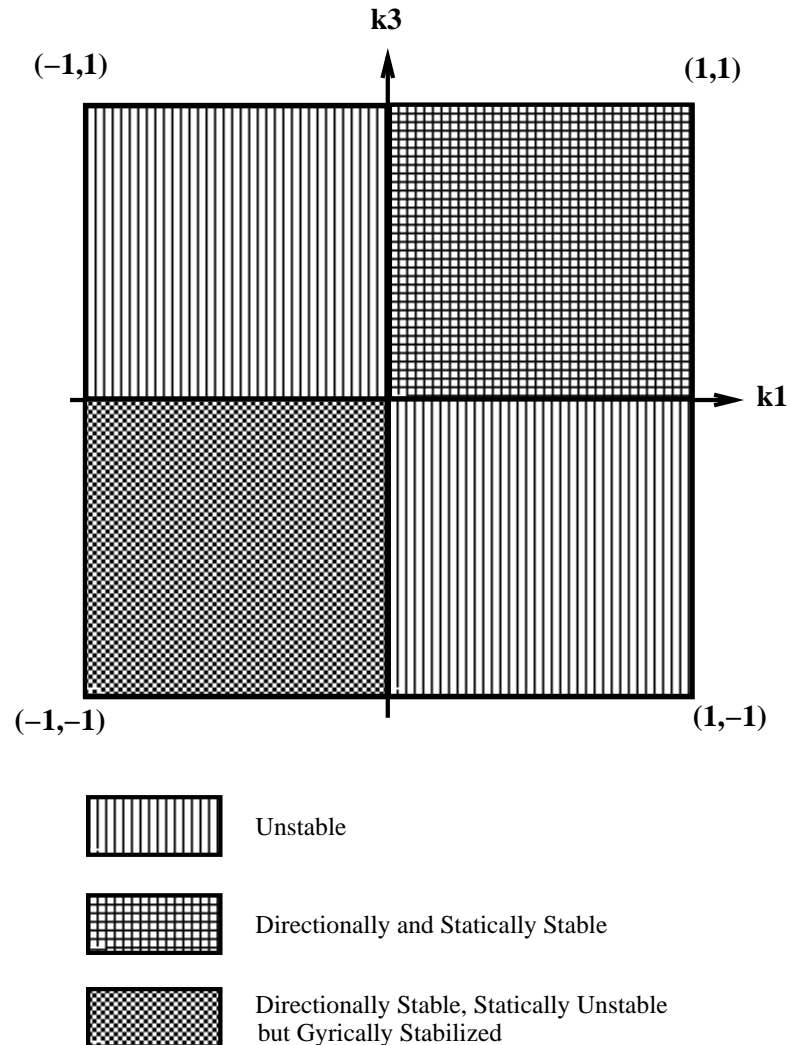


Figure 2-3: Stability diagram for the simple spin solutions of a rigid body. Rigid body rotational stability depends only upon the two non-dimensional inertia ratios k_1 and k_3 . We assume the body is rotating about the principal axis corresponding to I_2 for this diagram.

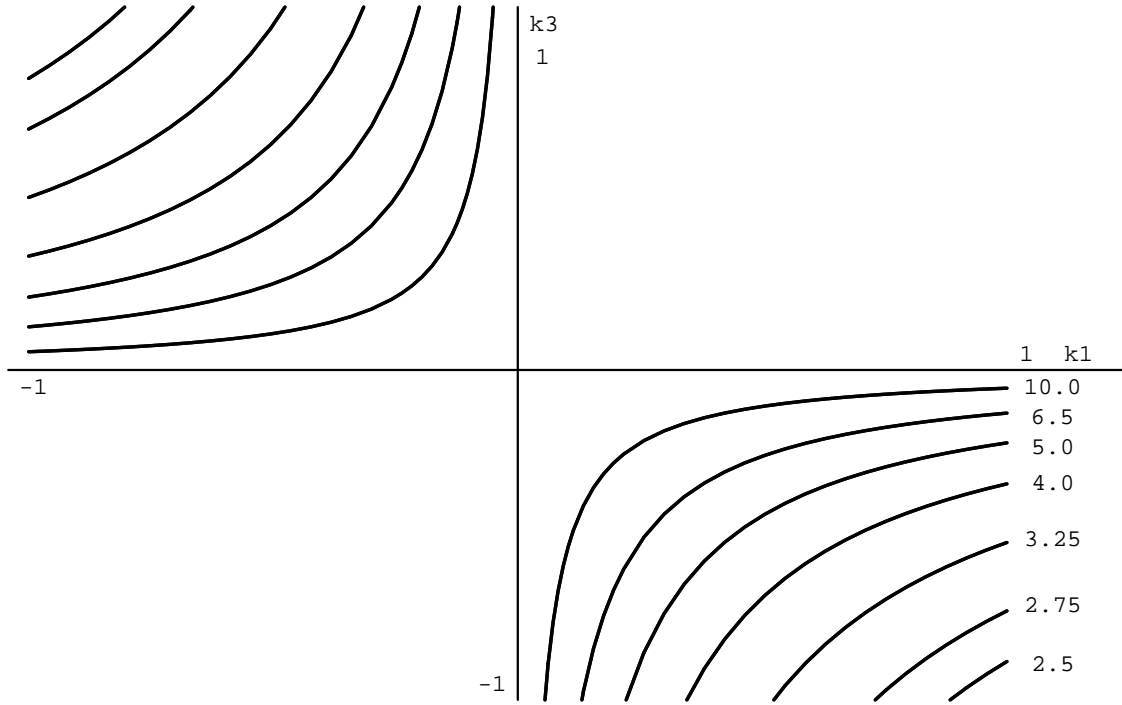


Figure 2-4: All rigid bodies with inertia ratios on a single curve have an unstable mode that grows at the same rate. The value of a curve, indicated in the figure, is the somersault angle (in radians) the body must execute before the unstable twist mode grows by a factor of ten. The most unstable systems are those with inertia ratios in the corners $\{k_1, k_3\} = \{1, -1\}$ or $\{-1, 1\}$. This plot is symmetric about the origin.

of N .

$$\Phi = \dot{\Phi}t = \frac{\ln(N)}{(-k_1 k_3)^{1/2}} \quad (2.14)$$

Figure 2-4 shows curves of constant Φ on the $\{k_1, k_3\}$ axes for $N = 10$.

2.4 Rotational Stability of the Rigid Human Body

For any particular configuration of the human body, we can solve for the orientation and magnitude of the principal axes of inertia. This allows us to compute the corresponding inertia ratios which in turn provide a valuable reference for the stability

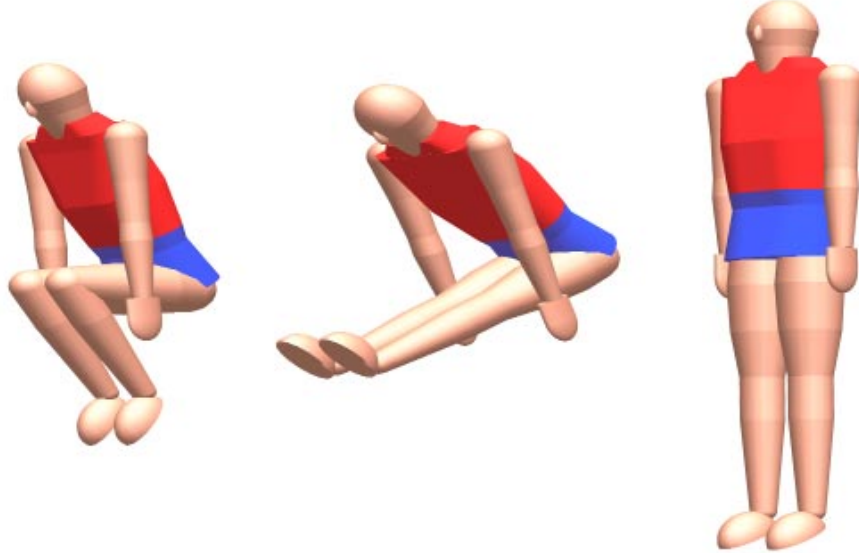


Figure 2-5: Tuck, pike, and layout positions for a human.

of the human body in rotation about the principal axes. Figure 2-5 shows from left to right a human in the tuck, pike and layout positions. Figure 2-6 shows the inertia ratios of a human performer moving from a tuck position through a pike position to a layout position. To make this figure, I assumed that I_2 was the principal inertia along the somersault axis of the human. This analysis shows that for a rigid body, tuck and pike somersault configurations are stable in rotation about the somersault axis while steady rotation in the layout position is unstable. In the pike and tuck positions the inertia ratios are in the stable upper right quadrant of the inertia ratio diagram while the inertia ratios of the layout somersault are in the unstable lower right quadrant.

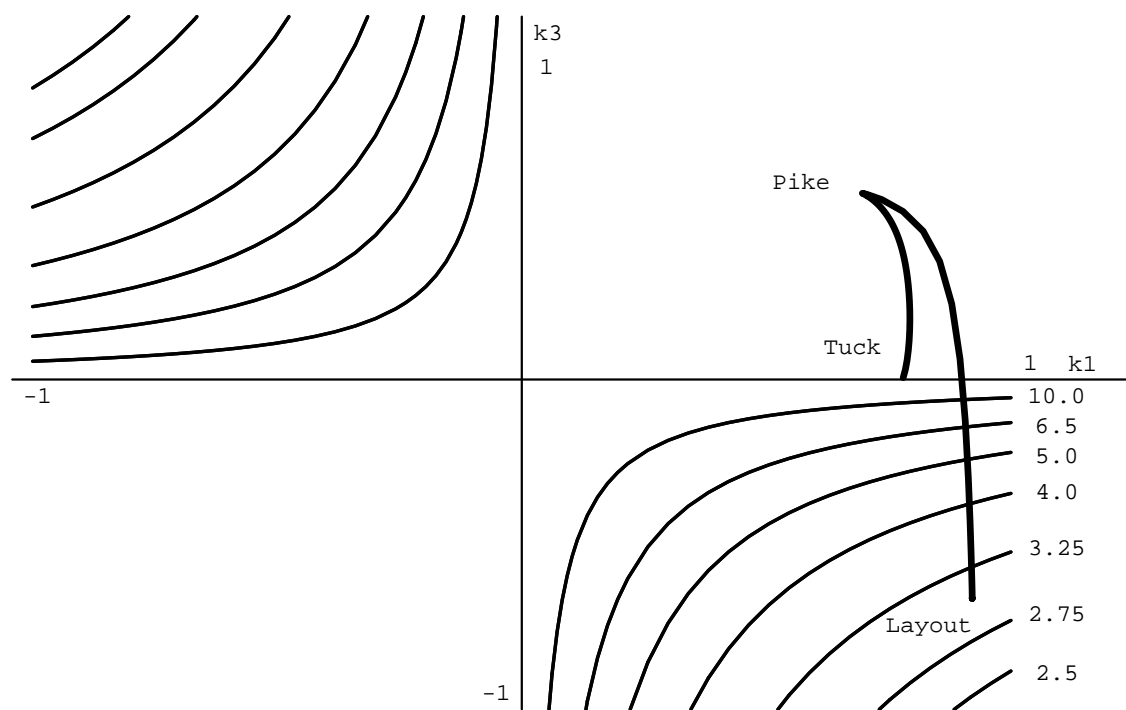


Figure 2-6: Inertia ratios of a human performer for a sequence of configurations connecting tuck, pike and layout positions. The tuck and pike positions are stable (for a rigid body) while the layout is unstable.

2.5 A Map of Rigid Body Rotation

The linear analysis we have used so far is restricted to three solutions for rigid body rotation, pure spin about each of the principal axes. A general solution for the torque-free motion of a rigid body tumbling in space would be useful for understanding the range of behavior a rigid body can exhibit between these three special solutions. Solving for such a solution is one of the classic problems of dynamics. The contribution that this solution offers today is a concise description of the states and non-dimensional parameters that govern rigid body rotation (see Appendix A.4). In addition, the analytic solutions give rise to elegant geometric interpretations of rigid body rotation that help to provide intuition of this otherwise complex movement. In this section, I present one form of geometric tool derived from the analytic solution that is useful in visualizing rigid body rotation. I think of this tool as a map of rigid body rotation because it shows graphically two of the three Euler angle trajectories involved in non-linear rotational motion of a rigid body. This map not only makes clear the stable and unstable axes of rotation but also shows two distinct regions of qualitatively different motion. A performer can exert control over his rotational motion by moving within and inbetween these two regions.

Two integrals of motion are used to define a map of rigid body rotation. During flight, a rotating rigid body must conserve angular momentum, \vec{h} , and kinetic energy, T . The magnitude of both of these quantities can be written as the equation for an ellipsoid in angular velocity space

$$h^2 = I_1^2\omega_1^2 + I_2^2\omega_2^2 + I_3^2\omega_3^2 \quad (2.15)$$

$$2T = I_1\omega_1^2 + I_2\omega_2^2 + I_3\omega_3^2. \quad (2.16)$$

Assume, with no loss of generality, that the angular momentum vector is aligned with the inertially fixed '2' axis. Using the direction cosine matrix, (2.2), we can solve for

the components of \vec{h} in the principal coordinate frame.

$$\vec{h} = hc_1 \hat{i}_{p1} + hc_2 \hat{i}_{p2} + hc_3 \hat{i}_{p3}$$

where $\{c_1, c_2, c_3\}$ are the direction cosines of \vec{h} and \hat{i}_{pj} is the j^{th} unit vector in the principal axis system. Alternatively, the principal axes components of angular momentum can also be written as follows

$$\vec{h} = I_1 \omega_1 \hat{i}_{p1} + I_2 \omega_2 \hat{i}_{p2} + I_3 \omega_3 \hat{i}_{p3}$$

Thus we have established that

$$hc_1 = I_1 \omega_1, \quad hc_2 = I_2 \omega_2, \quad hc_3 = I_3 \omega_3,$$

The ellipsoid describing angular momentum (2.15) can now be written as the equation of a sphere in direction cosine space.

$$c_1^2 + c_2^2 + c_3^2 = 1$$

Similarly the kinetic energy can be written as the equation of an ellipsoid.

$$\frac{c_1^2}{I_1} + \frac{c_2^2}{I_2} + \frac{c_3^2}{I_3} = \frac{2T}{h^2}$$

For a fixed kinetic energy and angular momentum, the direction cosines must simultaneously lie on the surface of both the momentum sphere and energy ellipsoid. Therefore, the intersection of these two shapes describes a trajectory in direction cosine space that the body must ‘follow’.

Figure 2-7 shows a sample map for the possible rotational trajectories of a ‘rigid’ human body. Each trajectory shown on the sphere corresponds to a different kinetic energy of rotation. The axes of the sphere are the direction cosine axes. The sphere



Figure 2-7: A map of rigid body rotation for a human in the layout position. The axes of the sphere and the principal axes of the body remain parallel as the body rotates. The inertially fixed angular momentum vector (black) paints trajectories onto the surface of the sphere as the sphere rotates. Each trajectory on the sphere corresponds to a different rotational energy. The trajectories indicate the tilt and twist angles of the body as it rotates. This map does not include somersault angle and does not show the time dependence of the tilt and twist Euler angles.

rotates with the body so that its axes remain parallel to the principal axes of the body. The angular momentum vector is shown protruding from the sphere. The sphere (and body) must move so that the (inertially fixed) angular momentum vector remains in the 'slot' that is appropriate for the given kinetic energy.

The stable and unstable axes of rotation are obvious from this map. The stable principal axes are surrounded by trajectories that enclose the axes while the unstable middle principal axis shows trajectories that converge then diverge from that axis. This map also shows that the trajectories are divided into two qualitatively different regions. This division is based on the rotational kinetic energy.

For a fixed angular momentum, the energy of rotation is bounded above and below by the rotational energy in pure spin about the minimum and maximum principal axes respectively.

$$\frac{h^2}{2I_{max}} \leq T \leq \frac{h^2}{2I_{min}}$$

Between these extremes exists a continuum of energy levels of rotational motion. The dividing point among these trajectories is the energy required to spin about the middle principal axis, $T = \frac{h^2}{2I_{mid}}$. Those trajectories with higher energy involve monotonically increasing (or decreasing) twist while those with less energy involve oscillatory twisting. In Figure 2-7, the trajectories which enclose the minimum principal axis (head-to-toe axis) of the performer involve monotonic twist while those that enclose the maximum principal axis of inertia involve twist angles that oscillate between 0 and $\pm\pi$ depending on which region the trajectory is located in.

We can read the twist and tilt Euler angles of a trajectory from this map in an intuitive way. Using Equation 2.2 we can derive an explicit relationship between the direction cosines and the Euler angles as follows

$$\begin{bmatrix} c_1 \\ c_2 \\ c_3 \end{bmatrix} = \begin{bmatrix} S_\Psi C_\Theta \\ C_\Psi C_\Theta \\ -S_\Theta \end{bmatrix}$$

Drawing the components of the angular momentum vector as shown in Figure 2-8, we realize that the spherical coordinates of the unit angular momentum vector are defined by the tilt and twist Euler angles, $\{\Theta, \Psi\}$. The tilt angle, Θ is the (negative) latitude of the energy curve and the twist angle, Ψ , is the (negative) longitude. Therefore we can simply read the tilt and twist Euler angles of the body from the polar coordinates of the angular momentum vector on this map. For example, the attitude of the body shown in Figure 2-7 is approximately $\Theta = 3^\circ, \Psi = 0$.

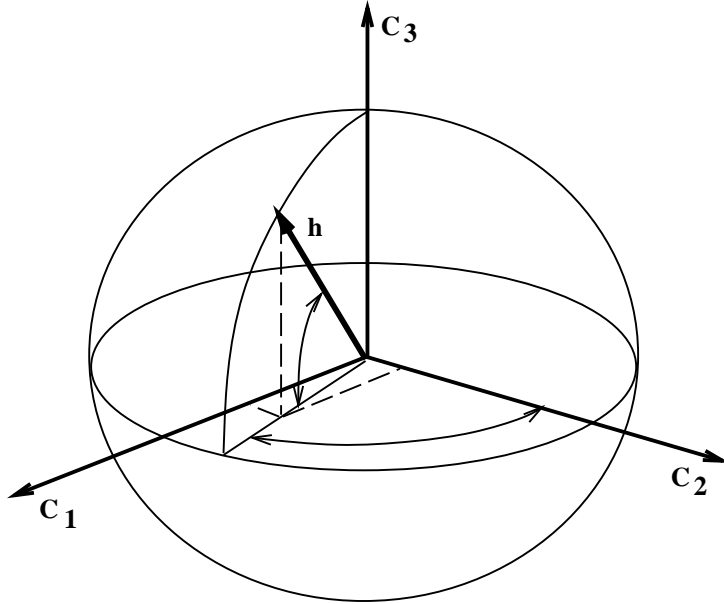


Figure 2-8: The spherical coordinates used to define orientation of the unit angular momentum vector in direction cosine space are the negative of the tilt and twist Euler angles.

2.6 Dynamic Simulation Environment

The analytic and experimental results presented in this thesis are complemented with numeric results from non-linear dynamic simulation of the creature in question. This section briefly describes the simulation environment used to compute the motion and produce graphic output from dynamic simulations.

The simulation environment consists of three parts that allow us to compute the movement of a creature, make a movie of its motion using computer graphics, and analyze its motion using time histories of simulated data. Using software developed in this laboratory, the Leg Laboratory at MIT, we have integrated the simulation environment so that the three parts are all generated automatically from a single input file that describes the shape, topology, and mass properties of the system. The part that computes the motion does so by numerically integrating the non-linear equations of motion for a given creature. The non-linear equations of motion are derived using the commercially available software package, SD-FAST. This package derives the

equations of motion for a rigid link, multi-body system using the description file as input. The equations of motion are automatically incorporated into a dynamic simulation that handles user interface to the software. The computer graphic and analysis software is also generated automatically from the description of the creature allowing us to animate movement from simulation data using either a simple “working” picture or a higher quality, computer graphic image. The only part of the simulation environment that is not automatically generated is the control software. This software is used to specify the desired behavior of the system. It does so by computing joint torques or other actuator inputs that we assume the creature to have. Passive forces like those due to springs, dampers and gravity are input to the equations of motion in a manner similar to active joint torques. The ability to quickly produce dynamic simulations of a variety of creatures has made this simulation software a useful research tool in the investigation of machine, human or animal movement.

2.7 Summary

Material in this chapter is derived from the text of [Hughes 86]. In this chapter, I reviewed the dynamic and kinematic equations of rigid body rotation. Linear equations of motion describe rigid body rotation in the neighborhood of the equilibrium solution of pure spin about a principal axis. A stability analysis of these equations shows that rigid body rotation is stable about the major and minor principal axes but is unstable about the intermediate axis. The linear stability analysis can be simplified by the use of the non-dimensional inertia ratios, k_1 and k_3 . A stability diagram simply demarcates stable and unstable regions in the k_1 , k_3 parameter space. I show the values of k_1 and k_3 that a (rigid) human body would assume in the tuck, pike, and layout positions in order to provide a stability reference for the rotating human body. A geometric map derived from the closed-form solution of rigid body rotation captures the range of possible rotational modes. This map intuitively shows the stable

and unstable axes of rotation. It also demarcates between two regions of qualitatively different rotational motion.

Chapter 3

Robot Tucked Somersaults

3.1 Introduction

The somersault is a maneuver in which a performer jumps into the air and rotates once about a side-to-side axis before landing on the ground. The main requirement of a successful somersault is a balanced landing which in turn requires that the performer finish the somersault with a pre-specified body attitude. In this chapter, I explore attitude control techniques for producing stable landing configurations for the tucked somersault of a 3D biped running robot.

The tucked somersault is distinguished by maintaining the tuck position during most of the maneuver. Humans ‘tuck’ by holding their knees close to the chest with the knee joints flexed to fold the lower legs under the body. An important dynamic feature of the tuck somersault is that in most humans it involves rotation about the major principal axis of inertia. Since a rigid body rotating about its major principal axis is directionally stable, we might expect the tuck somersault to be stable in the sense that the axis of rotation will tend to maintain its inertial orientation. This stability in turn simplifies the control of body attitude at landing in the tuck somersault.

Directional stability of the spin axis during a tucked somersault means that a



Figure 3-1: Photograph of the 3D Biped used for experiments. The body is an aluminum frame on which are mounted hip actuators and computer electronics. Each ball and socket hip joint has three low friction hydraulic actuators that can position the leg forward and aft, side-to-side, and can rotate the leg along the axis of the leg. A hydraulic actuator within each leg changes its length, while an air spring makes the leg springy in the axial direction. Sensors measure the lengths of the legs, the positions of the hip actuators, pressure in the hip actuators and contact between the foot and the floor. Gyroscopes measure the inertial attitude of the body. An umbilical cable connects the machine to hydraulic, pneumatic, and electrical power supplies. Control computations are done by microprocessors, some located on board and some nearby in the laboratory. Communications cables connect all processors.

somersault control strategy need deal primarily with avoiding over-rotation or under-rotation about the somersault axis. Rotation rate about the somersault axis can be controlled by changing rotational inertia. Since angular momentum must be conserved during flight, increasing inertia will slow down the somersault rate while decreasing inertia will increase somersault rate. If the performer knows the time of flight, then control of somersault rate provides a means of controlling the somersault angle at landing.

In this chapter, I discuss somersault experiments with a 3D biped robot, (Figure 3-1). Figure 3-2 shows a sequence of photographs of the 3D Biped taken while the robot performed a successful somersault. The somersault axis of the robot is coincident

with the maximum principal axis of inertia making the robot somersault dynamically similar to the tuck somersault in humans. To initiate the somersault the biped runs forward, jumps to attain a double stance phase, then thrusts with both legs while pitching its body forward. Once airborne, the robot shortens its legs (tucks) to accelerate the forward rotation and swings its legs to a predetermined position with respect to the body. During flight the robot uses a feedback algorithm that changes the leg length to produce a rotation rate that will yield the desired somersault angle at landing. To accommodate errors in the estimated time of landing, the robot moves its feet to track the desired landing configuration as the system approaches the ground. The robot does not use any active control of out-of-plane rotation during flight. Rather it uses a broad stance during takeoff to minimize tilt rotation at the beginning of flight and it uses a broad stance during landing to minimize the effect of landing tilt errors. The robot has successfully performed the somersault in the laboratory. On its best day, the robot regained balance on landing to continue stable running on seven out of ten somersault attempts.

3.2 The Mechanics of the Somersault

The most basic requirement of a somersault is that the performer neither over-rotate nor under-rotate the landing. Accurate control of the landing attitude allows careful placement of the foot relative to the center of mass of the robot which is a requirement for stable dynamic running [Raibert 84]. Considering only the somersault degree of freedom, the attitude requirement is expressed by equating the time of flight and the time to rotate through the desired change in somersault attitude,

$$\frac{\Delta\Phi}{\dot{\Phi}_o} = \frac{\dot{z}_o + \sqrt{\dot{z}_o^2 + 2g(z_o - z_{td})}}{g} \quad (3.1)$$

where

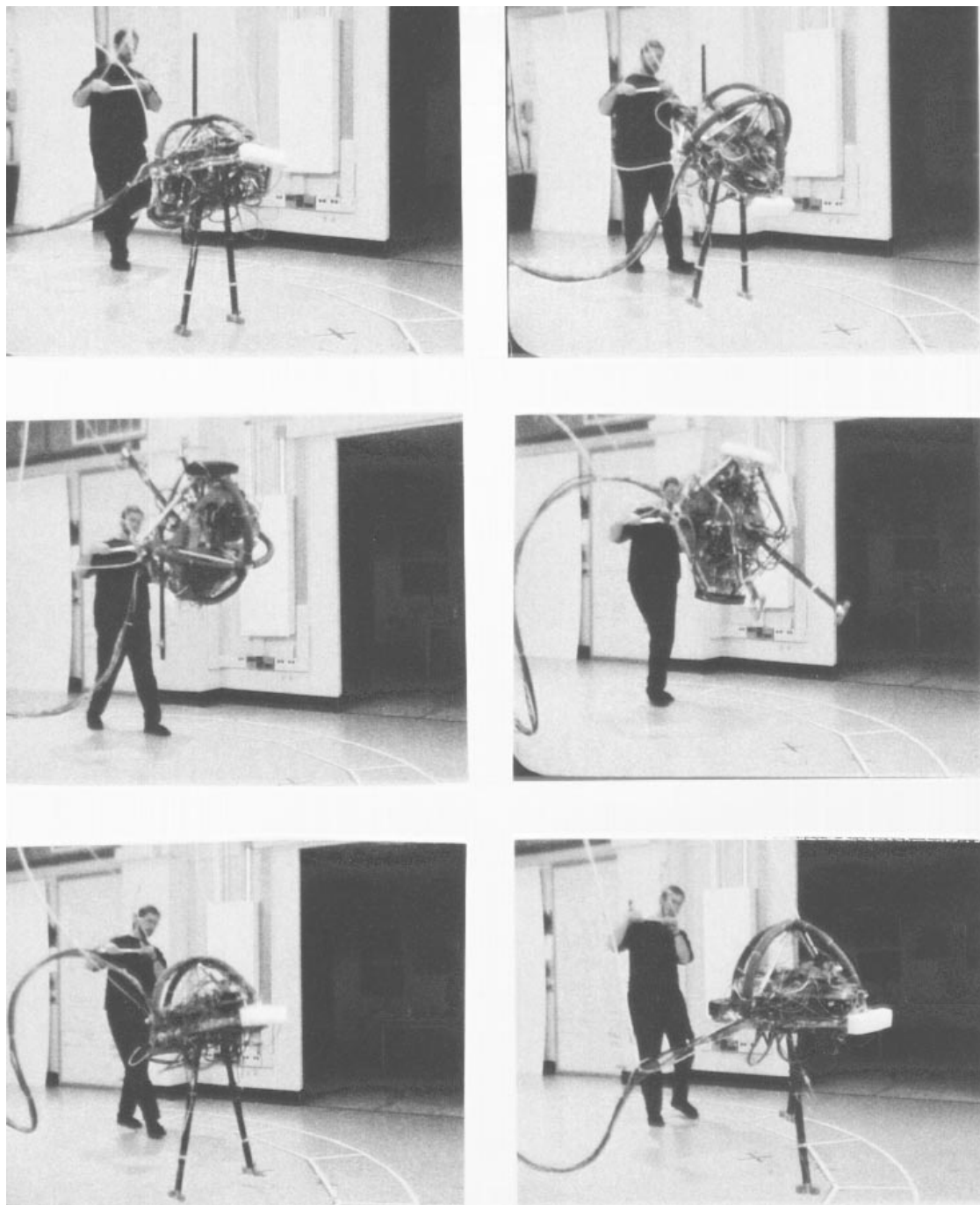


Figure 3-2: A sequence of photographs (arranged in left-right order starting upper left) taken during the execution of a somersault. The robot is running from left to right. Approximate relative time of each image: upper left-0.0 s, upper right-0.15 s, middle left-0.33 s, middle right-0.66 s, lower left-0.80 s, lower right-1.02 s.

$\Delta\Phi$ is the change in somersault angle required during flight

$\dot{\Phi}_o$ is the somersault rate of the body at lift-off

z_o is the height of the center of mass (c.o.m.) at lift-off

\dot{z}_o is the vertical velocity of the c.o.m. at lift-off

z_{td} is estimated height of the c.o.m. at touchdown

g is the acceleration of gravity

Equation 3.1 relies on several simplifying assumptions: 1) the somersault dynamics are governed by the planar equation $I\ddot{\Phi} = 0$, implying that the external torques due to supply cables or wind resistance are negligible, and 2) only the rotation in somersault is significant and the somersault axis is a maximum principal axis of inertia so that tilt and twist angles will stay small if they start small thus allowing us to ignore them, and 3) the legs do not swing with respect to the body during the flight phase, so $\dot{\Phi}_o$ represents the angular rates of both the body and the legs.

When the 3D Biped robot somersaults it rotates about its major principal axis. Figure 3-3 shows that the region of stable rotation about the somersault axis is large. We may then expect that as long as the somersault is initialized with the angular momentum vector close to the major principal axis then it will remain close to that axis. This in turn means that the tilt and twist angles of the robot at landing will be small and the somersault dynamics simplify as indicated above. In the remainder of this chapter we assume that this simplification is valid in computations involving rotational dynamics of the robot.

3.3 Somersault Control Strategies

The goal of the somersault control strategy is to produce a landing attitude that allows the robot to maintain balance. To regain balance on the landing, it is important that the robot achieve a desired horizontal displacement of the foot relative to the center

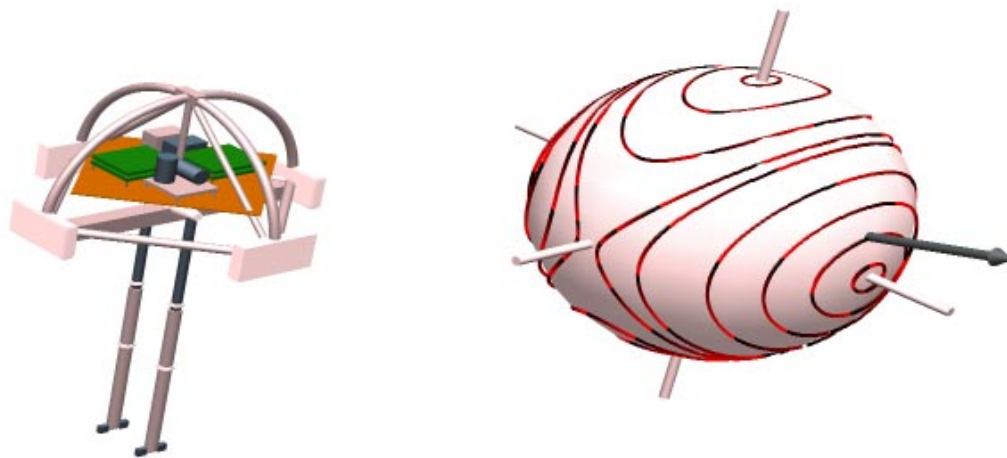


Figure 3-3: The somersault axis of the 3D Biped is coincident with the major principal axis of inertia. With the legs in the fully extended position, as shown here, the minor principal axis is the 'head-to-toe' axis.

of mass. In the plane of the somersault this horizontal displacement is given by

$$d = l \sin \beta \quad (3.2)$$

where l is the leg length and β is the leg inclination angle, the angle the leg makes with vertical in the plane of rotation (Figure 3-4). If the legs are held fixed relative to the body, then the desired landing attitude, or equivalently $\Delta\Phi$, can be found from d . If the initial conditions of flight, $\dot{\Phi}_o$, \dot{z}_o , and z_o , are established accurately so that for a desired z_{td} and $\Delta\Phi$ Equation 3.1 is satisfied, then the desired landing attitude will be achieved. More generally, one approach for generating somersaults is to establish accurately the initial conditions of flight to a state that is empirically determined, then to execute an open loop pattern of actuator signals to produce components of the desired behavior. Hodgins and Raibert used this approach in programming a planar biped robot to perform front somersaults with a 90% success rate. The success of such an approach depends upon how precisely one can reproduce the state of the robot and how sensitive the desired movement is to variations in the state.

For a running robot with less regular and repeatable motion, such as the 3D Biped, precise initialization is more difficult. Therefore, reliable production of a desired landing attitude might be improved with an in-flight feedback strategy that modifies the performance of the somersault based on the state of the robot in flight.

To the extent a system with non-zero angular momentum can change its inertia, it can also change its rotation rate. For a somersault, if the time until landing is known then control over rotation rate amounts to control over the landing attitude. The basis of the somersault control strategy is to change the robot somersault inertia to produce a rotation rate that will yield the desired body attitude at the time of landing.

The robot can change its inertia by extending or retracting (untucking or tucking) its prismatic legs. In flight, if the angular rate and moment of inertia of the robot in one configuration are $\dot{\Phi}_1$ and I_1 then with constant angular momentum the angular

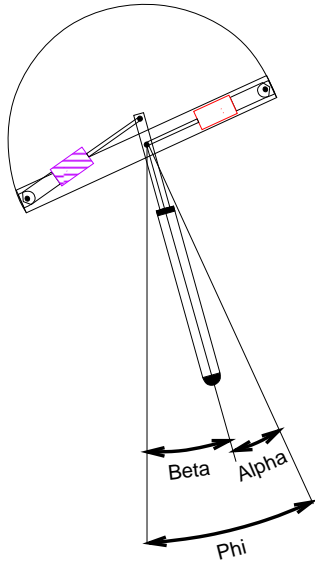


Figure 3-4: In order to maintain balance at landing the leg inclination angle, β , must be near the desired value. β is the angle the leg makes with the local vertical. It is a function of the the hip angle, α and the body attitude, Φ .

rate in a configuration with inertia I_2 is $\dot{\Phi}_2 = (I_1/I_2)\dot{\Phi}_1$. Joint limits restrict the range of inertia and thus limit control over the rotation rate. For the 3D Biped robot, the inertia about the somersault axis ranges from 1.22 kg m^2 with legs retracted to 1.50 kg m^2 with legs fully extended. In moving from a fully retracted to a fully extended position the robot can reduce its somersault rate to 81% of its initial value. We will refer to the regulation of somersault rate and landing attitude via leg length as the *tuck servo*.

3.3.1 Control of Somersault Angle

To implement the tuck servo with state feedback, we first pose the requirement of Equation 3.1 as a function of the state during flight rather than at lift-off.

$$\frac{\Phi_{td} - \Phi}{\dot{\Phi}} = \frac{\dot{z}_o + \sqrt{\dot{z}_o^2 + 2g(z_o - \cos \beta_{td} l_{td})}}{g} - (t - t_o) \quad (3.3)$$

where

- Φ_{td} is the desired somersault attitude at touch down,
- Φ is the current somersault attitude,
- $\dot{\Phi}$ is the current somersault rate,
- β_{td} is the desired leg inclination angle at touch down,
- l_{td} is the leg length at touch down,
- t is the current time,
- t_o is the lift off time.

The robot inertia and thus $\dot{\Phi}$ are functions of l_{td} , so we solve for the l_{td} that will make Equation 3.3 an equality.

We nominally require the hip angle to be zero on landing. If this is the case then $\beta_{td} = \Phi_{td}$ and the landing attitude and leg length determine the height of the hip. The center of mass is coincident with the hip, so z_{td} is given by

$$z_{td} = \cos \Phi_{td} l_{td} \quad (3.4)$$

We have also assumed that the tilt angle at touchdown is zero.

Define a function, f , as the difference between the left and right hand sides of (3.3).

$$f = \frac{\dot{z}_o + \sqrt{\dot{z}_o^2 + 2g(z_o - \cos \Phi_{td} l_{td})}}{g} - (t - t_o) - \frac{\Phi_{td} - \Phi}{\dot{\Phi}} \quad (3.5)$$

If the desired landing attitude is to be achieved then $f = 0$. Otherwise, the pitch rate needs to be increased or decreased depending on the sign of f . The control algorithm we use changes the leg to a length that will make $f = 0$. The function, f , is a non-linear function of the leg length, so we use a Newton search [Strang 86] to recursively solve for the desired leg length. The recursion uses the first order, Taylor series expansion of $f = 0$,

$$0 = f(l) + \frac{df}{dl} \Delta l \quad (3.6)$$

This yields the following equation for Δl

$$\Delta l = \frac{-f}{df/dl} \quad (3.7)$$

Ideally, once the desired leg length is achieved, f remains zero for the rest of the somersault and the desired leg length becomes the leg length at touch down, $l \rightarrow l_{td}$.

During each control cycle the tuck servo executes the following process

1. measure the state of the robot
2. compute f and df/dl_{td}
3. compute Δl_{td}
4. estimate the next value of f using $l_{td} = l_{td} + \Delta l_{td}$.
5. if $f \approx 0$ go to (6), else go to (2) using new values of f and l_{td}
6. servo the leg length to l_{td} .

To perform step 2 above we need to solve for df/dl_{td} . Taking the derivative of (3.5) with respect to l_{td} results in

$$df/dl_{td} = \frac{-\cos \Phi_{td}}{\sqrt{\dot{z}_o^2 + 2g(z_o - \cos \Phi_{td} l_{td})}} + \frac{\Phi_{td} - \Phi}{\dot{\Phi}^2} d\dot{\Phi}/dl_{td} \quad (3.8)$$

To obtain $d\dot{\Phi}/dl_{td}$ we use the fact that the angular momentum is a constant so that

$$\dot{\Phi} = \frac{h}{(I_o + 2m_l r^2)} \quad (3.9)$$

where

h angular momentum

r distance from the lower leg c.o.m. to the robot c.o.m.

m_l lower leg mass

I_o robot pitch inertia about c.o.m. when $r = 0$.

The total inertia of the robot as a function of leg length is $(I_o + 2m_l r^2)$. The $2m_l r^2$ term represents that inertia due to the distance of the lower legs from the robot c.o.m. This is the component of inertia that we control as the legs change length. From (3.9) we get

$$d\dot{\Phi}/dl_{td} = -\frac{2m_l r h}{(I_o + m_l r^2)^2} dr/dl_{td} \quad (3.10)$$

The robot center of mass moves very little when the legs are extended or retracted so we assume $dr/dl_{td} = 1$. Substituting for h from (3.9) results in

$$d\dot{\Phi}/dl_{td} = -\frac{2m_l r \dot{\Phi}}{(I_o + m_l r^2)} \quad (3.11)$$

Now by substituting (3.11), (3.8), and (3.5) into (3.7), we can compute the required Δl_{td} .

The computation of the desired leg length depends upon knowledge of robot parameters such as inertia and leg mass. However, since the process is repeated each control cycle based upon the sensed state of the robot, sensitivity to precise knowledge of these parameters is reduced. In exchange for this robustness to uncertainty we give up the ability to pre-specify both the landing attitude *and* the leg length at touchdown.

3.3.2 Accommodating Landing Time Errors

A limitation of the tuck servo strategy is its dependence upon accurate knowledge of the time until landing. With somersault rates on the order of 500 deg/s , small errors in the predicted landing time can result in intolerable landing attitude errors. Because we have no measurement of the vertical position or speed while airborne these quantities must be derived from estimates of the lift-off conditions. To accommodate

errors in these estimates, we have modified the landing strategy to allow the robot to land with the desired configuration anywhere within a ‘window’ of the predicted landing time.

The leg inclination angle in (3.2) is the difference between the somersault angle and the hip angle, $\beta = \Phi - \alpha$. By changing the hip angle the control algorithm makes the foot track the desired displacement for a short time just prior to or after the expected landing time. In this way, the robot maintains the desired landing configuration during a ‘landing window’ that is centered about the nominal landing attitude. In order to maximize the landing window the legs are moved ‘back’ relative to the body ($\alpha > 0$) early in the flip. Prior to landing, the foot is swept forward in order to track the desired foot position until touchdown.

3.3.3 Control of Tilt and Twist Angles

Achieving a takeoff attitude with no tilt and twist is challenging with the 3D Biped. As the robot runs its body somersault angle stays close to zero but its body tilts and twists in phase with the stepping cycle as it runs. During a normal running cycle, the robot uses hip actuators during stance to apply torques to the body in order to control body attitude. However, we found that it was difficult to achieve small tilt and twist angles and rates at takeoff using only the hip servos. We found that the best method for keeping tilt and twist angles and angular rates small during takeoff was to use a wide double stance during the flip initiation in combination with the normal attitude control used during stance ([Raibert 84]). This wide double stance helps stabilize the robot’s tipping motion during takeoff. An important component of this approach was to achieve simultaneous touch down of both feet at the beginning of the double stance phase. Similarly, a wide double stance during somersault landing and simultaneous touchdown of both feet were observed to minimize the effect of tilt and twist errors on the somersault recovery.

3.4 Experiments with 3D Biped Somersaults

The 3D Biped is a two-legged robot that is free to translate and rotate in 3D space. Each leg is mounted adjacent to the center of gravity of the body with a ball and socket hip joint. The hip joint allows leg rotation about the x , y , and z axes ($\pm 20^\circ$, $\pm 60^\circ$, $\pm 15^\circ$ see Fig. 1). Hydraulic actuators control each of these degrees of freedom. The robot's telescoping legs contain a fourth hydraulic actuator that acts in series with a pneumatic compression spring. Mass properties of the 3D Biped are included in Table 3.1 Some of the kinetic energy of the machine is stored in compression of the air spring during each bounce, and returned to power the subsequent flight phase. Energy is added to the hopping oscillation by actively compressing the air spring with the hydraulic piston during stance. The 3D Biped maintains balance while running by performing three control tasks [Raibert 84]:

1. during stance, the robot maintains body posture by applying hip torques between the legs and the body,
2. during stance, the robot adds energy to the air spring to maintain the hopping oscillation, and
3. during flight, the robot positions the foot in anticipation of the next stance phase in order to control forward velocity.

To execute a somersault, the 3D Biped modifies three steps in an otherwise normal running sequence. The robot performs a hurdle step during which it hops higher than normal as it prepares to land on both feet for the flip step. The flip step is initiated by thrusting with both legs while pitching the body forward. During the landing step the robot lands on both feet then resumes a normal running gait. The control actions used to execute the flip are summarized in Table 3.2.

In laboratory experiments, the 3D Biped has successfully performed the forward somersault and regained a stable running cycle afterwards (Figure 3-2).

Table 3.1
3D Biped Parameters

| Symbol | Description | Quantity |
|-----------|-----------------------|--------------------|
| m | total mass | 31.44 (kg) |
| m_l | lower leg mass | 0.652 (kg) |
| I_o | somersault inertia | 1.02 ($kg\ m^2$) |
| r_{min} | min. lower leg radius | 0.404 (m) |
| l_{min} | min. leg length | 0.647 (m) |
| l_{max} | max. leg length | 0.862 (m) |

Three sets of data from a successful somersault and a nearly successful somersault are shown in Figures 3-5, 3-6, and 3-7. Figure 3-5 shows data for the approach, flip, landing, and continuation of running for a successful somersault. The nominal desired landing attitude was set to 350° . The robot ran steadily until the hurdle step at which time it hopped higher than normal as it prepared to land on both feet. During the flip step the body is thrust upwards and accelerated in somersault. The desired leg inclination angle was set to -5.7° based on the forward speed in flight. The robot lands 0.080s earlier than anticipated with a somersault attitude of 325° and with a leg inclination angle of -11° . The actual leg inclination angle is much closer to its desired value than the corresponding values in somersault because of the feet-back position in flight. The foot positioning servo was not used in this somersault because the desired foot position was always slightly in back of the actual foot position, and the legs were already in a swept back configuration. Balance is regained on landing, but since the robot lands with a slight backward lean, forward speed is lost. Forward speed and posture are quickly restored during the following steps.

Note the oscillation in tilt angle during flight. This oscillation occurs because the robot took off with a non-zero tilt rate. Since rotation about the somersault axis is passively stable, the oscillation does not grow. We found that in order to regain

Table 3.2
Control Summary for the Somersault

| Step | Action |
|-----------|---|
| Approach | Run forward ($\approx 1m/s$) with alternating gait |
| Hurdle | Pitch up slightly Hop with increased leg thrust Prepare to land simultaneously on both feet |
| Flip | Jump with maximum thrust Pitch body forward with maximum torque Shorten legs once airborne Servo hips to feet back position Engage tuck servo Prepare to land simultaneously on both feet Track desired foot position |
| Landing | Dissipate energy on landing Return somersault rate to zero, restore posture Adjust nominal leg length based on l_{td} |
| Following | Resume running with alternating gait |

balance after the somersault, the tilt angle on landing must be kept moderately small, $|\Theta| < 15^\circ$. To do this we increased the stance width during the flip step, thereby providing a passively stable stance configuration in tilt during initiation.

The data in Fig. 4 shows the somersault action on a larger scale to illustrate the function of the tuck servo. Between the beginning of the flip step and lift off, the magnitude of the somersault rate, hip angle rate, and leg length all increase. At lift off, the somersault rate of the body declines rapidly as the legs are accelerated to the rotation rate of the body. The conservation of momentum constraint produces the symmetry between the absolute angular rate of the body and the relative angular rate of the hips. During this time, the legs are tucked to the shortest possible length.

The tuck servo is engaged as the hips reach the desired feet-back position and come to rest relative to the body. The robot has a somersault rate of 606 deg/s at the time the tuck servo is engaged. At this somersault rate, it is estimated that the robot will over-rotate by 84° . This error is illustrated by the third graph of Fig. 4 which compares the estimated time until touchdown and the estimated time until the desired somersault attitude is achieved. The tuck servo extends the legs to the maximum possible length to slow down the somersault rotation to 463 deg/s at which point it is estimated that the robot will land at nearly the desired attitude. The robot maintains this configuration until landing.

Data from another nearly successful somersault is shown in Fig. 5. In this somersault, the robot uses the foot positioning servo to keep from over-rotating. Once again the desired somersault landing attitude was 350° . The desired leg inclination angle was set to -5.9° . The robot lands 0.065s later than anticipated with a somersault attitude of 391° and with a leg inclination angle of -3.2° . As the robot detected that it was over-rotating it swept the feet forward quickly to track the desired foot position. This increased the somersault rate because of the conservation of angular momentum and contributed to the somersault attitude error on landing. A velocity measurement error during stance after landing led to the loss of forward speed of the

Table 3.3
3D Biped Flip Attempts

| File | Outcome | β_{td} deg | Φ_{td} deg | $\dot{\Phi}$ deg/s | \dot{z}_0 (est) m/s | \dot{z}_0 (meas) m/s | $\dot{z}_0\%err$ | speed _{lo} m/s |
|-----------|---------|---------------------|--------------------|-----------------------|--------------------------|---------------------------|------------------|----------------------------|
| 92.346.4 | success | 0.12 | -10.8 | 547 | 3.08 | 3.04 | -1.2 | 1.04 |
| 92.346.5 | success | -0.14 | -6.29 | 529 | 3.48 | 3.33 | -4.3 | 0.77 |
| 92.346.6 | success | 0.33 | -8.47 | 524 | 3.41 | 3.32 | -2.8 | 0.89 |
| 92.346.7 | success | -0.31 | -13.7 | 549 | 3.53 | 3.48 | -1.4 | 1.10 |
| 92.346.8 | 6 steps | -1.95 | -18.9 | 553 | 3.69 | 3.70 | 1.6 | 1.02 |
| 92.346.9 | success | -0.39 | -12.7 | 551 | 3.45 | 3.47 | 0.7 | 1.04 |
| 92.346.10 | success | -0.04 | -11.6 | 545 | 3.54 | 3.48 | -1.7 | 0.96 |
| 92.346.11 | success | -0.28 | -15.3 | 541 | 3.15 | 3.13 | -0.5 | 0.90 |
| 92.346.12 | fall | -3.42 | -1.04 | 529 | 3.28 | 3.04 | -7.4 | 0.89 |
| 92.346.13 | fall | -1.87 | -17.7 | 503 | 3.33 | 3.20 | -3.9 | 0.88 |

robot so that it was momentarily supported by safety ropes before resuming running and therefore not considered a complete success.

Table 3.3 shows data compiled for ten somersault attempts performed by the 3D Biped in the laboratory. The robot successfully regained balanced running on seven of these attempts.

3.5 Summary

In this chapter, I discuss a strategy for robot somersaults that combines elements of feed forward control, feedback control, and passive dynamic stability. I also presented results from somersault experiments done in the laboratory on a 3D biped running robot. The somersault is initialized using pre-programmed patterns of action. In

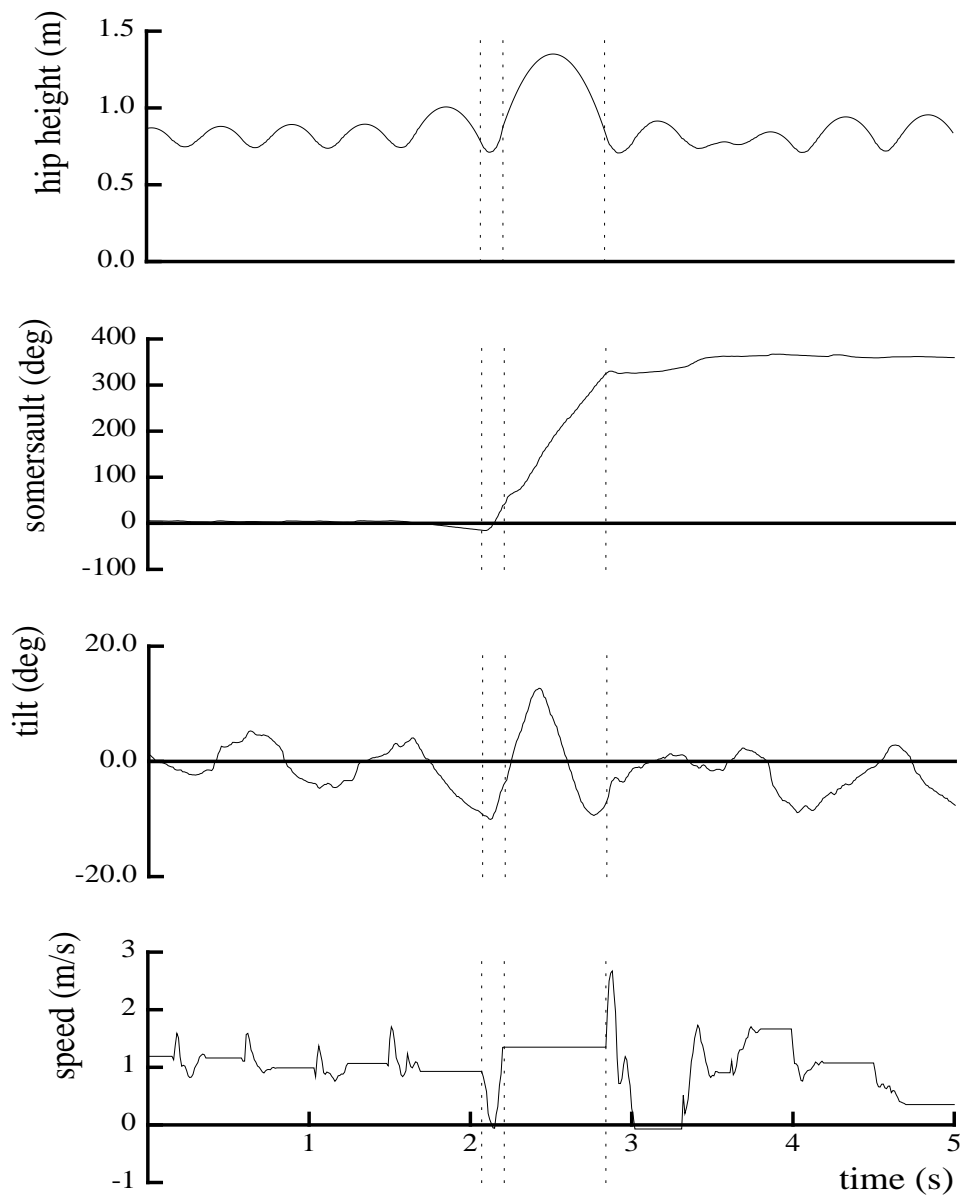


Figure 3-5: Hip height, somersault, and tilt angles, and forward speed of the 3D-Biped during a somersault. Vertical lines indicate initiation of flip, lift-off and landing. Data file B92.181.3

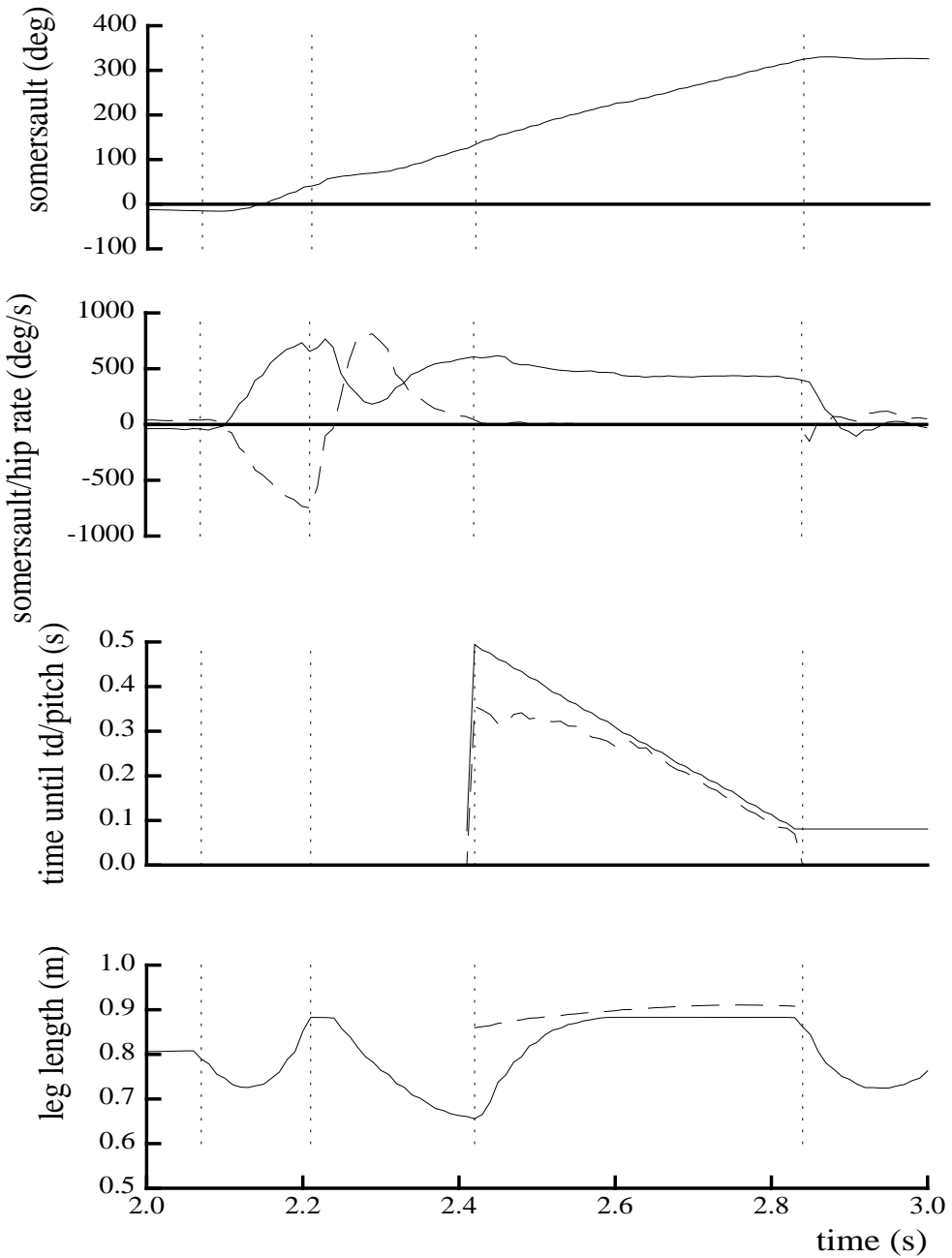


Figure 3-6: Somersault angle, absolute somersault rate (solid) and relative hip rate (dashed). The third graph shows the estimated time until touch down (solid) and estimated time until desired somersault attitude is achieved (dashed). The last graph is the measured leg length (solid) and desired leg length(dashed) for one leg. Vertical lines indicate initiation of flip, lift-off, tuck servo initiation, and landing. Data file B92.181.3.

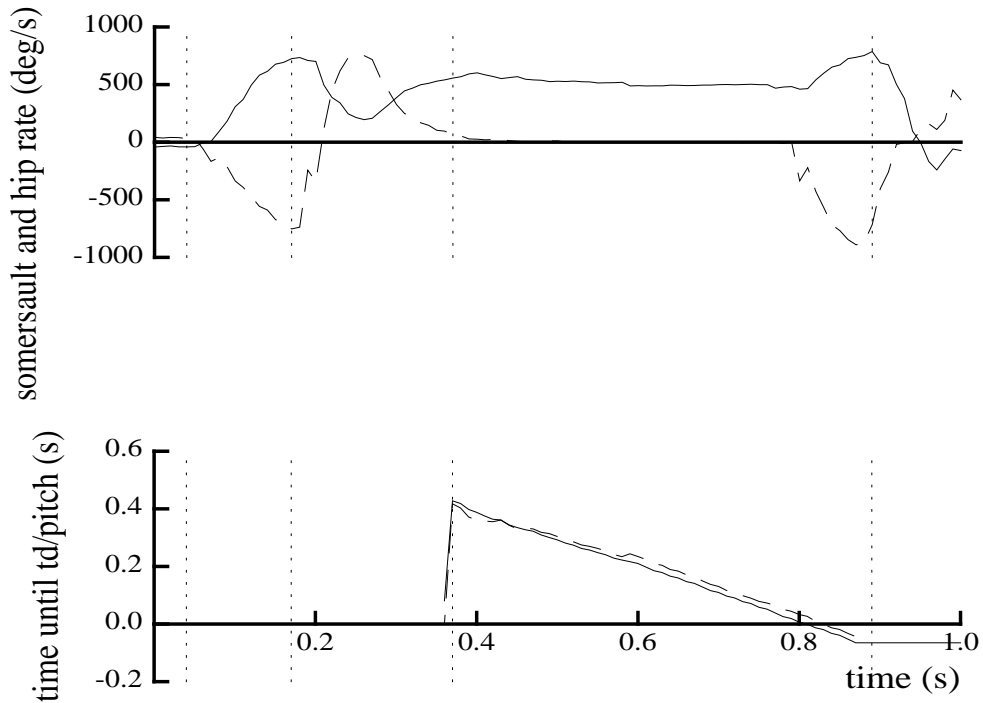


Figure 3-7: This somersault was over-rotating so the feet were swept forward at the end to track a desired foot position. Data shows absolute somersault rate (solid) and relative hip rate (dashed) and estimated time until touch down (solid) and estimated time until desired somersault attitude is achieved (dashed). Vertical lines indicate initiation of flip, lift-off, tuck servo initiation, and landing. Data file B92.181.4.

flight, a feedback strategy changes robot inertia to control the landing attitude of the somersault. The robot actively positions its feet to maintain a desired landing configuration during an interval surrounding the predicted landing time. The passive tilt stability inherent in a wide double stance is used to reduce tilt angle and rate on takeoff. The passive stability of a rigid body rotating about its maximum principle axis of inertia accounts for moderate tilt angles on touch down given moderate tilt angles and rates on lift-off.

Chapter 4

Passively Stable Layout Somersaults

4.1 Introduction

The layout somersault is an airborne maneuver in which the performer rotates about a side-to-side axis while maintaining an erect body configuration. The layout somersault is often considered to be inherently unstable because it involves rotation about the middle principal axis of inertia, an unstable mode of rotation for a rigid body. I found that passive arm movement could neutrally stabilize the layout somersault. These passive movements are generated by dynamic forces that arise from body motion and from compliant shoulders. Figure 4-1 shows a sketch of the type of three-body model used for simulation, analysis, and experimental tests in the laboratory. This simple three-body model of a human can exhibit passively stable layout somersaults if an appropriately tuned spring is used at the shoulder.

Layout somersaults are considered stable if steady somersaulting is achieved without exhibiting any 'large' oscillations in the tilt or twist angles. For example, Figure 4-2 shows simulation data of the simple human model for two cases:

1. **Rigid body (dashed lines):** this model has very stiff shoulder springs and

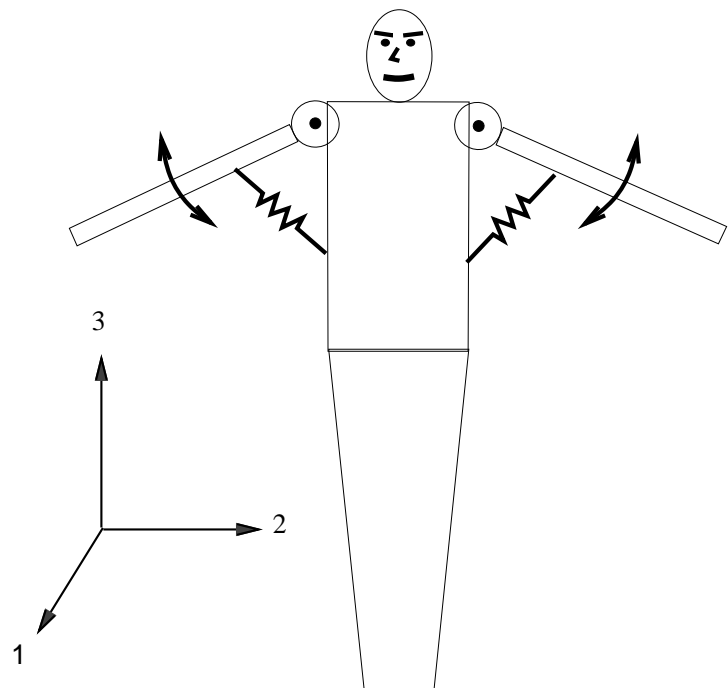


Figure 4-1: Diagram of a dynamic model used to study layout somersaults. The head, torso, and legs comprise a single rigid body. The arms are connected to the body with pin joints that allow rotation about the 1 body axis. Joint torques are provided by torsional springs and (possibly) dampers.

dampers to approximate the rigid body case. As with the true rigid body, the tilt and twist angles periodically move through large excursions from zero as the body somersaults.

2. **Passively stable body (solid lines):** this model has tuned shoulder springs without dampers that allow considerable passive arm movement. The tilt and twist angles of the body stay near zero.

The rigid body tilt and twist angles shown in Figure 4-2 are shown in another form in the map of Figure 2-7 which is repeated here in Figure 4-3. The rigid body instability is evident by the trajectories that converge and diverge upon the somersault axis. The twisting oscillation of the simulation data corresponds to a trajectory on the map that is centered about the maximum principal axes (front-to-back).

In this chapter, I present results of studies on the passive layout somersault using non-linear dynamic simulation and linear stability analysis. By deriving a linearized model of the dynamics of a three-body model, I show that passive layout stability depends upon both the arm angle and the shoulder spring constant. I show conditions under which passive layout stability can theoretically be achieved. Using the simplest possible model of the layout somersault, I explain the fundamental dynamics of passive stabilization. I also present summarized results of non-linear dynamic simulations that support the linear stability analysis.

4.2 Simple Human Model

Figure 4-1 shows a simplified human body model used to study the dynamic stability of somersaulting motion. From the non-linear equations of motion of this model I analytically derive linearized equations that govern the motion of the body relative to pure somersaulting rotation. The linear equations of motion decouple into two distinct subsystems which allow further model simplifications. When inertial parameters for a human are used in this model, a linear stability analysis indicates that stability of

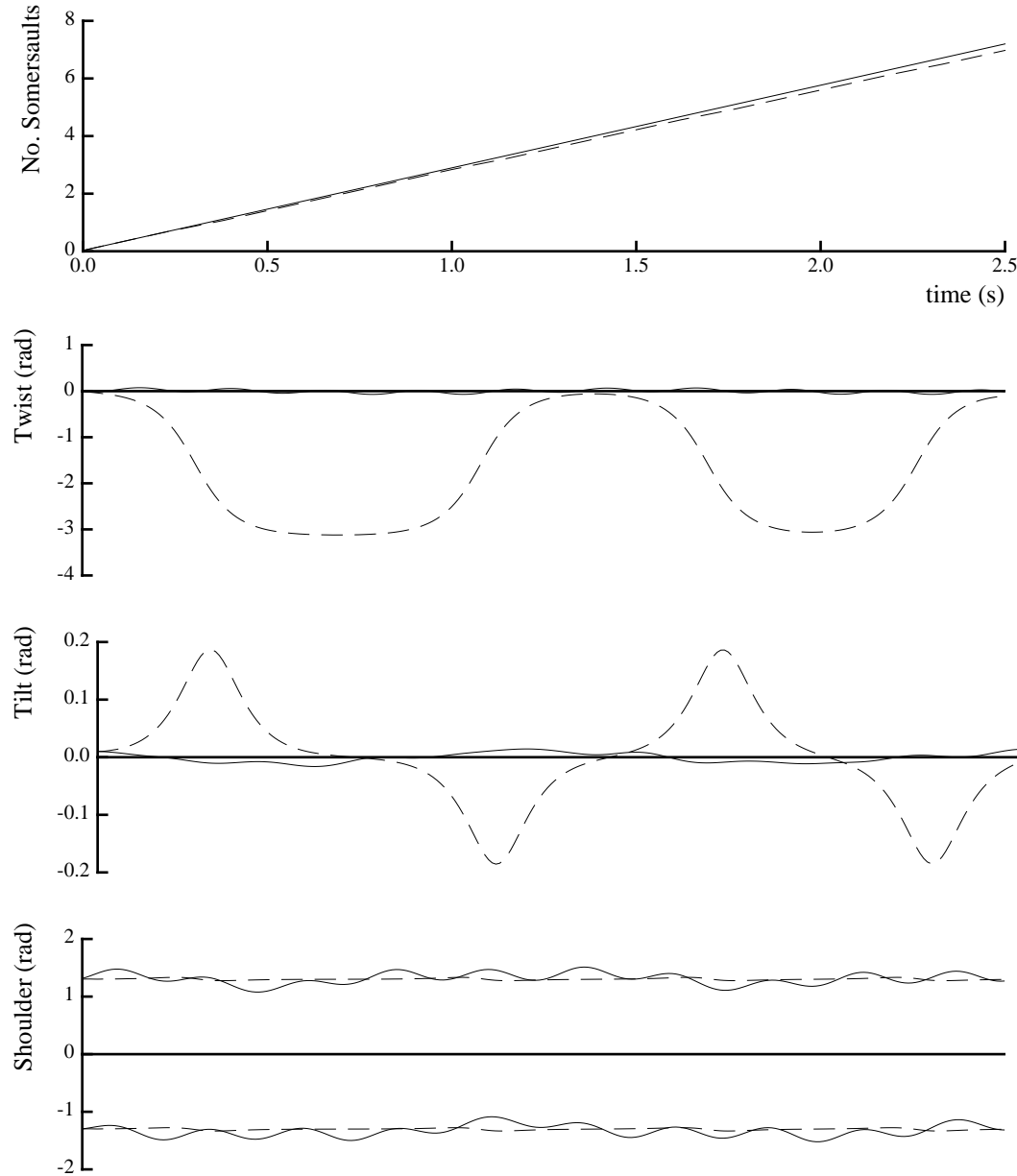


Figure 4-2: Number of complete somersault revolutions, twist and tilt Euler angles describing body attitude, and left and right shoulder angles for two simulations. The solid lines indicate the passively stable case. The dashed lines indicate the rigid body case. The data for the passively stable case shows nearly eight stable somersaults about the middle principal axis.



Figure 4-3: A map of rigid body rotation for a human in the layout position. The inertially fixed angular momentum vector (black) paints trajectories onto the surface of the sphere as the sphere rotates. The axes of the sphere and the principal axes of the body remain parallel as the body rotates. Each trajectory on the sphere corresponds to a different rotational energy. The trajectories indicate the tilt and twist angles of the body as it rotates. This map does not include somersault angle and does not show the time dependence of the tilt and twist Euler angles.

the layout somersault can be achieved for a range of nominal arm angles and shoulder spring constants.

The human body model has shoulder pin joints that allow the arms to be raised and lowered in the ‘2-3’ plane of the body. The head, torso, and legs are modeled as a single rigid body. Torques at the shoulder joints are provided by torsional springs and dampers. Neglecting translation of the center of mass, the model has five degrees of freedom (d.o.f.): three for rotation of the body with respect to inertial space and two for relative movement of each arm. The orientation of the body with respect to an inertial coordinate frame is described using a 2-1-3 sequence of Euler angles (Figure 2-1.) To describe the attitude of the body relative to the inertial frame, a coordinate system initially parallel to the inertial reference frame is first rotated through the somersault angle about the inertially fixed ‘2’ axis, then rotated through the tilt angle about the intermediate ‘1’ body axis, and finally rotated through the twist angle about the body fixed ‘3’ axis.

The rotation of the right and left arms relative to the body are given respectively by the angles γ_r and γ_l . An arm angle is equal to zero when the hand is held next to the thigh. Positive rotation of the arm about the ‘1’ axis is given by the right hand rule. The right and left arm angles are rewritten in terms of symmetric (γ_s) and asymmetric (γ_a) components as follows:

$$\begin{aligned}\gamma_s &= 1/2(\gamma_l - \gamma_r) \\ \gamma_a &= 1/2(\gamma_l + \gamma_r)\end{aligned}$$

The parameters necessary to describe the three-body system in the non-linear equations of motion are given below. The body is assumed to be symmetric from left to right when the arms are held in a symmetric orientation.

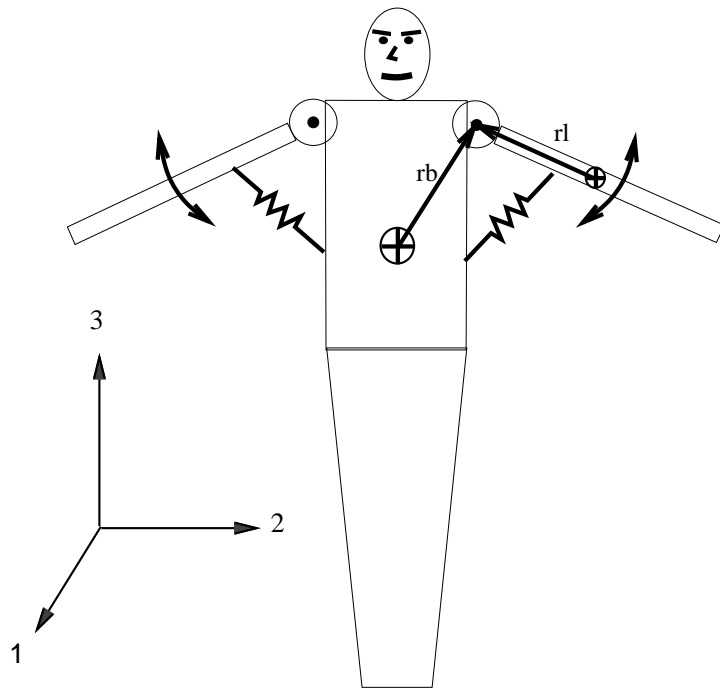


Figure 4-4: Diagram of a five d.o.f. model with body axes and vectors labeled.

m_b mass of the body

m_l mass of arms

Ib_1, Ib_2, Ib_3 body principal inertias in body fixed axes

Il_1, Il_2, Il_3 arm principal inertias in arm fixed axes $\Gamma_{s0} = 0.0$

rb_1, rb_2, rb_3 vector components from body c.g. to left arm pin joint

rl_1, rl_2, rl_3 vector components from left arm c.g. to pin joint

k_{sh}, b_{sh} shoulder spring and damping constants

Figure 4-4 shows vectors and body axes defined in the above list.

In order to study the layout somersault as performed by humans, I will use data for a human performer, Carl Furrer, 1982 World Trampoline Champion [Yeadon 84].

Table 4.1
Inertia Data for Carl Furrer

| Parameter | Value | Units |
|-----------|--------|-------------------|
| m_b | 58.3 | kg |
| m_l | 3.743 | kg |
| Ib_1 | 10.19 | kg m ² |
| Ib_2 | 9.93 | kg m ² |
| Ib_3 | 0.52 | kg m ² |
| Il_1 | 0.128 | kg m ² |
| Il_2 | 0.128 | kg m ² |
| Il_3 | 0.0037 | kg m ² |
| rb_1 | 0.0 | m |
| rb_2 | 0.18 | m |
| rb_3 | 0.479 | m |
| rl_1 | 0.0 | m |
| rl_2 | 0.0 | m |
| rl_3 | 0.262 | m |

The data for Furrer's body parameters are included in Table 4.1.

4.2.1 Nonlinear Equations of Motion

I derive the non-linear equations of motion¹ as a starting point for a linear analysis that will follow. I used Kane's method [Kane 85] to derive the equations. Rather than include the lengthy equations here I include the Mathematica code used to produce them in Appendix A.1. The equations are derived using a reference coordinate frame located at the center of mass of the three body system. Therefore, the rotational equations are decoupled from the translational equations.

¹Non-linear equations used for dynamic simulation were derived using a commercially available package, SD-FAST. This version of the equations was not amenable to analytic linearization.

4.2.2 Linearized Equations of Motion

The linearized equations will describe the motion of the system with respect to a reference frame that is steadily rotating about the 2 axis with rate $\dot{\Phi}$. Pure somersault rotation about a principal axis of inertia is an equilibrium solution for this system if a constant feed forward shoulder torque is applied to cancel the centrifugal forces due to steady rotation. This steady torque can be achieved by pre-tensioning the shoulder spring. The magnitude of this torque will be a function of the nominal symmetric arm angle, Γ_{s0} , and the rotation rate, $\dot{\Phi}$. Any deviation of the arm from Γ_{s0} will result in additional shoulder torques from the springs and dampers.

The linearized equations of motion for this model follow:

$$M\ddot{x} + \dot{\Phi}(G + D)\dot{x} + \dot{\Phi}^2(K + K')x = 0 \quad (4.1)$$

where

$$M = \begin{bmatrix} m_{11} & 0 & m_{13} & 0 & 0 \\ 0 & m_{22} & 0 & 0 & 0 \\ m_{13} & 0 & m_{33} & 0 & 0 \\ 0 & 0 & 0 & m_{44} & 0 \\ 0 & 0 & 0 & 0 & m_{55} \end{bmatrix} \quad (4.2)$$

$$G = \begin{bmatrix} 0 & g_{12} & 0 & 0 & 0 \\ -g_{12} & 0 & g_{23} & 0 & 0 \\ 0 & -g_{23} & 0 & 0 & 0 \\ 0 & 0 & 0 & 0 & g_{45} \\ 0 & 0 & 0 & -g_{45} & 0 \end{bmatrix} \quad (4.3)$$

$$D = \begin{bmatrix} 0 & 0 & 0 & 0 & 0 \\ 0 & 0 & 0 & 0 & 0 \\ 0 & 0 & 2b_{sh}/\dot{\Phi} & 0 & 0 \\ 0 & 0 & 0 & 0 & 0 \\ 0 & 0 & 0 & 0 & 2b_{sh}/\dot{\Phi} \end{bmatrix} \quad (4.4)$$

$$K = \begin{bmatrix} k_{11} & 0 & k_{13} & 0 & 0 \\ 0 & k_{22} & 0 & 0 & 0 \\ k_{31} & 0 & k_{33} & 0 & 0 \\ 0 & 0 & 0 & 0 & 0 \\ 0 & 0 & 0 & 0 & k_{55} \end{bmatrix} \quad (4.5)$$

$$K' = \begin{bmatrix} 0 & 0 & 0 & 0 & 0 \\ 0 & 0 & 0 & 0 & 0 \\ 0 & 0 & 2k_{sh}/\dot{\Phi}^2 & 0 & 0 \\ 0 & 0 & 0 & 0 & 0 \\ 0 & 0 & 0 & 0 & 2k_{sh}/\dot{\Phi}^2 \end{bmatrix} \quad (4.6)$$

The state vector, x , is comprised of (in order): θ - the tilt angle, ψ - the twist angle, γ_a - the asymmetric deviation of the two arms from the nominal arm angle, ϕ - the deviation of the somersault angle from the frame steadily rotating at rate $\dot{\Phi}$, and γ_s - the symmetric deviation of the two arms from the nominal arm angle.

The expressions for individual components of M , G , and K are listed in Appendix A.3. In Equation 4.1 the nominal rotation rate, $\dot{\Phi}$, scales the rate terms and $\dot{\Phi}^2$ scales the spring terms. This is evidence of the fact that the coriolis forces involving somersault rate give rise to rate dependent terms and the centrifugal forces involving somersault rate give rise to spring terms. The terms in D and K' arise from the spring and damper model of the shoulder torques (τ_l, τ_r) for each arm.

$$\tau_l = -k_{sh}(\gamma_l - \Gamma_{s0}) - b_{sh}\dot{\gamma}_l \quad (4.7)$$

$$\tau_r = -k_{sh}(\gamma_r + \Gamma_{s0}) - b_{sh}\dot{\gamma}_r \quad (4.8)$$

Non-dimensional states (z, \dot{z}, \ddot{z}) are derived by scaling \dot{x} , and \ddot{x} by $\dot{\Phi}$ or $\dot{\Phi}^2$ as follows

$$\begin{aligned} z &= x \\ \dot{z} &= \dot{x}/\dot{\Phi} \\ \ddot{z} &= \ddot{x}/\dot{\Phi}^2 \end{aligned}$$

Rewriting the equations of motion as functions of the non-dimensional states results in the following

$$\dot{\Phi}^2 (M\ddot{z} + (G + D)\dot{z} + (K + K')z) = 0 \quad (4.9)$$

It is now clear that $\dot{\Phi}$ serves only as a time scale of Equation 4.9. We may consider $\dot{\Phi} = 1$ for simplicity in studying stability as long as we are willing to work with scaled shoulder spring and damping terms. In the following stability analysis we use a non-dimensional shoulder spring defined as follows

$$K_{sh} = \frac{k_{sh}}{\dot{\Phi}^2 I_{sh}}$$

where I_{sh} is the inertia of the arm about the shoulder. For Furrer's data $I_{sh} = 0.3849 \text{ kg m}^2$.

The reason for describing arm angles in terms of symmetric and asymmetric components is clear upon examination of the matrices of Equations 4.2 - 4.6. This decomposition allows us to see that in general the linearized system decouples into two distinct subsystems; the upper 3-by-3 system that couples tilt and twist with asymmetric arm movement and the lower 2-by-2 system that couples rotation rate with symmetric arm movement. We consider these two subsystems separately in a linear stability analysis. It will turn out that the parameters which stabilize the composite

system are nearly, but not exactly, identical to those that stabilize the 3-by-3 system.

4.3 Stability Analysis

In this section, I present a linear stability analysis of the layout somersault. To start, I present the stability of the equivalent rigid body, that is the rigid body that would result if the arms were rigidly fixed to the body. As expected, if the body were rigid the layout somersault would be unstable. Then I proceed to an analysis of the three-body system. The goal is to determine the shoulder spring constants and arm angles that produce stable somersaults when the remaining body parameters are fixed. A root locus plot shows how the location of the linear system poles move as the shoulder spring constant is systematically varied. The root locus plot shows that under some conditions, all poles of the linear system are simultaneously on the imaginary axis, implying (neutral) stability. The results of the root locus are also presented in the form of stability diagrams that show under what values of shoulder spring and arm angle the passive stability can be realized.

4.3.1 Rigid Body

As a start, let us examine the characteristics of the equivalent rigid body for this system. I consider the equivalent rigid body to be the rigid body that has the same principal inertia as the whole three body system. If we consider the arms to be fixed rigidly to the body then we can solve for the equivalent rigid body inertias, and thus the inertia ratios, k_1 and k_3 , (see Section 2.3.2) as a function of the nominal arm angle, Γ_{s0} . The inertia ratios k_1 and k_3 capture the inertia of the equivalent rigid body and therefore determine its stability.

For a true rigid body rotating about its intermediate axis, the unstable mode of

motion will grow at a rate given by Equation 2.13

$$z = z_0 e^s \text{ where } s = (-k_1 k_3)^{1/2} \dot{\Phi} t$$

Since $\dot{\Phi} t$ is simply the nominal somersault angle, the change in somersault angle, Φ , required for the unstable mode to grow by a factor of N is given by Equation 2.14

$$\Phi = \dot{\Phi} t = \frac{\ln(N)}{(-k_1 k_3)^{1/2}}$$

Using the data for Furrer (Table 4.1) in the three d.o.f. model with a symmetric arm angle of $\Gamma_{s0} = 1.3$ rad. the resulting rigid body inertia ratios are $k_1 = 0.65$ and $k_3 = -0.87$. Using these numbers with $N = 10$ results in $\Phi = 3.1$ rad, or the unstable mode will grow by a factor of 10 in less than one half somersault. Figure 4-5 shows a plot of the inertia ratios of the five d.o.f. model for symmetric arm angles between 0.0 and 3.0 radians. These inertia ratios are superposed upon curves of constant Φ .

4.3.2 Multi-Body

Some useful information regarding the stability of this system is available by a simple examination of the form of the matrices in Equation 4.1. If shoulder damping, b_{sh} , is zero then $D = 0$ and Equation 4.1 describes a conservative gyric system. As discussed in Section 2.3.1, the strongest stability result one may expect from a conservative gyric system is neutral stability, i.e. the system will be a perfect oscillator. A sufficient condition for stability is for the net stiffness matrix to be positive definite, $K + K' > 0$. This is not possible since $K + K'$ is not even full rank for the five d.o.f. system. This happens because the system is unstable to perturbations in somersault rate as was the case for the rigid body system in Chapter 2. However, even the three-by-three subsystem of tilt, twist, and asymmetric arm movement does not have a positive definite stiffness matrix for the fixed body parameters used here. Therefore, if the system is to be stable it must be gyroscopically stabilized.

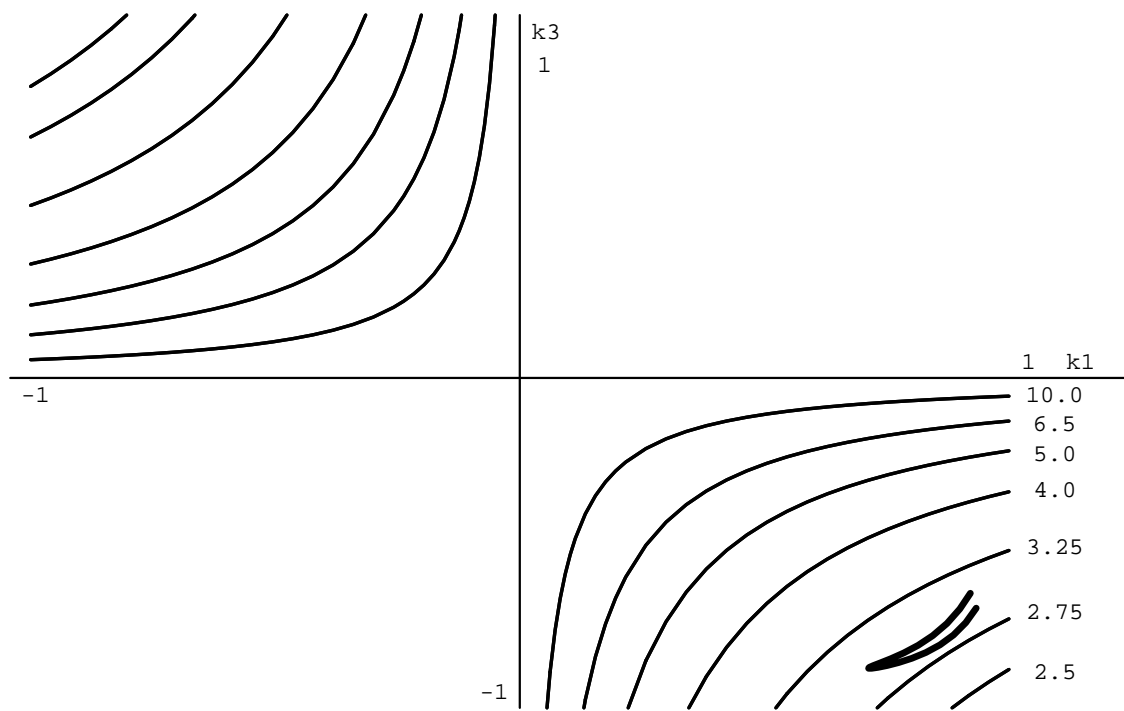


Figure 4-5: Rigid body stability diagram for Furrer's data. The dark lines show k_1 and k_3 for $0 < \Gamma_{s0} < 3.0$. The light lines are lines of constant Φ , the change in somersault angle required for the unstable rigid body mode to grow by a factor of ten. The plot shows that the human form is relatively unstable in the rigid body sense.

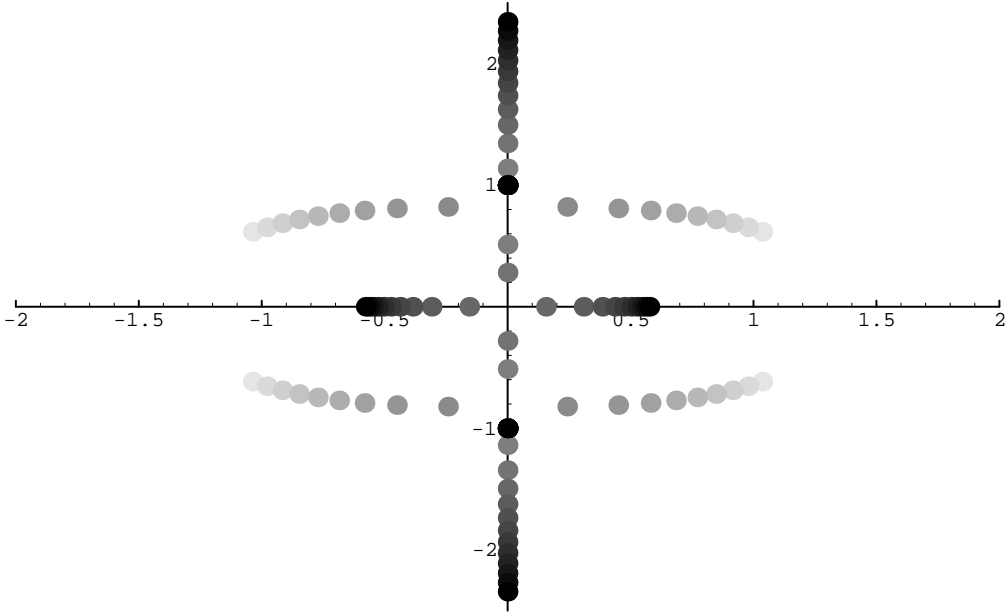


Figure 4-6: Root locus plot for the 3-by-3 subsystem of tilt, twist, and asymmetric arm movement. $b_{sh}/\dot{\Phi} = 0.0$ and the nominal symmetric arm angle, Γ_{s0} , is 1.3 rad. Light dots indicate root locations for $K_{sh} \approx -2.0$. Dots get progressively darker as K_{sh} increases to 4.0.

Root Locus

In this section I present plots of the roots of the characteristic equation of 4.9 as the shoulder spring constant and nominal symmetric arm angle are systematically varied. Figure 4-6 is a root locus for the 3-by-3 subsystem of tilt, twist, and asymmetric arm angle. This plot shows how the 3-by-3 system roots move as the shoulder spring stiffness is gradually increased when $\Gamma_{s0} = 1.3$ rad. Note the symmetry about the imaginary axis as predicted for a conservative-gyric system.

When the nondimensional shoulder spring, K_{sh} , is set to -2.0 the four symmetrically located roots have both real and imaginary components. As the shoulder stiffness is increased the symmetric right and left half plane roots converge on the imaginary axis where they split. One set moves away from the origin along the imaginary axis for as long as shoulder stiffness increases. The other pair converge at the origin where they again split one traveling along the positive real axis the other along the negative real axis. At very high shoulder stiffness these two real roots approach

the real (stable and unstable) rigid body roots. At high shoulder stiffness the high frequency imaginary pair correspond to an arm-body oscillation.

There are two poles of this system at $\pm i$ that do not move with changing shoulder spring constant. These are the roots of the *stroboscopic* mode of rotation. This mode is a rigid body mode of motion that does not include arm movement. Examination of the eigenvectors associated with this mode reveals that the attitude and velocity vectors are parallel. This indicates that this mode involves pure spin about the middle principal axis, the equilibrium condition, when that axis is perturbed slightly from the original orientation. This rigid body mode will exist for all values of the parameters.

For some values of shoulder spring all of the roots of this system are located on the imaginary axis. These marginally stable conditions suggest that for these values of the parameters the physical system may be stable. Note that even though equal size steps in K_{sh} were used to numerically evaluate the root locus, the loci do not move in even steps. In particular the loci ‘jump’ to the imaginary axis from the right and left half planes. This indicates that the edge of the stable region in parameter space is steep.

Figure 4-7 shows a root locus for the same system with the addition of a viscous damper at the shoulder joint. Note the loss of symmetry about the imaginary axis and the lack of a set of spring values that stabilize the system. This result agrees with the spirit of Hughes proof that damping tends to destabilize gyroically stabilized systems. However, this model does not exactly fit the requirements of his proof since the damping matrix is not positive definite. Finally, Figure 4-8 shows how the root loci plots change as Γ_{s0} is varied between 0.0 and 2.8 radians.

The root loci of this section suggest that neutral stability of the layout somersault is possible for certain combinations of nominal arm angle and shoulder spring constant. It appears that asymptotic stability is unlikely as shoulder damping tends to destabilize the system. In the next section we will examine more precisely the dependence of stability on arm angle and shoulder spring constant.

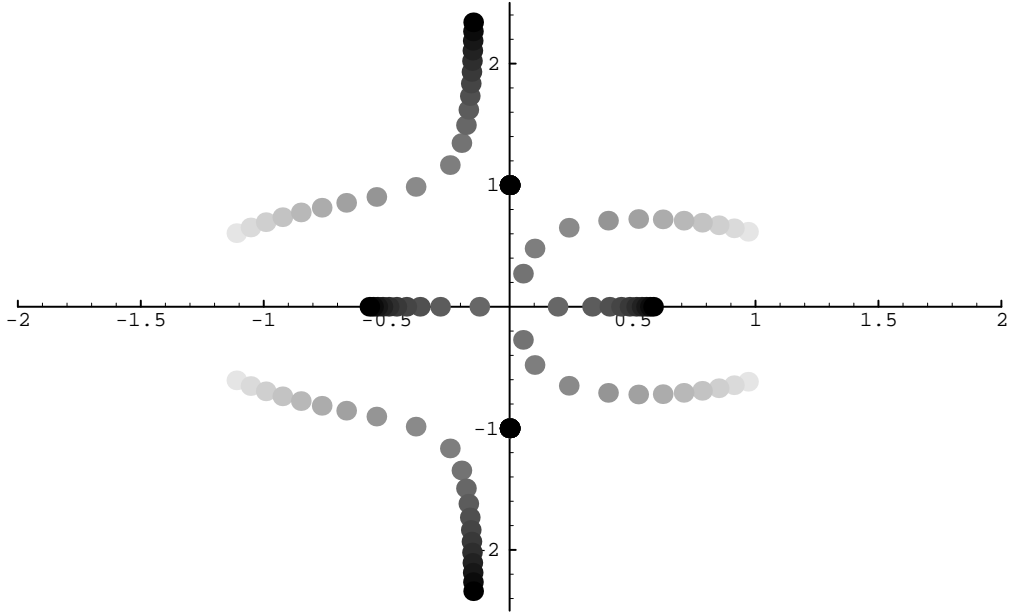


Figure 4-7: Root locus plot for the 3-by-3 subsystem of tilt, twist, and asymmetric arm movement. $b_{sh}/\dot{\Phi} = 0.1$ and the nominal symmetric arm angle, Γ_{s0} , is 1.3 rad. Light dots indicate root locations for $K_{sh} \approx -2.0$. Dots get progressively darker as K_{sh} increases to 4.0.

Stability Diagrams

In this section, I present plots that show precisely how stability depends on the shoulder spring constant and nominal arm angle.

Figure 4-9 shows the results of a search in the Γ_{s0} - K_{sh} parameter space for conditions that stabilize the five d.o.f. linearized system. This collection of points suggests a region in the parameter space that stabilizes the system. The stable points in Figure 4-9 are an intersection of the stable points of the two decoupled linear systems that comprise the five d.o.f. system. Figures 4-10 and 4-11, are the corresponding plots of stable points for the 3-by-3 subsystem of tilt-twist-asymmetric arm and the 2-by-2 subsystem of somersault-symmetric arm. Comparison of Figures 4-9 and 4-10 shows that stability of the five d.o.f. system is well represented by the stability of the simpler 3-by-3 system, i.e. few conditions that stabilize the 3-by-3 system fail to stabilize the 5-by-5 system.

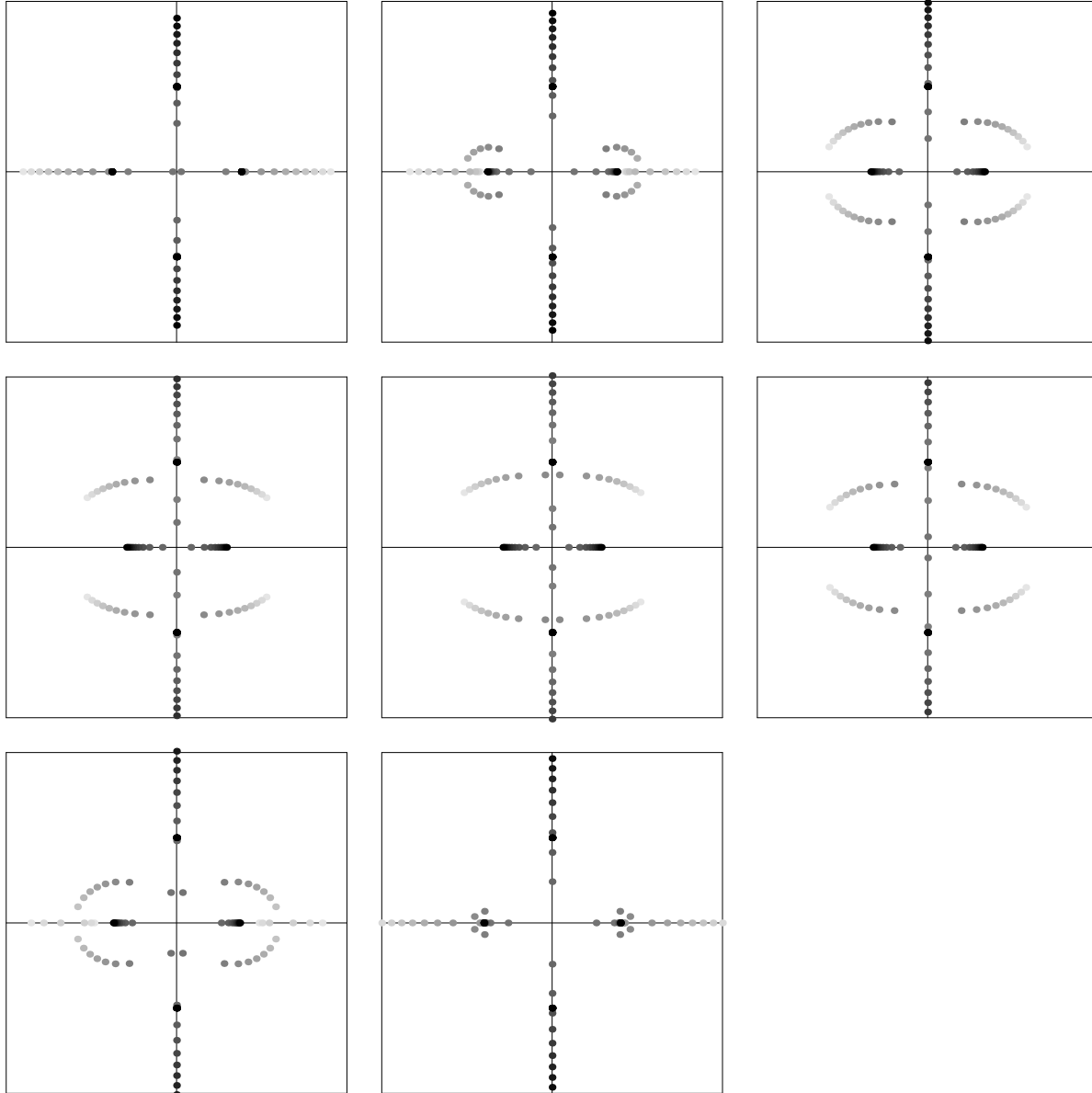


Figure 4-8: Root loci for the 3-by-3 subsystem of tilt, twist, and asymmetric arm movement as the nominal symmetric arm angle, Γ_{s0} , is varied between 0.0 (top left) and 2.8 rad (bottom center) , $b_{sh} = 0$, $-2.0 < K_{sh} < 4.0$.

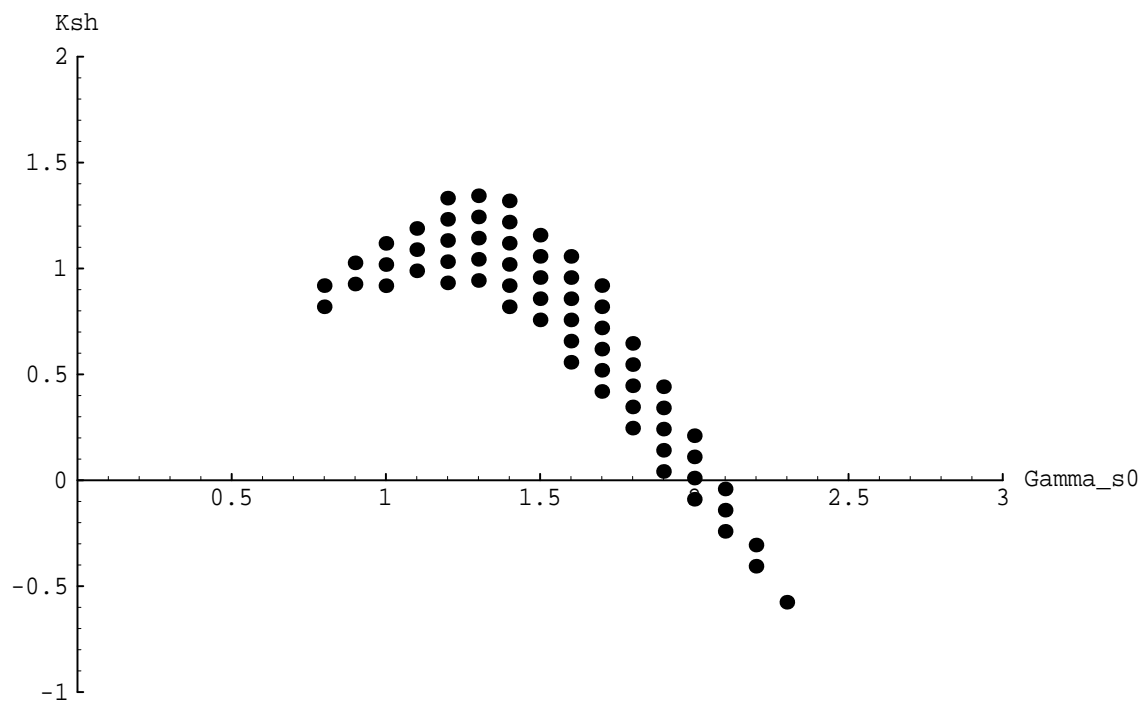


Figure 4-9: Each darkened point in this plot corresponds to a specific choice of K_{sh} and the nominal symmetric arm angle (Γ_{s0}) that stabilize the full five d.o.f. linear system, $b_{sh}/\dot{\Phi} = 0$.

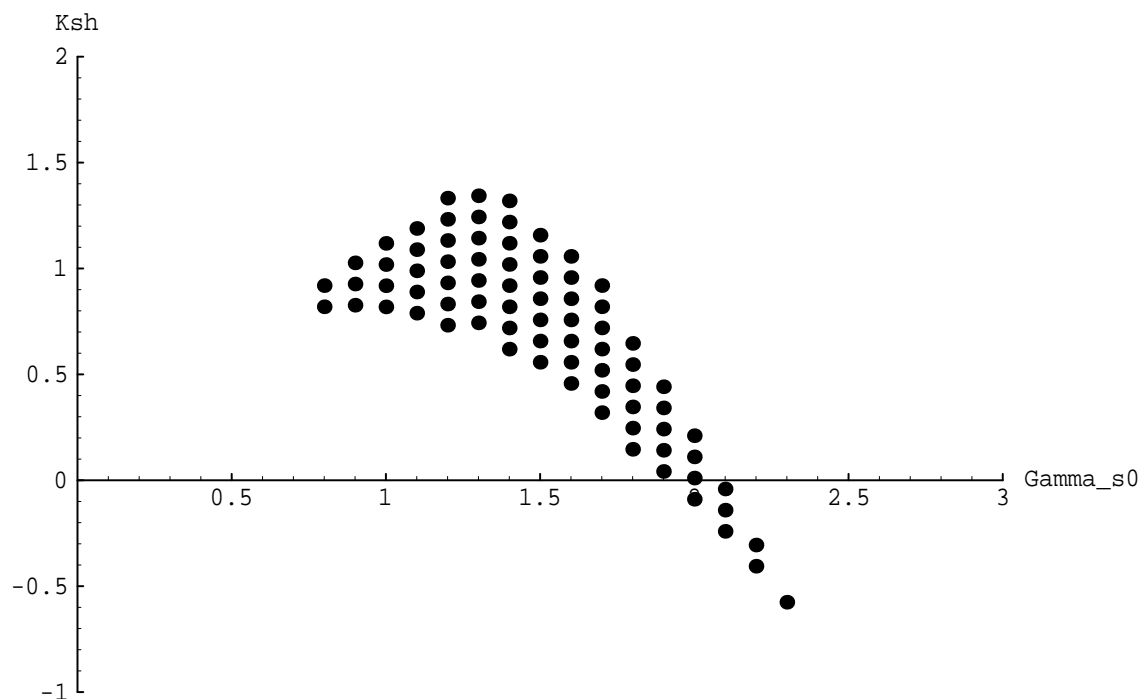


Figure 4-10: Each darkened point in this plot corresponds to a specific choice of K_{sh} and the nominal symmetric arm angle (Γ_{s0}) that stabilize the three d.o.f. linear system of tilt, twist, and asymmetric arm movement, $b_{sh}/\dot{\Phi} = 0$.

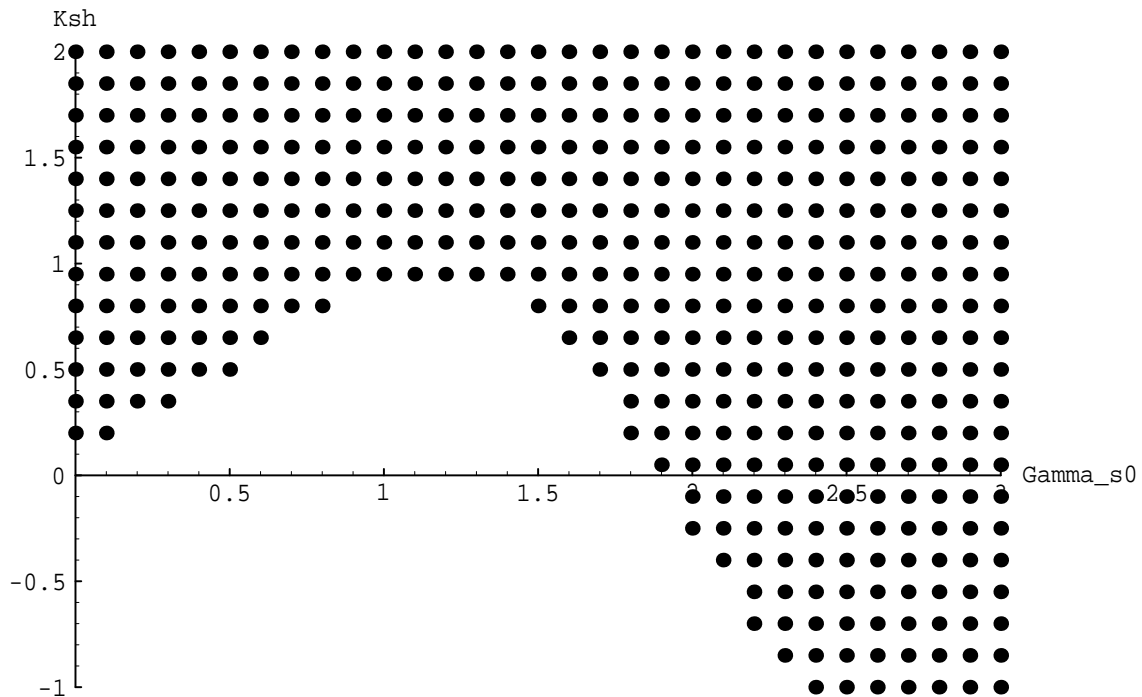


Figure 4-11: Each darkened point in this plot corresponds to a specific choice of K_{sh} and the nominal symmetric arm angle (Γ_{s0}) that stabilize the two d.o.f. linear system of somersault and symmetric arm movement, $b_{sh}/\dot{\Phi} = 0$. Higher values of K_{sh} than are shown on this plot are suspected to also stabilize the system.

4.3.3 Non-Linear Stability via Dynamic Simulation

The linear stability analysis (Figure 4-9) predicts that passive layout somersault stability can be achieved for nominal symmetric arm angles between 0.8 and 2.0 radians (assuming only positive shoulder spring constants are allowed.) We would normally expect the linear analysis results to be valid only in some region of the linearizing condition. Stability to perturbations away from the linearizing condition will depend upon the size of the perturbations. Since in the case of passive layout somersaults the linear analysis can only predict neutral stability we can not conclude that the non-linear system is stable even for arbitrarily small perturbations. While non-linear dynamic simulation can not prove non-linear stability it can provide a fast and easy check on whether or not the non-linear system is likely to be stable. In this section, I use non-linear dynamic simulation as a check on the linear stability results.

Figure 4-12 shows results summarizing a series of dynamic simulations of the five d.o.f. human model. Each three dimensional plot shows how many stable somersaults the five d.o.f. model exhibited in simulation as a function of the nominal symmetric shoulder angle, Γ_{s0} , and the shoulder spring, K_{sh} . Each point in the grid represents a separate simulation. A somersault was considered stable if it did not exhibit a twist angle of at least $\pm\pi/2\text{ rad}$. There was little ambiguity between stable and unstable layout somersaults. Either the twist angle remained small while the model somersaulted or the twist angle would grow significantly beyond one-quarter twist making it easy to distinguish stable and unstable motion. The plots show that the region in parameter space that the linear analysis predicted to be stable is also the region that produces the most stable layout somersaults in non-linear simulation.

The height of the plots in Figure 4-12 has been limited to eight somersaults. Several simulations exceeded this limit. For selected cases, the non-linear dynamic simulations indicated that the maneuver may remain stable indefinitely as long as energy is conserved. Two simulations starting from an initial tilt angle of 0.01 radians and zero twist angle were stopped after running for 2000 simulated seconds. During

these simulations the performer produced over 2750 stable layout somersaults. The shoulder springs and nominal arm angles that produced these long running maneuvers were $\{K_{sh}, \Gamma_{s0}\} = \{1.2, 1.4\}, \{1.0, 1.6\}$. Other conditions may also have produced stable, long running maneuvers. I did not perform an exhaustive search.

4.4 How Passive Layout Stability Works

In the last section we showed that under certain conditions a five d.o.f. dynamic model of a human can exhibit passively stable layout somersaults. We used numerical searches to find combinations of shoulder springs and nominal arm angles that stabilized the layout somersault. This search process does not provide much insight into how or why passive stabilization works. In this section, I describe what I consider to be the fundamental dynamic processes that make passive layout stability possible. First, I look at the differences in state trajectories between the passively stable case and the unstable rigid body case. The differences in trajectories between the two cases make evident that arm motion can change the orientation of the principal axes in a way that stabilizes the layout somersault. We then look more closely at how this arm movement arises. To do this I focus on the simplest possible model that captures passive layout stability. I define the important non-dimensional parameters that govern this model and show how stability depends upon these parameters. Then I provide an intuitive explanation of the passive dynamic process that stabilizes the layout somersault.

4.4.1 Stabilization Via Principal Axes Reorientation

Batterman [Batterman 68] and later Frohlich [Frohlich 79] showed how an athlete can control the orientation of his principal axes during a rotating maneuver using arm movement. This control allows an athlete to initiate twist in a somersault without using any external forces or torques. Using symmetry, Yeadon [Yeadon 84] has argued

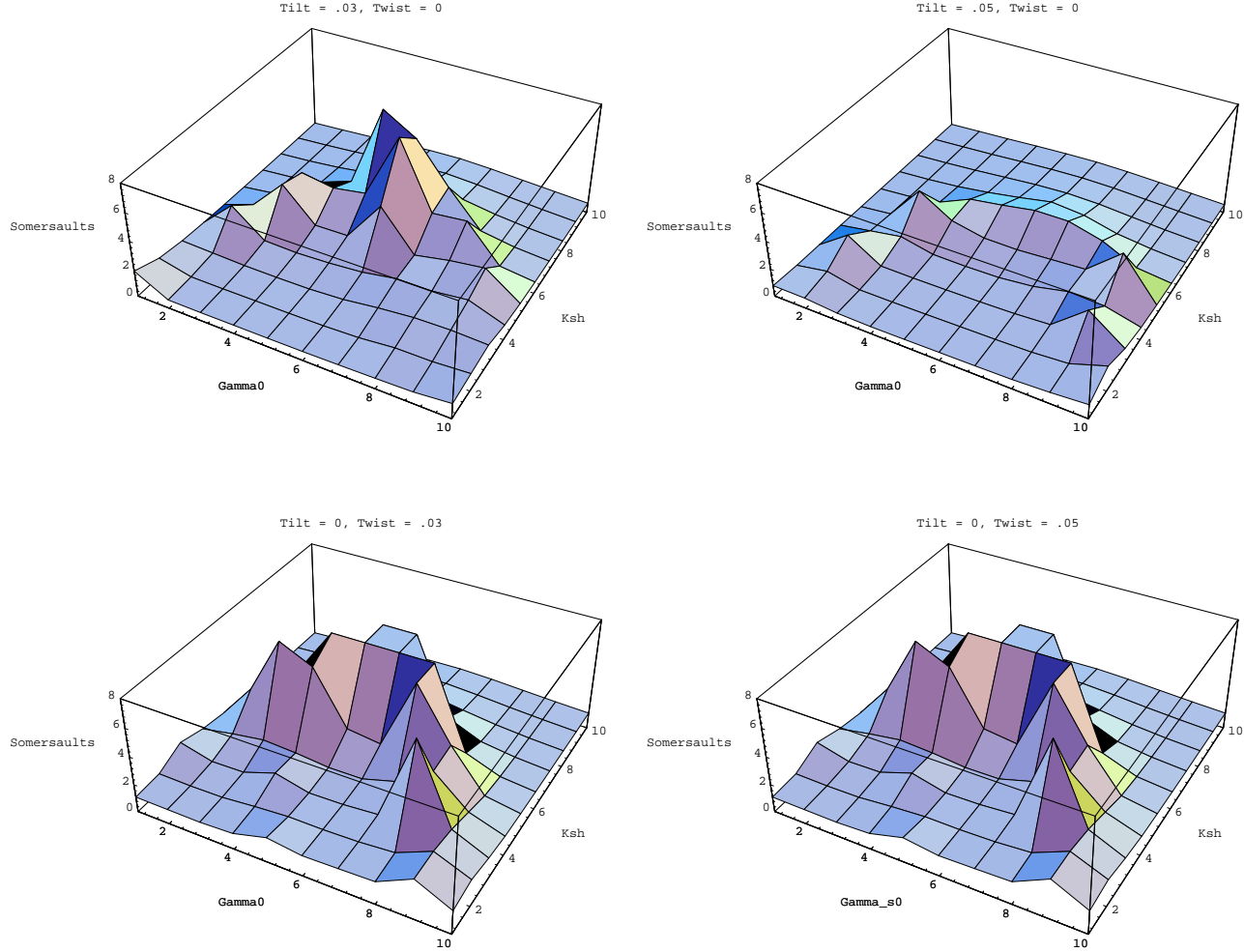


Figure 4-12: These plots show that the regions (in Γ_{s0} - K_{sh} space) of stable somersaulting motion of a non-linear dynamic simulation are similar to those regions predicted to be stable by the linear analysis (Figure 4-9). The height of each grid point indicates the number of stable layout somersaults performed during a separate dynamic simulation of the five d.o.f. model. The axes of each grid indicate the symmetric arm angle, $0.4 \text{ rad} \leq \Gamma_{s0} \leq 2.2 \text{ rad}$, and the non-dimensional shoulder spring, $0.0 \leq K_{sh} \leq 1.8$, used for each simulation. The different plots show that the number of stable somersaults performed is sensitive to the initial tilt and twist angles.

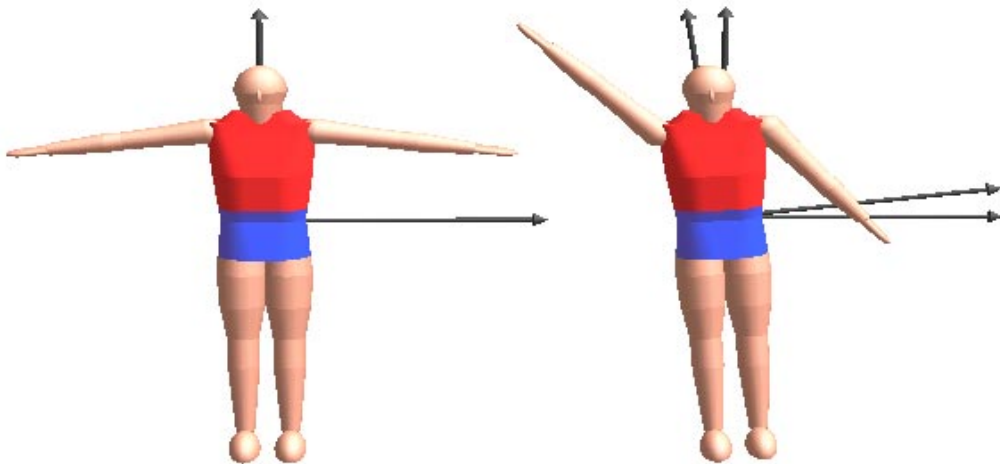


Figure 4-13: The orientation of the principal axes of inertia can be controlled with arm rotation. The tilt of the principal axes of the figure on the right is a result of body axis tilt due to airborne reorientation of the body plus principal axes tilt due to body asymmetry.

that an athlete has an equal opportunity to remove twist from a twisting somersault using arm motion. In this section I will show how arm movement is used to control the orientation of the principal axes. Then I will show how principal axis orientation can be used to influence rotational maneuvers.

The orientation of a human's principal axes relative to a set of body fixed axes depends upon the configuration of the arms and legs of the performer. Figure 4-13 shows a human figure in two different body configurations. The tilt of the body on the right is the result of the airborne reorientation of the arms from the symmetric configuration of the figure on the left to the asymmetric configuration of the figure on the right. Also shown are inertially fixed axes and principal axes of the figures. The principal axes of the figure on the left are aligned with the inertial axes. Notice

that the principal axes of the figure on the right are tilted with respect to the inertial axes and also inclined relative to the body axes. This inclination of the principal axes from the body fixed axes is due to asymmetry of the body and it has the effect of changing the ‘gain’ on principal axis reorientation due to arm movement. To see how principal axis orientation can be used to control twist we will examine a plot of rigid-body rotational trajectories.

Figure 4-14 shows the twist angles plotted as a function of tilt angle for several rigid body trajectories of the human model while in the layout configuration. This plot is essentially a close up view of the $\{c_1, c_3\}$ axes of the map shown in Figure 4-3. The different trajectories correspond to different energy levels of rigid body rotational motion. While time is not explicitly shown on the plot, the data points are all 0.01 sec. apart. Thus dot spacing shows that twist rate increases with tilt magnitude. Arrows have been drawn on this plot to show the direction of motion. The instability of rotation about the middle principal axis is evident from the converging and diverging trajectories near the origin. These trajectories show that if body attitude deviates slightly from the origin then it will depart the origin in a direction that depends upon which ‘side’ of the equilibrium it is located.

Tilting the principal axes using arm movement has the effect of moving the body from one energy trajectory to another. While an instantaneous change in tilt can not change the twist angle, it can change the twist rate by putting the body on a trajectory with a different twist rate. Stabilization of the layout somersault can be viewed as a process of selectively adding or subtracting twist over time using arm movement so that the trajectory remains in the vicinity of the origin of Figure 4-14. Figure 4-15 shows a trajectory of a non-linear dynamic simulation of the passive, five d.o.f. model of the human. This trajectory of tilt and twist angles is superposed upon the rigid body trajectories of the same model. The passively stable trajectory circles the origin in a counter-clockwise fashion periodically increasing then decreasing the twist and tilt angles. The counterclockwise rotation of the trajectory means that

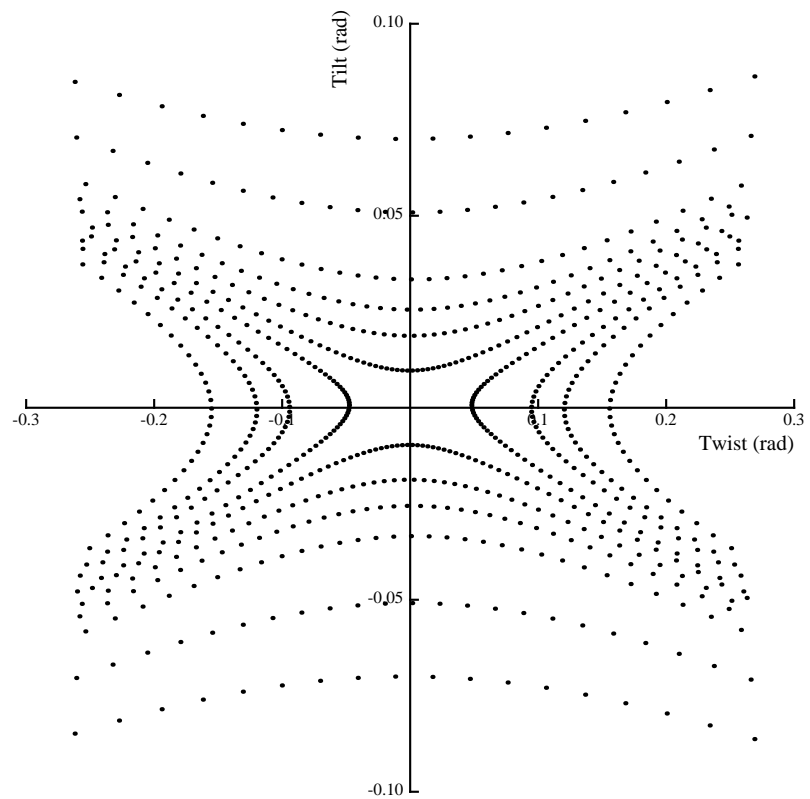


Figure 4-14: Tilt angles plotted as a function of twist angle for several different energy levels of rigid body rotation of a human. Arrows indicate the direction of motion with increasing time. Dots are all 0.01 seconds apart. The arms of the rigid human model were abducted to a symmetric angle of 1.3 radians.

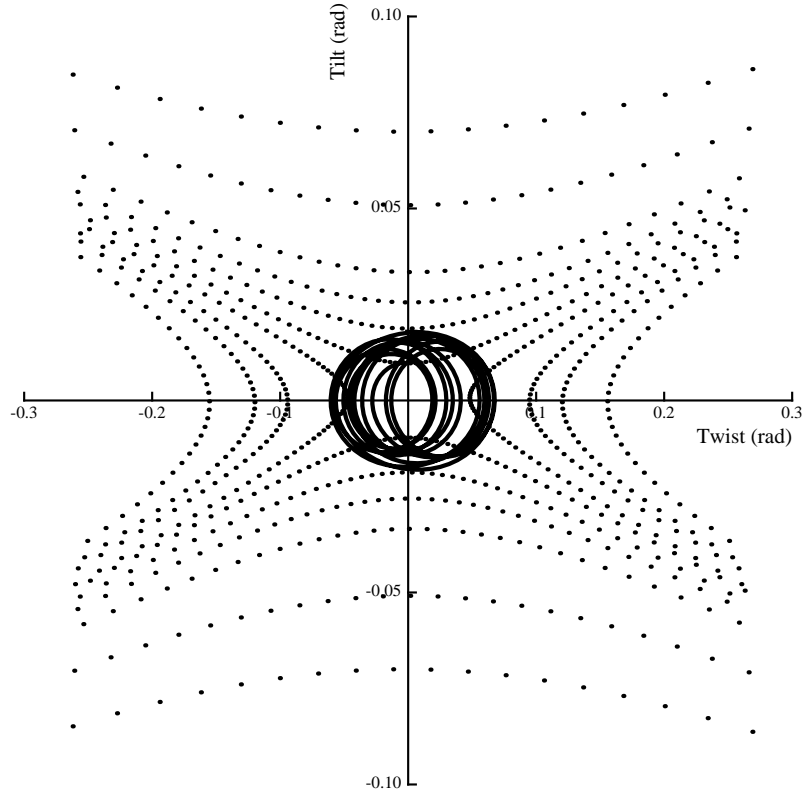


Figure 4-15: Tilt angles plotted as a function of twist angle for a non-linear dynamic simulation of the five d.o.f. passive model of the human. The simulated trajectory is superposed upon rigid body trajectories of the same model. This simulation was initialized with a tilt angle of 0.01 rad, zero twist angle and symmetric arm angle of 1.3 rad.

while the body twists ‘with the flow’ in the upper and lower halves of the plane it has to move ‘upstream’ with regard to the tilt angle. How is this accomplished?

The system uses arm movement to accomplish this ‘upstream’ tilting action. In Figure 4-15 we see that by starting with an initial condition of positive tilt angle, zero twist angle, and arms symmetric the body begins to twist in the negative direction. From this initial condition the tilt of the principal axes apparently decreases despite the rigid body tendency to increase the tilt angle. This decrease in principal axis tilt is a result of the arms moving asymmetrically (left arm up, right arm down) in response to the negative twist rate. The arm tilting (rotation about the ‘1’ axis) arises from the combination of somersaulting (rotation about the ‘2’ axis) and twisting (rotation

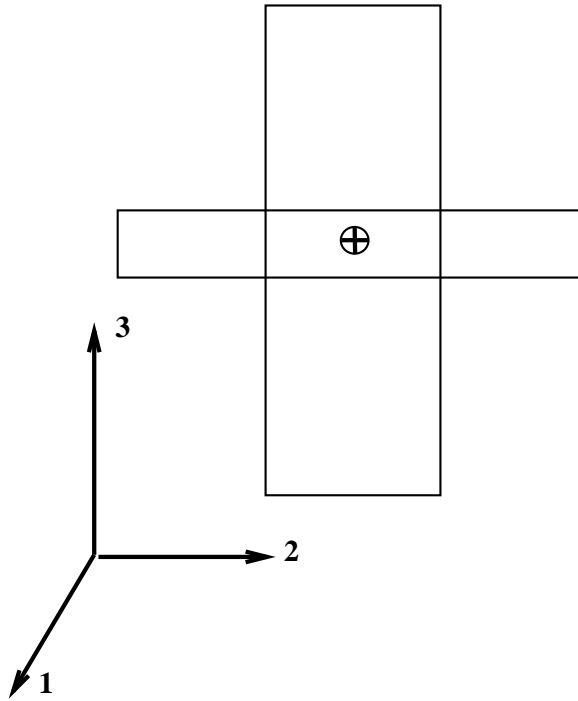


Figure 4-16: A simple model that captures the essential dynamics for passive layout stability. The single arm is allowed to pivot about its center. The arm and body centers of mass are coincident.

about the ‘3’ axis.) This gyroscopic affect will tend to move the arm in a direction that reduces the tilt angle of the principal axes as long as the body is twisting.

This oscillation is a passive behavior that emerges from the mechanical properties of the system interacting with the environmental forces due to rotation. The gyroscopic forces which provide the inherent correction of this model depend upon the shape and position of the arm. To see how this passive behavior emerges we will look at a simplified model of the dynamics.

4.4.2 The Simplest Model

The simplest model that I can think of that captures the essential dynamics of passive layout stability is shown in Figure 4-16. This model has the feature that only asymmetric arm motion is allowed. Recall from Section 4.3.2 that symmetric arm motion could be ignored when looking for stability of the five d.o.f. model. Also, since the

center of mass of the arm is coincident with the center of mass of the body, the equations of motion will be significantly simplified as compared to the more complex human model.

The linear equations of motion for this four d.o.f. model will show that the somersault degree of freedom again decouples from the remaining dynamics. Ignoring this degree of freedom and assuming no damping at the pin joint of the arm results in the following three d.o.f. linear model.

$$M \ddot{x} + \dot{\Phi} G \dot{x} + \dot{\Phi}^2 (K + K') x = 0 \quad (4.10)$$

$$M = \begin{bmatrix} m_{11} & 0 & m_{13} \\ 0 & m_{22} & 0 \\ m_{13} & 0 & m_{33} \end{bmatrix}$$

$$G = \begin{bmatrix} 0 & g_{12} & 0 \\ -g_{12} & 0 & g_{23} \\ 0 & -g_{23} & 0 \end{bmatrix}$$

$$K = \begin{bmatrix} k_{11} & 0 & k_{13} \\ 0 & k_{22} & 0 \\ k_{13} & 0 & k_{33} \end{bmatrix}$$

$$K' = \begin{bmatrix} 0 & 0 & 0 \\ 0 & 0 & 0 \\ 0 & 0 & k_{sh}/\dot{\Phi}^2 \end{bmatrix}$$

where the state vector, x , is comprised of (in order) tilt, twist, and arm angle and k_{sh} is the spring between the arm and the body. The model parameters are given in Table 4.2.

This dynamic model still requires us to define the six inertia parameters of the body before we consider stability. Recall from Chapter 2 that the rotational dynamics

Table 4.2
Simplest Model Parameters

| Parameter | Definition |
|-----------|---|
| m_{11} | $Ib_1 + Il_1$ |
| m_{13} | Il_1 |
| m_{22} | $Ib_3 + Il_3$ |
| m_{33} | Il_1 |
| g_{12} | $(Ib_1 + Il_1) - (Ib_2 + Il_2) + (Ib_3 + Il_3)$ |
| g_{23} | $-Il_1 + Il_2 - Il_3$ |
| k_{11} | $(Ib_2 + Il_2) - (Ib_3 + Il_3)$ |
| k_{13} | $Il_2 - Il_3$ |
| k_{22} | $-(Ib_1 + Il_1) + (Ib_2 + Il_2)$ |
| k_{33} | $Il_2 - Il_3$ |

of a rigid body depend only upon two non-dimensional inertia parameters. Following the spirit of this result, in the next section we reduce the model to non-dimensional form in order further simplify the analysis.

Non-Dimensional Linear Equations of Motion

I now present a non-dimensional version of the linear dynamic equations of motion of the model shown in Figure 4-16 for the case of steady somersaulting about the ‘2’ axis. The purpose of this step is to discover the important non-dimensional parameters of this model. The states are made non-dimensional through scaling by the nominal somersault rate. Casting the equations in terms of non-dimensional parameters is accomplished by dividing each equation by the corresponding inertia term on the diagonal of the mass matrix. A few more simple algebraic manipulations will bring the system of equations into the following form. (In this form these equations do not reflect the symmetry that we expect of a conservative gyric system. However, they can easily be made to fit this canonical form.)

$$\dot{\Phi}^2 (M\ddot{z} + G\dot{z} + Kz) = 0 \quad (4.11)$$

$$M = \begin{bmatrix} 1 & 0 & I_{rel} \\ 0 & 1 & 0 \\ 1 & 0 & 1 \end{bmatrix}$$

$$G = \begin{bmatrix} 0 & 1 - k_1 & 0 \\ -(1 - k_3) & 0 & \frac{-(1 - k_1)(1 - k_3)I_{rel}}{1 - k_1} \\ 0 & 1 - kl_1 & 0 \end{bmatrix}$$

$$K = \begin{bmatrix} k_1 & 0 & kl_1 I_{rel} \\ 0 & k_3 & 0 \\ kl_1 & 0 & kl_1 + K_{sh} \end{bmatrix}$$

The five independent non-dimensional parameters are defined as follows:

$$k_1 = \frac{(Ib_2 + Il_2) - (Ib_3 + Il_3)}{Ib_1 + Il_1}$$

$$k_3 = \frac{(Ib_2 + Il_2) - (Ib_1 + Il_1)}{Ib_3 + Il_3}$$

$$I_{rel} = \frac{Il_1}{Ib_1 + Il_1}$$

$$kl_1 = \frac{Il_2 - Il_3}{Il_1}$$

$$K_{sh} = \frac{k_{sh}}{Il_1 \dot{\Phi}^2}$$

Equation 4.11 depends upon only five non-dimensional parameters. The parameters k_1 and k_3 are the principal inertia ratios for an equivalent rigid body system. They describe the inertia properties of the system that would result if the arm were fixed in place. Notice that if the arm degree of freedom were eliminated from Equation 4.11 then the remaining equations are identical to the rigid body equations (2.11). I_{rel} defines how big the inertia of the arm is relative to the inertia of the rigid body. It is important in determining how much the body moves in response to arm movement. The next term, kl_1 is an inertia ratio analogous to k_1 involving only arm parameters.

Table 4.3
Furrer's Non-dimensional Parameters

| Parameter | Value |
|-----------|-------|
| k_1 | 0.65 |
| k_3 | -0.87 |
| I_{rel} | 0.06 |
| kl_1 | -0.99 |

It is important in determining the tendency of the arm to tilt in response to twist rate.

We use data from the human model (Table 4.1) to derive sample values for these dimensionless parameters. These parameter values are shown in Table 4.3. These parameters are computed assuming the arms are held straight out to the side of the body. To compute the arm inertia of the model in Figure 4-16 I let $Il_1 = Il_3 = 2.0 \times 0.3849 \text{ kg m}^2$, the sum of the arm inertias about their shoulder axes in the given configuration.

With these numbers in mind, we can inspect the individual terms of the matrices of Equation 4.11 to help us develop an understanding of the relevant dynamic forces. Without arm movement the system reduces to the rigid body equations of motion which are unstable for the set of parameters in Table 4.3. For this reason I will focus on the arm related terms only. First consider the 3-2 term of G . This term is nearly equal to 2.0. If the twist rate of the model is negative then this term will contribute to a positive acceleration of the arm angle which is precisely the corrective tendency that we observed in the plot of Figure 4-15. Additional arm accelerations come from the centrifugal forces associated with somersault rotation. These forces are represented by the 3-1 and 3-3 terms in the stiffness matrix, K . If $K_{sh} = 0$ then the 3-3 term of the stiffness matrix is negative. This reflects the fact that if the arm is deviated from its equilibrium position then it will experience centrifugal forces from somersault rotation that tend to drive the arm further away from zero. This

is because the centrifugal forces on either side of the arm are opposite one another due to asymmetry and the forces increase with deflection of the arm. Without a shoulder spring this term could overwhelm the helpful gyroscopic accelerations from the 3 - 2 term in G to destabilize the system. However, the shoulder spring offsets this destabilizing force. In fact, a rule of thumb for choosing the shoulder spring constant to stabilize the passive system is to choose the spring that *exactly cancels* the destabilizing term due to centrifugal forces.

Performing a root locus search for stabilizing spring constants of this simple 3 d.o.f. system results in the following range of stabilizing shoulder springs:

$$0.98 \leq K_{sh} \leq 1.08$$

which approximately cancels $kl_1 = -1$.

This rule for picking stabilizing shoulder springs generalizes to the more complicated model of the human. The most important difference in the human model is that the nominal symmetric angle of the arms can range from 0.0 radians (hands next to legs) to π radians (hands overhead). The non-dimensional shoulder spring constants that stabilize the human model are plotted as a function of nominal symmetric arm angle in Figure 4-17 (repeated from Figure 4-10). Also shown in this plot is the value of K_{sh} that would exactly cancel the spring term due to centrifugal forces on the arm. Again, the region of stabilizing spring constants seems to be defined by the negative of this centrifugal force term. Finally, it is interesting to note that for a nominal symmetric arm angle of $\pi/2$ the non-dimensional stabilizing shoulder spring constant is approximately $K_{sh} = 1.0$.

Stability Diagrams for the Simplest Model

The stability analyses performed thus far have all assumed that we have known values of the body inertia parameters. The small number of non-dimensional parameters of Equation 4.11 make it possible to study how linear stability depends upon these

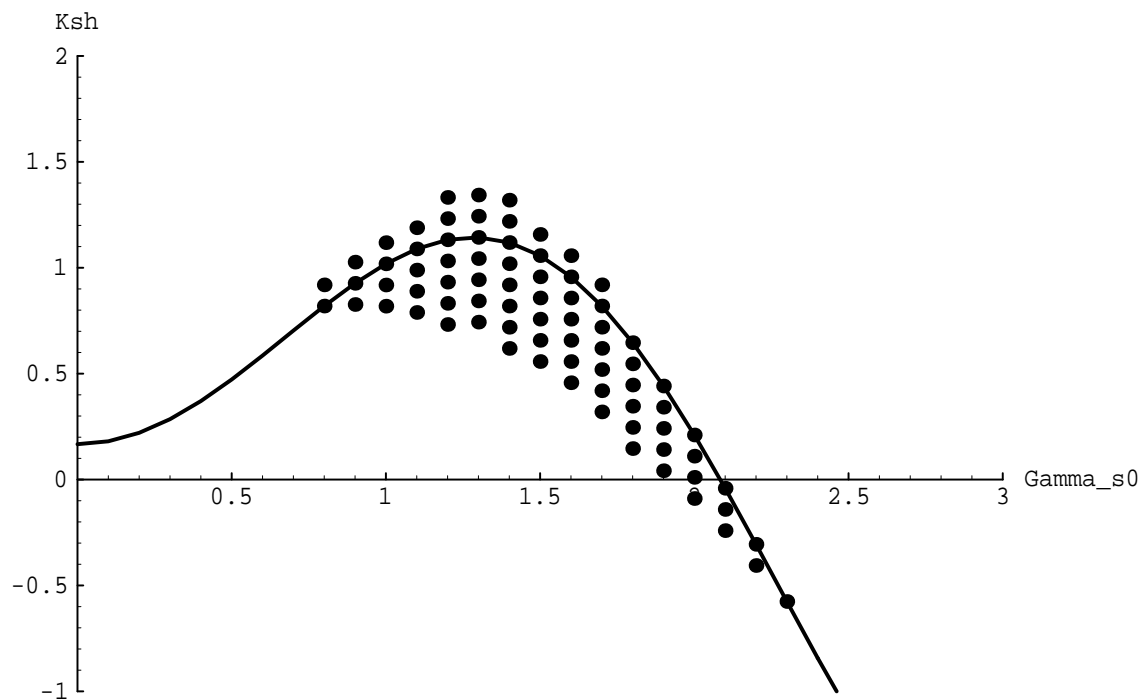


Figure 4-17: Plot of the stabilizing K_{sh} for a the 3-by-3 subsystem of the human model. The solid curve shows the value of K_{sh} that will exactly cancel the spring term due to centrifugal forces on the arm.

inertia parameters as well. In this section I present two stability diagrams that show how linear stability depends upon the parameters k_1 , k_3 , I_{rel} , and K_{sh} . The stability diagrams consist of a sequence of plots of the $\{k_1, k_3\}$ parameter space. The darkened regions of these plots represent values of k_1 and k_3 that are stable for the specified values of I_{rel} and K_{sh} .

Figure 4-18 shows that the value of K_{sh} that stabilizes the largest region of the unstable fourth quadrant of the $\{k_1, k_3\}$ parameter space is $K_{sh} \approx 1.1$. Figure 4-19 shows that larger the value of I_{rel} the easier it is to stabilize the bottom two quadrants of the $\{k_1, k_3\}$ parameter space. Large I_{rel} corresponds to relatively larger arms.

The parameter kl_1 is a shape parameter for the arm that describes the tendency of the arm to tilt in response to twisting motion. Figures 4-9, 4-10, and 4-11 indicate that the effectiveness of the arm to stabilize the layout somersault decreases as the arms are moved away from $\Gamma_{s0} = \pi/2$ (hands held straight out to the side.) I believe this change in effectiveness is due the change in the parameter kl_1 . To check this, I allowed the shape of the arm in Figure 4-16 to reflect the symmetric arm angle Γ_{s0} . Then I searched for the K_{sh} that would stabilize the simple three d.o.f. model with fixed body parameters representative of those for a human. The stable Γ_{s0} - K_{sh} configurations are shown in Figure 4-20. The shape of this plot is suggestive of the shape in the stability diagrams for the five d.o.f. model. An important difference between the diagrams for the simple three d.o.f. model and the five d.o.f. model is that the center of mass of the arm for the three d.o.f. model is coincident with the pin joint. I think this may lead to the extra stable conditions in Figure 4-20.

4.5 Summary

In this chapter I presented results from a study of the stability of several simple models of the layout somersault. A rigid body analysis of the layout somersault predicts that the maneuver is inherently unstable. A linear analysis of a passive three-

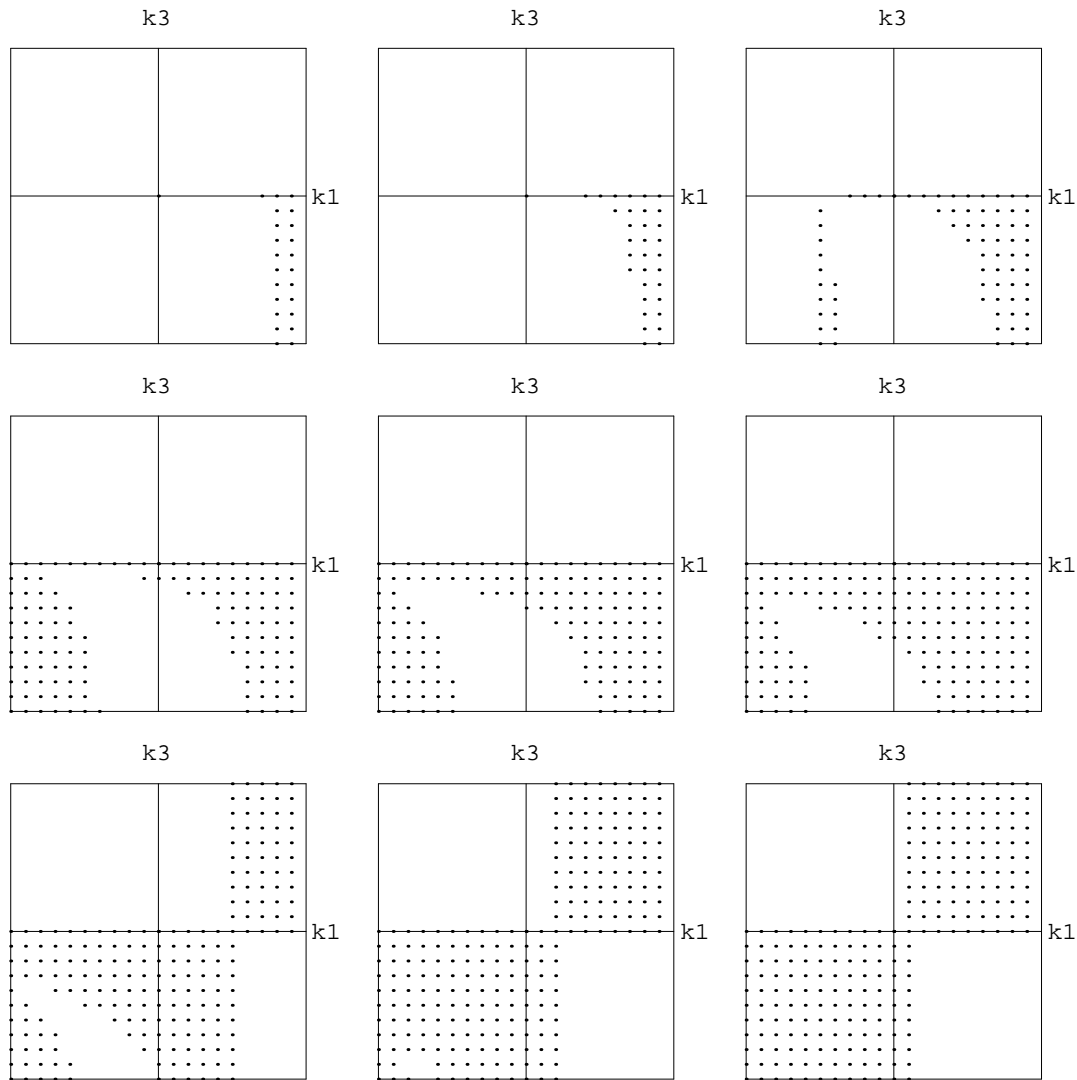


Figure 4-18: These plots show that $1.0 \leq K_{sh} \leq 1.1$ produces the largest region of stable configurations for rotation about the middle principal axis for the “simplest model”. Each dark point represents a stable configuration in k_1 - k_3 space for rotation about a principal axis. $k_1 = -1, I_{rel} = 0.1$ Each plot is for a different value of K_{sh} . $K_{sh} = 0.0, 0.5, 0.8, 0.9, 1.0, 1.1, 1.2, 1.5$ and 2.0 for plots positioned from left to right and down the page.

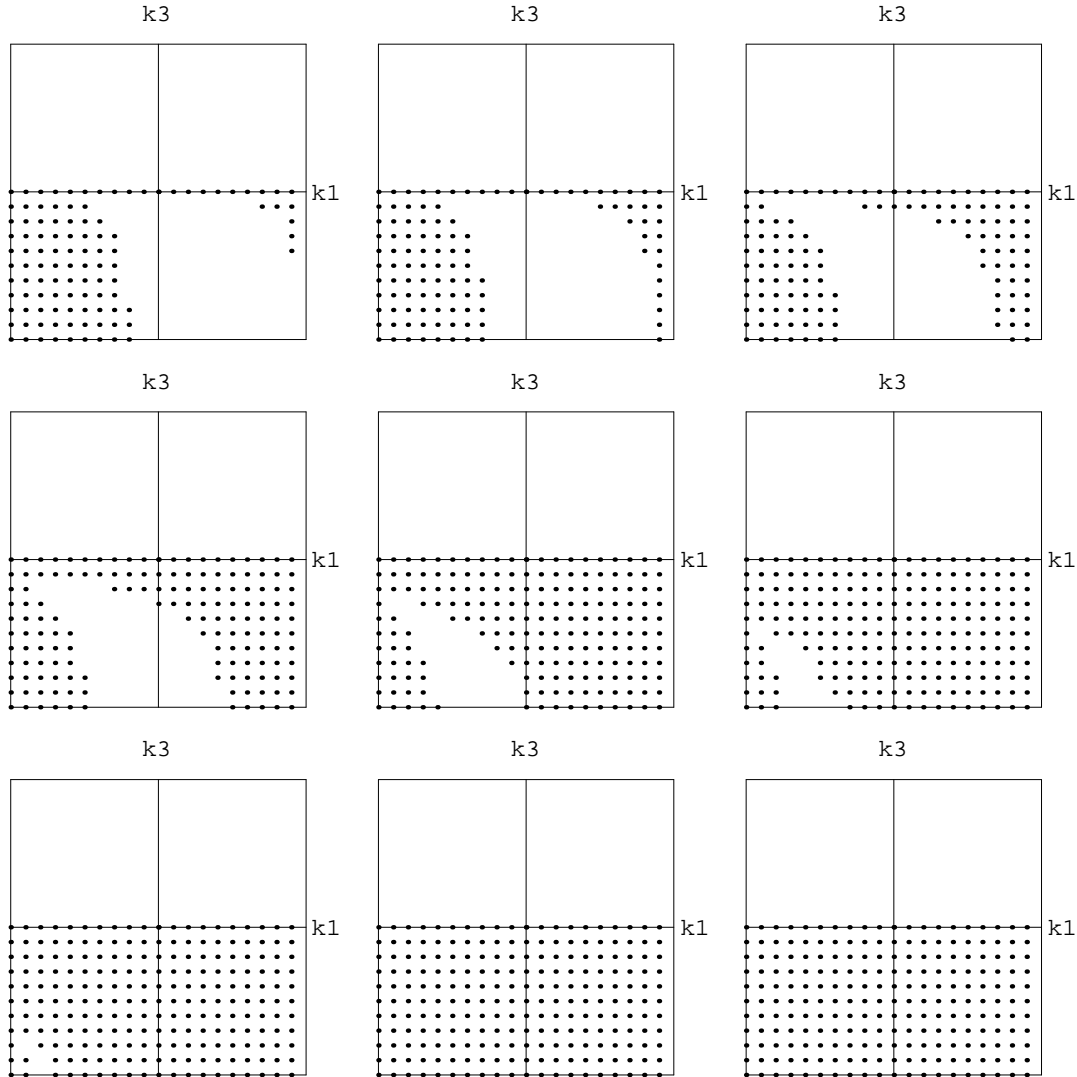


Figure 4-19: These plots show that stabilization gets easier with larger arms. Each dark point represents a stable configuration in k_1 - k_3 space for rotation about a principal axis. $k_1 = -1, K_{sh} = 1.0$. Each plot is for a different value of I_{rel} . $I_{rel} = 0.01, 0.02, 0.05, 0.1, 0.2, 0.3, 0.4, 0.5$ and 0.6 for plots positioned from left to right and down the page.

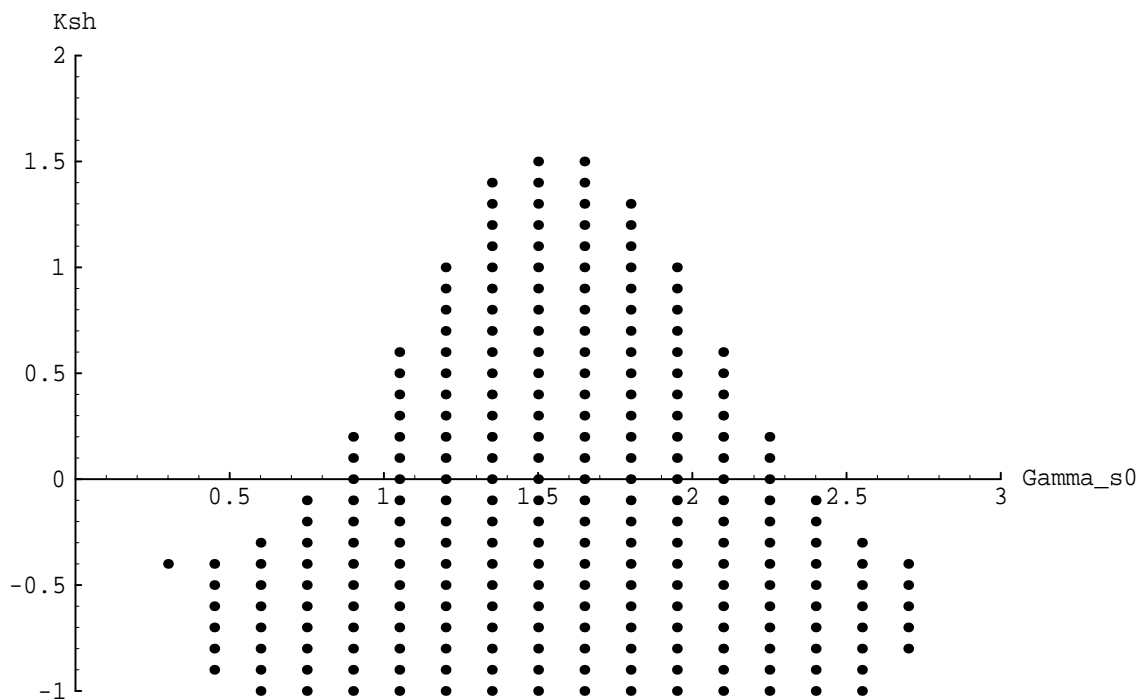


Figure 4-20: This plot shows that the stability of the “simplest model” can reflect the dependence on arm position that we saw in the five d.o.f. model (Figure 4-9.) Each dark point represents a stable configuration of the simple three d.o.f. model. The shape of the arm of the “simplest model” is changed with the value of Γ_{s0} to resemble the nominal symmetric arm angles of the five d.o.f. model.

body human model of the layout somersault predicts that neutral stability can be achieved for a range of nominal symmetric arm angles and shoulder spring constants. The model is considered passive because the joint and body motion is the result of the passive dynamic interaction of the bodies and the environmental forces. No active control or sensing is used in the model. Non-linear dynamic simulation of the passive three-body model shows that the most stable configurations conform to the linear analysis results. The number of stable somersaults that the three body model performed in dynamic simulation before exhibiting a twist instability is sensitive to initial conditions. However, for selected cases, non-linear dynamic simulations of the layout somersault indicated that the maneuver may remain stable indefinitely as long as energy is conserved.

In order to provide a more intuitive understanding of how passive stabilization of the layout somersault works, we considered the impact of principal axis orientation on layout stability. I showed how the natural tendency of the arms to tilt in response to twisting movement of the body provides a built-in correction to the twist instability. The arm tilt forces the principal axes of the system to move in a direction that compensates for tilt and twist errors. This built-in correction eliminates the divergent tendency of the system as long as the compliance of the shoulders cancels the unstable centrifugal forces on the arms. This effect is clarified by studying a very simple two body model of the layout somersault. This simple model also allows us to derive five non-dimensional parameters that are important in studying passive layout stability. I present stability diagrams that show how stability of the simplest model depends upon these parameters.

Chapter 5

Layout Somersault Experiments

5.1 Introduction

To find out whether or not passively stable layout somersaults are physically possible, we built a somersaulting 'doll' that can be tested in the laboratory. The doll has springy shoulders that allow arm movement in the frontal plane. The non-dimensional inertia parameters of the doll show that it is dynamically similar to the five d.o.f. model of the human performer studied in Chapter 4. The goals of the experiments were 1) to determine if passive layout stability was physically possible, and, 2) empirically determine the shoulder spring constants that best stabilized the motion.

To initialize the somersaults, we built a mechanical launching device that throws the doll into the air with angular rotation about the somersault axis. The launcher helped us to achieve consistency in the experimental conditions and helped to minimize the human influence of the experiment. The operation of the launcher and doll is similar in appearance to a gymnast swinging around a horizontal bar then releasing the bar to perform a multiple somersaulting dismount.

In this chapter I describe the human-like doll and launching device used during experiments. Using models from the previous chapter, I perform an analytic stability analysis of the doll to determine under what conditions the doll is theoretically

stable in somersault rotation. Then, I describe the somersault experiments in which we repetitively launched the doll with different shoulder springs to determine which springs best stabilized the doll. During experiments we found that the doll could consistently perform at least three and one half stable layout somersaults during flight. The doll may have performed more layout somersaults if we had been able to observe longer flight times. The laboratory ceiling height limited our opportunity to observe more somersaults. Also, we found good agreement between theory and experiment in finding the shoulder springs that best stabilized the maneuver.

5.2 Experimental Apparatus

In this section I describe the human-like doll used during experiments. I compare three non-dimensional parameters of the doll and the human model studied in Chapter 4 to show that the two models are dynamically similar. I also describe the launching device used to initialize the somersaults during experiments.

5.2.1 Human-Like Doll

I built a mechanical version of the five d.o.f. human model studied in Chapter 4. This doll is a fifteen inch tall, scaled version of the human performer whose anthropometric data were used in the stability analysis of Chapter 4. A photograph of this doll is shown in Figure 5-1. The body is made of wood. The shoulder joint axes are $3/16$ in. diameter steel shafts that are fixed to the body via aluminum brackets screwed to the front and back of the doll body. The arms are made of $1/4"$ threaded steel rod. The arms are attached to the shoulder shaft via an aluminum block fitted with ball bearings that allow free shoulder rotation in the frontal plane. Three shoulder pulleys with $1/2$ in., $3/8$ in., and $5/16$ in. radii are mounted to the aluminum block to be concentric with the shoulder shaft. Linear springs attached between the body and the shoulder pulleys act as torsional springs about the shoulder shaft. The different

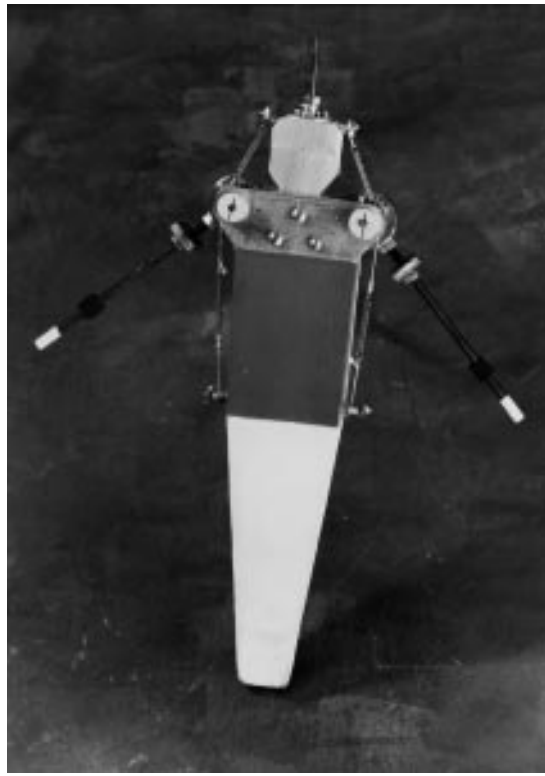


Figure 5-1: Photograph of the mechanical doll used for experiments with layout somersaults.

radii pulleys allow a single linear spring to be used as three different torsional springs. Two sets of springs were used in opposition to each shoulder. The shoulder springs could be pre-tensioned so that the arm had any desired equilibrium angle. The doll had a 1/4 in. diameter vertical shaft attached to its head. This shaft is used as a handle for the mechanical launcher to grasp. One 30g threaded weight was added to each arm. Moving the position of this weight on each arm allowed us to change the inertia of the arm without changing the total mass of the body.

The physical parameters of the five d.o.f. doll without added arm weights and with the arm weight located at a radius of $0.043m$ from the shoulder center of rotation are given in Table 5.2.1. The arm inertias are given in an axis system located at the center of mass of the arm and parallel to the body axis system when the arm is held straight down at the side, $\Phi_{s0} = 0.0$. Data for this chapter are all for the doll with arm weight at a radius of $0.043 m$ from the shoulder.

Table 5.1
Doll Body Parameters

| Parameter | No weight | | 30g weight $r = 0.043$ m | |
|-----------|-----------|-------------------|-----------------------------|-------------------|
| m_b | 0.466 | kg | 0.466 | kg |
| m_l | 0.0275 | kg | 0.0575 | kg |
| Ib_1 | 0.00411 | kg m ² | 0.00411 | kg m ² |
| Ib_2 | 0.00391 | kg m ² | 0.00391 | kg m ² |
| Ib_3 | 0.000354 | kg m ² | 0.000354 | kg m ² |
| Il_1 | 0.0000559 | kg m ² | 0.0000789 | kg m ² |
| Il_2 | 0.0000559 | kg m ² | 0.0000789 | kg m ² |
| Il_3 | 0.000001 | kg m ² | 0.000001 | kg m ² |
| rb_1 | 0.0 | m | 0.0 | m |
| rb_2 | 0.0413 | m | 0.0413 | m |
| rb_3 | 0.0664 | m | 0.0664 | m |
| rl_1 | 0.0 | m | 0.0 | m |
| rl_2 | 0.0 | m | 0.0 | m |
| rl_3 | 0.0832 | m | 0.0572 | m |

Figure 5.2.1 shows a plot of the rigid body inertia ratios of the doll and of the human performer for symmetric arm angles between 0.0 and 3.0 radians. These are superposed upon curves that show how quickly the unstable somersault mode grows for a rigid body. Comparison of the inertia ratios shows that the doll has nearly the same rigid body inertia ratios as the human model. Figure 5-3 shows a plot of the non-dimensional parameter I_{rel} for both the doll and the human model for arm angles between 0.0 and 3.0 radians. Comparing these curves shows that the doll has relatively more massive arms than the human which makes stabilization slightly easier.

5.2.2 Launching Device

We built a launching device so that we could initialize the somersaults with consistency and with minimum direct human influence. A photograph of the launcher is

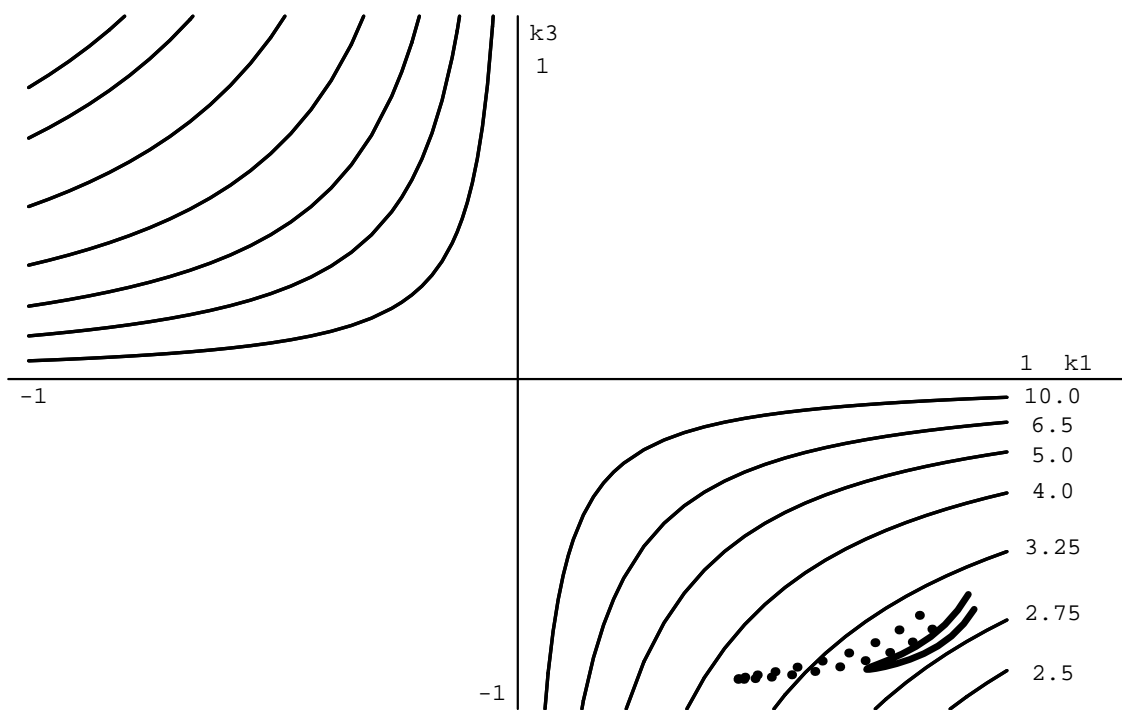


Figure 5-2: Rigid body inertia ratios of the doll (dotted line) and the human model (solid line) for arm angles between 0.0 and 3.0 rad.

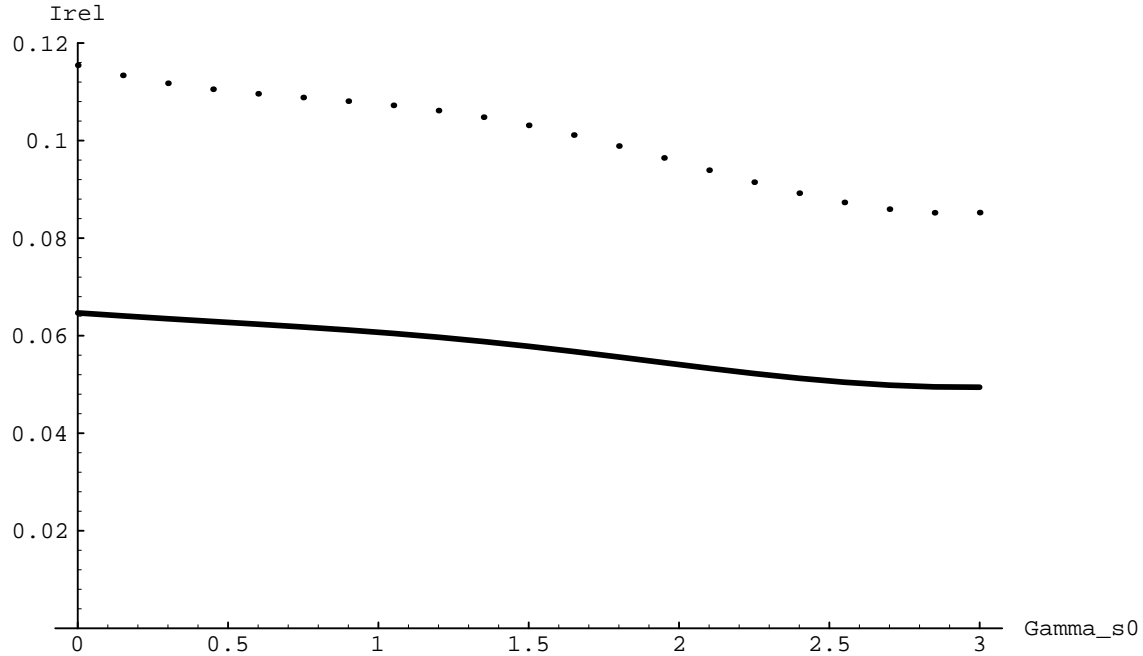


Figure 5-3: Plot of I_{rel} as a function of nominal symmetric arm angle, Γ_{s0} , for the doll (dotted line) and the human model.

shown in Figure 5-4. The launcher functioned by accelerating the doll in rotation around a horizontal bar then releasing the doll at a fixed angle around the bar. The launcher consisted of three components: 1) a horizontal bar, 2) a bearing supported toggle clamp that was free to rotate around the bar, and 3) a torsion spring used to accelerate the clamp relative to the bar.

To initialize the somersaults, the steel rod fixed to the head of the doll was clasped in the toggle clamp. The doll and toggle clamp would then be wound around the horizontal bar to tension the launcher spring. When the doll and toggle clamp were released they would accelerate around the horizontal bar. When the toggle clamp lever hit a trigger bar, the toggle clamp popped open, releasing the doll into a somersaulting, parabolic trajectory. The position of the trigger bar around the horizontal bar could be changed so that the toggle clamp released the doll at an angle that produced the desired flight trajectory. The toggle clamp had adjustments that allowed the doll to be launched with initial tilt or twist angles, however, for all experiments

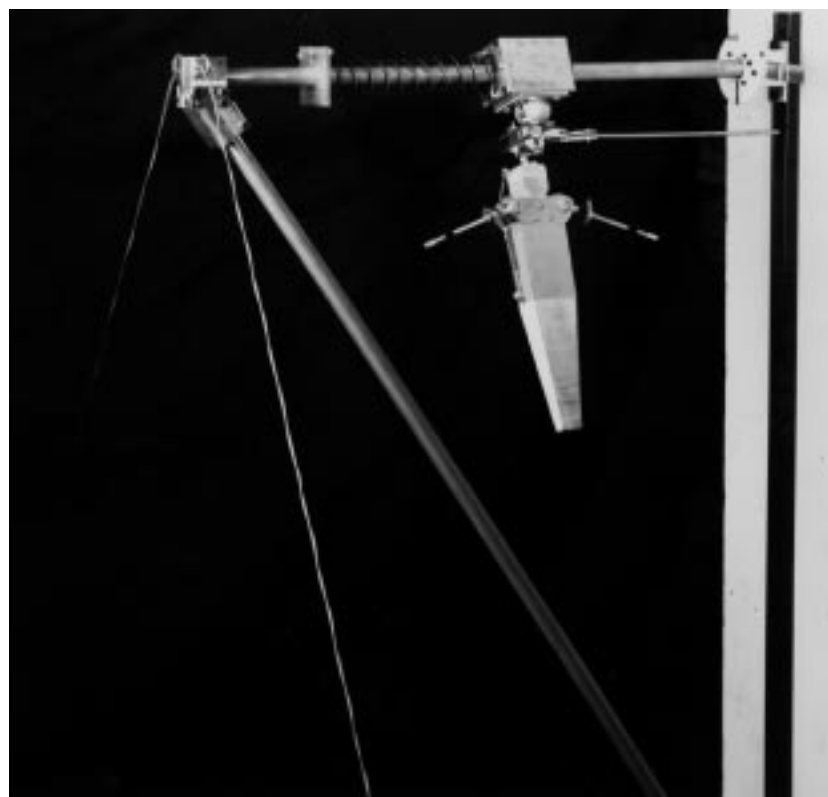


Figure 5-4: Photograph of the mechanical launcher used to initialize the doll somersaults in experiments.

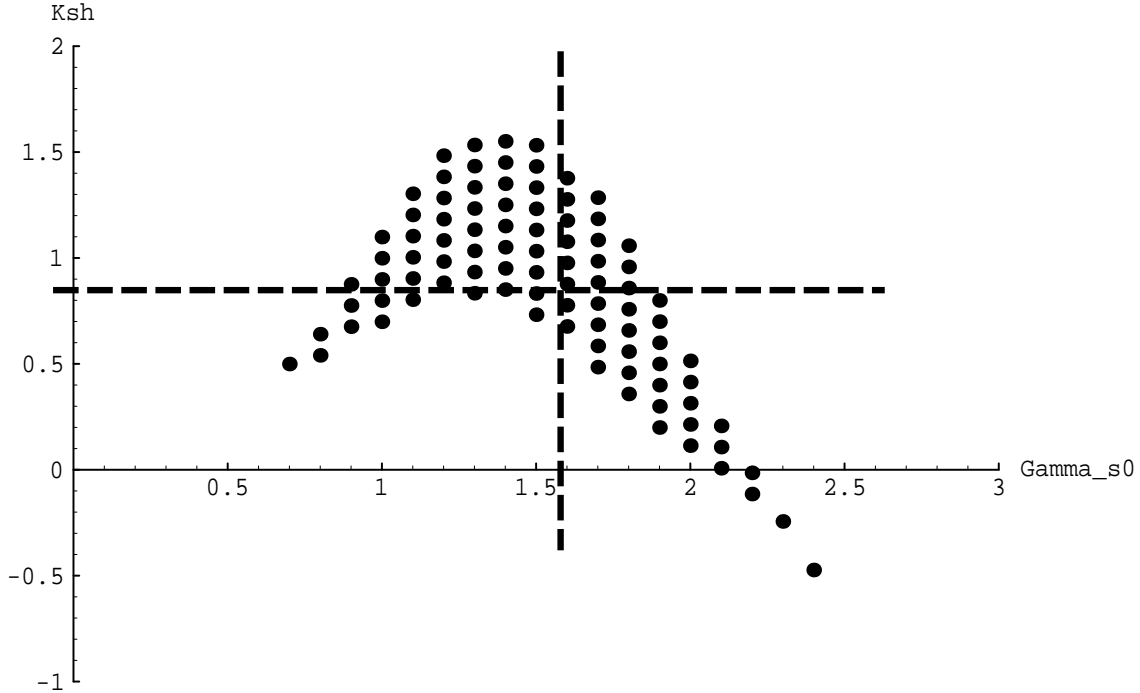


Figure 5-5: The points in this plot indicate the values of K_{sh} that theoretically will stabilize layout somersaults in the doll. The cross-hairs indicate the spring constant that best stabilized the doll during experiments.

we set the initial tilt and twist angles to be approximately zero.

5.3 Theoretical Predictions

Figure 5-5 shows the theoretically determined stabilizing values of K_{sh} as a function of symmetric arm angle for the doll. Also shown in this figure is the spring constant that best stabilized the doll with a nominal arm angle of $\Gamma_{s0} \approx 1.57$ during experiments. Note that this plot of the stabilizing K_{sh} is very similar to those for the human in Figure 4-9. The most notable difference is the larger range of stabilizing K_{sh} for the doll. This is due to the larger I_{rel} of the doll.

5.4 Description of Experiments

The experiments consisted of a sequence of launches of the doll to determine which shoulder springs stabilized the doll in somersault rotation. For each different shoulder spring used on the doll, we launched the doll twenty times using approximately the same launch spring pre-tension. The toggle clamp released the doll from the bar at a somersault angle of approximately $\frac{\pi}{2}$ rad. We video taped each experiment. Using the video tape for analysis, for each launch we recorded the number of somersaults performed before the doll exhibited a twist angle of approximately $\frac{\pi}{2}$ (one quarter twist). If during a dismount the doll never exhibited this large twist angle then the dismount was considered to be completely stable. For comparison, we also performed twenty launches with the arms of the doll fixed rigidly in place.

Recall from Chapter 4 that the nominal symmetric arm angle does affect the value of the stabilizing spring constant. During experiments we attempted to keep the nominal symmetric arm angle approximately equal to 1.6 radians by initializing the somersault with the appropriate arm angle and shoulder spring pretension. Large centrifugal forces on the arms during acceleration around the bar necessitated that we devise a method for fixing the arm position until the moment of release from the bar. In order to initialize the somersault with the desired arm angle we propped up the arms with thin steel rods held between the arms and small indentures near the feet of the doll. The rods were held in place by the shoulder spring pretension. As the doll rotated about the bar, centrifugal forces pushed the arms towards the feet helping to hold the steel rods and arms in place. Once free of the bar, the doll began rotating about its center of mass which tended to lift the arms off the steel rods allowing the rods to fall clear of the doll. The nominal arm angle was difficult to set precisely as it depended not only on initial position of the arms but also on the pretension of the springs necessary to hold the arms at this angle during rotation.

Figure 5-6 shows the beginning of two separate experiments with the doll.

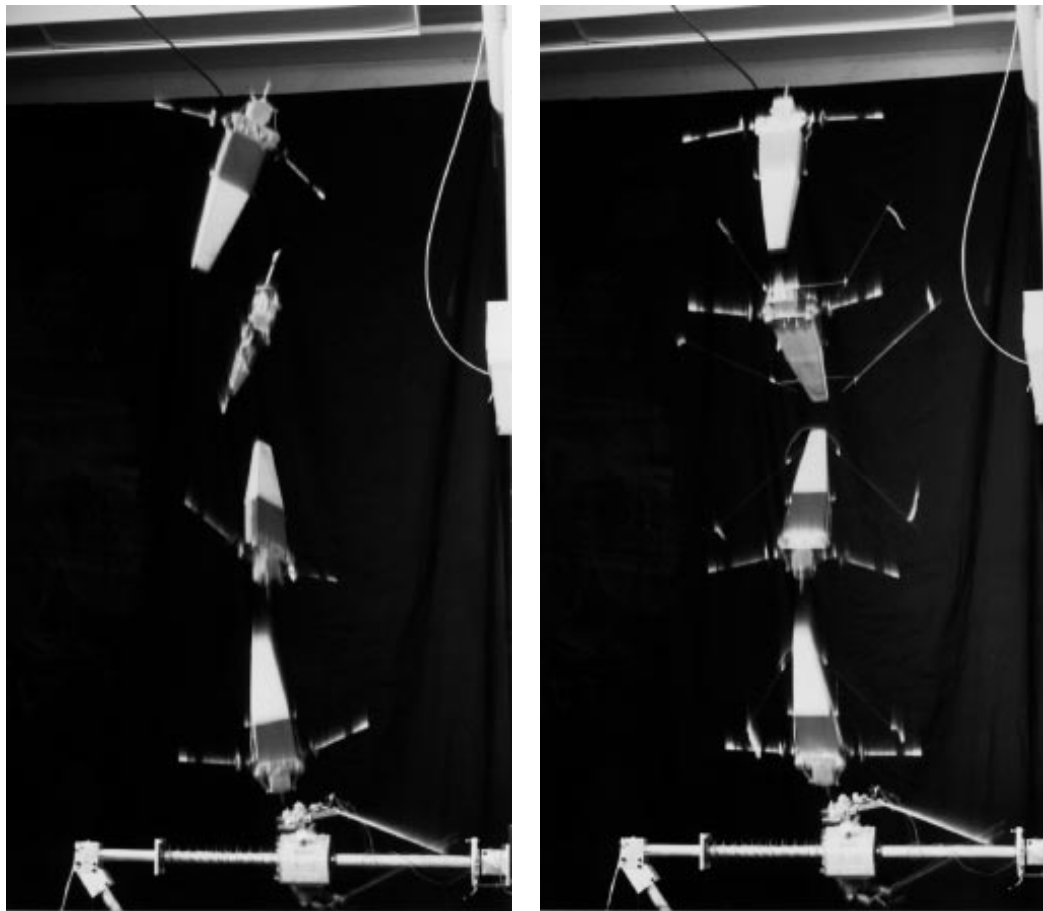


Figure 5-6: The photo on the left show the rigid doll with arms clamped in place. This doll exhibits the twist instability. The photo on the right shows the doll with flexible arms performing a stable layout somersault.

5.5 Experimental Results

There was little ambiguity between stable and unstable dismounts. Either the twist angle remained small while the doll somersaulted or it would grow significantly beyond one-quarter twist making it easy to distinguish stable and unstable cases. The rotation rate available from our launcher and laboratory ceiling height of 4.3 m limited the doll to approximately three and one half complete somersaults from release to landing in the hands of our human 'catcher'. Figure 5-7 shows the average number of stable somersaults performed as a function of the six different shoulder spring constants tested. The average is computed over twenty sequential launches for a single shoulder spring. The standard deviation for each condition is shown with error bars. The average somersault rate was 16.6 rad/sec, and $I_{sh} = 3.021 \cdot 10^{-4} \text{ Nm}^2$.

In addition to recording the number of stable somersaults exhibited during each launch we recorded whether or not the doll still appeared stable at the end of the maneuver (did not exhibit a quarter twist). If the doll had not exhibited a quarter twist by the end of the maneuver then it was considered to be a completely stable dismount. The percentage of completely stable dismounts as a function of K_{sh} is shown in Figure 5-8.

Of the six conditions tested, (five springs plus rigidly fixed arms) one shoulder spring value clearly outperformed the rest. The shoulder spring, $K_{sh} = 0.82$, performed 18/20 dismounts without exhibiting the twist instability. This high percentage of completely stable dismounts led to the very small variance in Figure 5-7. If we could have observed more somersaults, the doll may have exhibited a variance more in accordance with the remaining data. The variance in number of stable somersaults appears to increase with softer shoulder springs. While the doll became more erratic under these conditions, it never-the-less occasionally performed a completely stable dismount. At the other extreme, the doll with fixed arms reliably exhibited the twist instability at about one complete somersault from release.

The experimental results contained in Figures 5-7 and 5-8 are in agreement with

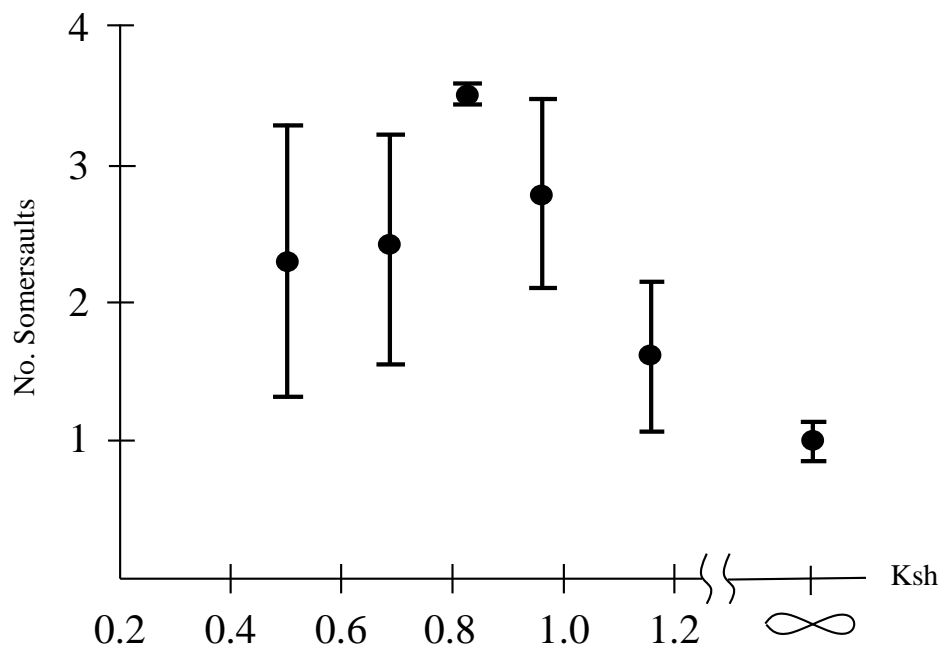


Figure 5-7: Plot of the average number of stable somersaults performed during twenty launches of the doll as a function of the shoulder spring constant, K_{sh} . The standard deviation is indicated by error bars. The data for the rigidly fixed arms is indicated by the infinite value of K_{sh} . The nominal arm angle was approximately 1.6 radians. The best value of $K_{sh} = 0.82$ falls within the range of stability predicted by theory as indicated in Figure 5-5.

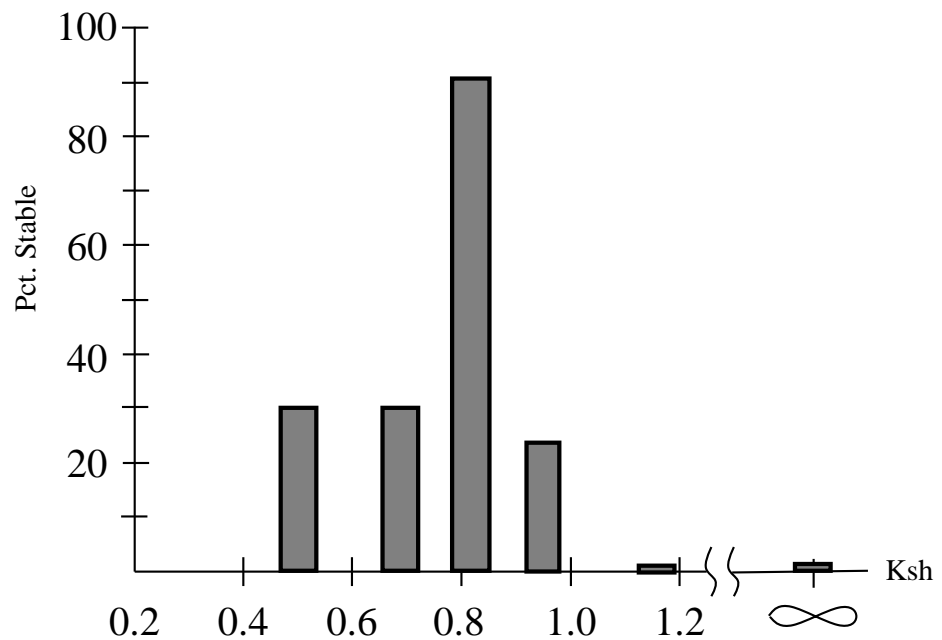


Figure 5-8: Plot of the percentage (of twenty) of completely stable dismounts as a function of the non-dimensional shoulder spring constant, K_{sh} . The two test conditions on the right side of the plot exhibited zero completely stable somersaults. The best value of $K_{sh} = 0.82$ falls within the range of stability predicted by theory as indicated in Figure 5-5.

the theoretical results for stable layout somersaults. Figure 5-5 shows that for a $\Gamma_{s0} \approx 1.57$, the stabilizing shoulder spring should have values in the range $0.7 \leq K_{sh} \leq 1.4$. The best experimental value for the doll, $K_{sh} \approx 0.8$ falls in this range with performance falling off on either side. Furthermore, this best value also falls in the range of stabilizing shoulder springs for the human model data as shown in Figure 4-9.

5.6 Summary

In this chapter I presented the results of layout somersault experiments on a mechanical human-like doll. Comparison of the non-dimensional model parameters of the doll and of a human indicate that the doll is dynamically similar to the human although slightly easier to stabilize due to relatively more massive arms. The experiments demonstrate that the doll can consistently perform at least three and one half stable layout somersaults. The consistency of the dismounts depends strongly upon the value of the shoulder spring. The best shoulder spring exhibited 18/20 completely stable dismounts, somersaulting dismounts without any evident twist instability. While softer shoulder springs make the dismount more erratic, they never-the-less allow the doll to occasionally perform a completely stable dismount and regularly perform two stable layout somersaults. On the other hand, stiff springs make the doll more reliable but less stable. The best value of the non-dimensional shoulder spring constant was $K_{sh} = 0.82$ which is within the region of stability predicted by the linear stability theory.

Chapter 6

Twisting Somersaults

6.1 Introduction

The twisting somersault is a maneuver in which the performer simultaneously rotates about the somersault and twist axes of the body. Multiple twisting, multiple somersaulting maneuvers are among the most exciting and complex aerial maneuvers performed by gymnasts and other athletes. Unlike the pure somersault, the twisting somersault must include non-linear rotational coupling between the different body axes. One effect of this non-linearity is that the effect of the performer's control actions will change during a maneuver making cause and effect relationships more complex than in the pure somersault. Navigation and feedback control of twisting maneuvers are challenging tasks. Does the accurate, reliable performance of this maneuver necessitate a feedback control strategy?

In this chapter I briefly discuss the open loop control of twisting somersaults. Open loop control means the performer's control actions are simply replayed from memory. We would like to know if twisting somersaults could exhibit passive dynamic stability when performed with an open loop control strategy. We discuss one test we performed to look for evidence of passive dynamic stability in the twisting somersault.

I present results from the non-linear dynamic simulation of a 1 1/2 twisting front

somersault. This maneuver requires that the performer execute a sequence of limb motions during flight. We found that when a simulated performer used a prescribed set of motions for executing this maneuver, the landing attitude of the performer was sensitive to initial conditions leading to poor landing attitudes. However, when the performer's control movements were compliant, the reliability of the landing attitude was significantly improved. There appears to be an optimal choice for the performer's compliance that leads to the most reliable landings.

I also discuss the control of twisting somersaults by the 3D Biped robot. We programmed a simulated 3D Biped robot to perform a front somersault with half twist. We found that in order to make the robot maneuver look like a front somersault with twist as performed by a human, we had to add weight to the robot to make its moments of inertia more like those of a human. We also had to use stronger actuators than available for the physical robot. Our experiments to make the real 3D Biped robot perform the maneuver in the laboratory were unsuccessful. The physical robot actuators had insufficient actuator power to perform the maneuver.

6.2 The Tilt of Twisting Somersaults

Frohlich [Frohlich 80] described two techniques for performing twisting somersaults. In the **torque twist** the athlete derives rotation about the somersault and twist axes from external forces as he or she leaves the ground, diving board or other apparatus. In the **torque-free twist with angular momentum** the athlete initiates twist from an airborne somersault with an asymmetric movement of the limbs (Figure 1-1). The net effect of either technique is to tilt the principal axes of the body relative to the angular momentum vector. A map of rotation, such as that in Figure 2-7, shows that even a small amount of tilt of the principal axes from the layout somersault position will result in twisting. (This is what makes layout somersaults challenging.) The greater the tilt angle, the greater will be the twist rate.

6.3 One and One Half Twisting Front Somersault

Yeadon [Yeadon 84] discusses a “torque-free” twist technique based on the hula movement for initiating twist from a piked front somersault. The hula movement involves a swiveling of the hips not unlike that required to swing a hula hoop about the hips. A quarter cycle of hula movement performed during a pike front somersault will tilt the performer’s principal axes relative to the angular momentum vector. This effect is increased if the arms are held in an abducted position during the movement. After the hula movement the performer extends from the pike and the arms are adducted to decrease the inertia about the twist axis. The extension from the hula movement should happen between the $1/4$ and $3/4$ twist positions to maximize the net tilt of the body. However, between these limits, Yeadon claims the timing of the extension is not critical to the final tilt angle.

6.3.1 The Nominal Case

I created a simulation of a human performing a one and one half twisting front somersault. The simulated athlete used the technique described in the previous paragraph to perform the maneuver in a weightless environment (Figure 6-1). The human model has thirteen joint degrees of freedom, including three in each shoulder, one at each elbow, two in each hip, and one in the torso allowing the upper body to twist relative to the lower body. The maneuver was initialized from an upright piked somersault position with the arms held straight out from the side of the body. The maneuver finished in a layout body position with the arms held straight out from the sides.

The control movements used to produce this maneuver were hand programmed so that the model looked natural during the movement and finished with the desired attitude and body configuration. The control movements consisted of a sequence of desired positions of the joints written as functions of time. The purpose of designing this maneuver was to empirically find a sequence of body configurations and joint

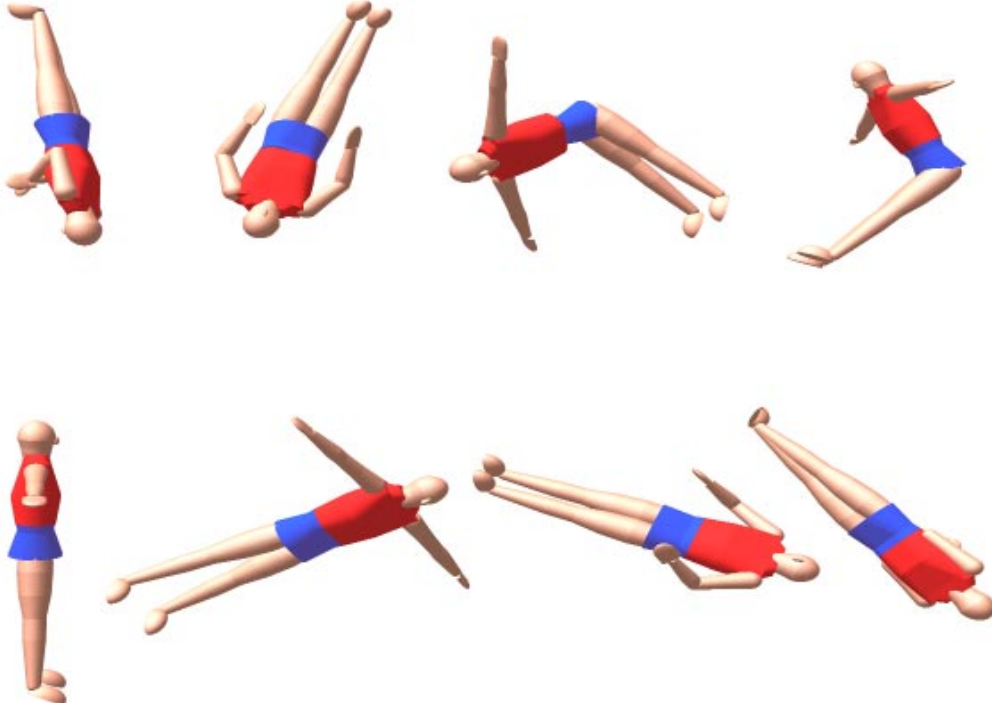


Figure 6-1: Images arranged in **right-to-left, top-to-bottom order** from a dynamic simulation of a 1 1/2 twisting front somersault. The maneuver was initialized from somersault rotation in the piked position. The control movements for this maneuver are a hand programmed sequence of joint angles written as functions of time.

torques that would produce the desired maneuver under nominal conditions. The nominal somersault rate at the beginning of the maneuver was 12.6 rad/sec and the maximum twist rate during the maneuver is 40.2 rad/sec .

6.3.2 Off-Nominal Performance, Prescribed Motion

If the simulated performer uses the prescribed set of control movements from a different set of initial conditions than the nominal case then the trajectory of the maneuver will change. How sensitive the maneuver is to variation in the initial conditions is important to the reliability of the maneuver. We tested the sensitivity of this maneuver to initial conditions by running a series of simulations, each starting from a different set of initial tilt (Θ_0) and twist (Ψ_0) angles of the body. We evaluated the reliability

of the maneuvers by comparing the landing attitude of the off-nominal simulations to that of the nominal case. (The landing attitude was considered to be the attitude at a fixed time after the start of the maneuver.) The error, e in landing attitude was computed as follows:

$$e^2 = 1/4((\Phi_d - \Phi)^2 + (\Theta_d - \Theta)^2 + (\Psi_d - \Psi)^2 + 1/13 \sum_{i=1}^{n_j o n t s} (qd_i - q_i)^2)$$

where Φ , Θ , and Ψ are the body attitude at landing q_i refers to the i^{th} joint position and the subscript d refers to the desired value. This equation for the error emphasizes the body attitude over body configuration. An error of 1.0 is large; it could mean the twist angle or somersault angle was off by 4.0 radians or about 270° .

The results of a series of simulations that varied the initial tilt and twist attitude of the body over a range, $-0.1 \text{ rad} \leq \Theta_0 \leq 0.1 \text{ rad}$, $-0.1 \text{ rad} \leq \Psi_0 \leq 0.1 \text{ rad}$ are shown in Figure 6-2.

The nominal maneuver, $\Theta_0 = 0$, $\Psi_0 = 0$, corresponds to the center grid point of this figure. The height of the surface there is zero. Away from the nominal the landing attitude error increases except for a narrow valley of initial tilt and twist attitudes along which the landing error remains small. It appears that a prescribed motion strategy would not produce reliable 1 1/2 twisting somersaults. Is there a simple open loop strategy that can improve this performance?

6.3.3 Off-Nominal Performance, Compliant Motion

It seems unlikely that people could accurately reproduce prescribed motions in a dynamic movement like the 1 1/2 twisting somersault. People use springy muscles and tendons to position their limbs. It seems likely that the change in environmental forces that would accompany a change in maneuver trajectory would mean that the limb movements change even if the athlete *tried to execute the exact same motions*. This idea is the basis for the following set of simulation experiments.

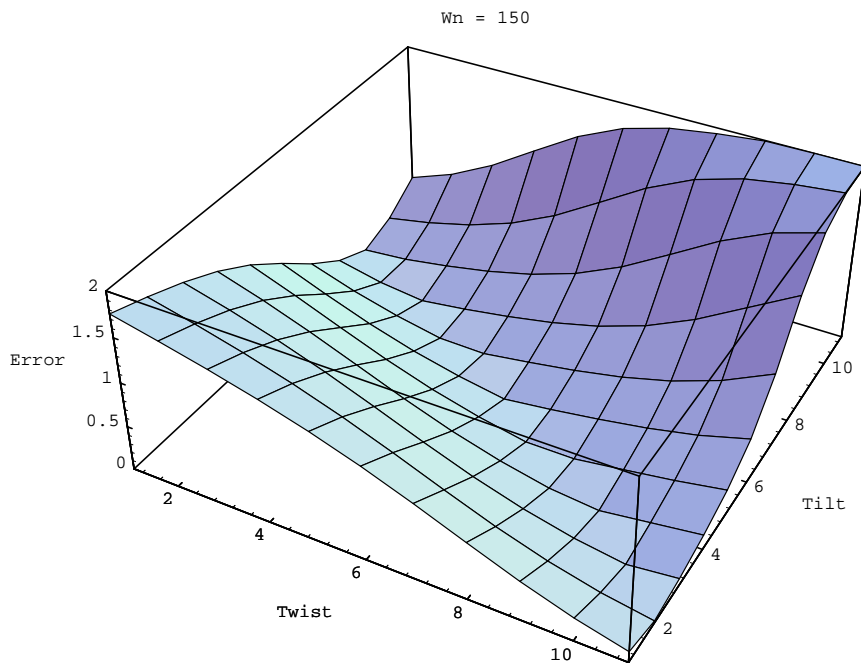


Figure 6-2: This figure shows the accuracy of a 1 1/2 twisting somersault in the presence of off-nominal initial conditions. The simulated performer used a prescribed set of joint angles to perform the maneuver. The two grid axes correspond to initial tilt and twist angles of the body, $-0.1 \text{ rad} \leq \Theta_0 \leq 0.1 \text{ rad}$, $-0.1 \text{ rad} \leq \Psi_0 \leq 0.1 \text{ rad}$. The height of the grid indicates the accuracy of the landing attitude of the simulation starting from the corresponding set of initial conditions.

We ran a series of simulations of the 1 1/2 twisting front somersault that used the joint torques from the nominal maneuver as feed forward commands. We also used the prescribed joint motion from the nominal maneuver as the commanded positions for a set of compliant, position plus derivative (pd) servos at the joints. In this open loop strategy, the net joint torques would be a combination of the feed forward torques plus pd servo torques. Since the pd servos use a prescribed set of positions as desired values, they act like passive springs and dampers at the joints. If the maneuver started from the nominal initial conditions then the joints would follow the prescribed trajectories. Then the torques from the pd servos would remain zero and the nominal maneuver would be reproduced.

Our goal in this part of the experiment was to find a set of pd servo gains (spring constants and damping coefficients) that produced the most reliable performances. Rather than search over the gain parameters of pd servos at thirteen joints, I chose to search over one parameter. Therefore, I compute the gains of all joint servos according to a single parameter, the body clamped natural frequency, ω_n . The intent behind this choice is that all body joints have a similar compliance or natural frequency of operation. We will then look for a body natural frequency that produces reliable 1 1/2 twisting somersaults.

To compute the servo gains at a given joint as a function of ω_n , I assume that the body inboard (towards the torso) from the joint is inertially fixed and all out-board joints are immobilized. This way the model simplifies to a single d.o.f. joint between the limb in question and ground. The equations reduce to a simple second order system of equations as follows

$$I \ddot{x} + c(\dot{x} - \dot{x}_d) + k(x - x_d) = 0$$

where I is the apparent inertia of the limb at the joint, c is the damping coefficient, and k is the spring constant of the joint. This simple system can be rewritten in the

canonical form

$$\ddot{x} + 2\zeta\omega_n(\dot{x} - \dot{x}_d) + \omega_n^2(x - x_d) = 0$$

therefore $c/I = 2\zeta\omega_n$ and $k/I = \omega_n^2$. We choose $\zeta = 0.7$ to achieve a well damped system response [Ogata]. Then choosing ω_n allows us to compute the stiffness and damping constants in a consistent manner.

We systematically varied the value of ω_n between 150 rad/s and 20 rad/s. At each of these values of the body natural frequency we performed a series of simulations starting from initial conditions just as in the case of prescribed motion at the joints. I plotted the results in the form of the 3D plot shown in Figure 6-2 for each frequency and subjectively evaluated them. There was a clear choice for the best natural frequency. Figure 6-3 shows the simulation results for the case of $\omega_n = 30 \text{ rad/s}$. This plot shows that the reliability of the 1 1/2 twisting somersault performed with the open loop strategy shows marked improvement over the prescribed motion case. Now, nearly half the set of initial conditions results in small final attitude errors. Furthermore, the landing attitude errors were worse for either smaller or larger values of ω_n . These basic results held true for variations in the angular momentum, h , of the maneuver as well ($0.9 h \leq h \leq 1.1 h$).

Figures 6-4 and 6-5 show data from two simulations using the nominal value of angular momentum and with $\Theta_0 = -0.1$, and $\Psi_0 = -0.1$. The data of figure 6-4 shows that when prescribed joint motion is used for an off-nominal maneuver, the body attitude error becomes large at the end of the maneuver. In contrast, the data of figure 6-5 shows that while the joint angles incur some error during the maneuver the body attitude is close to the desired value at the end of the maneuver.

Since the timing of this maneuver will scale with somersault rate it is instructive to show how the body clamped natural frequency compares to the nominal somersault rate, $\frac{\omega_n}{\Phi_0} = \frac{30}{12.6} = 2.38$. It appeared in simulations that the compliance that allowed the arms to open prematurely, thus increasing the body inertia about the twist axis, was important in off-nominal simulations. For this reason, one might consider scaling

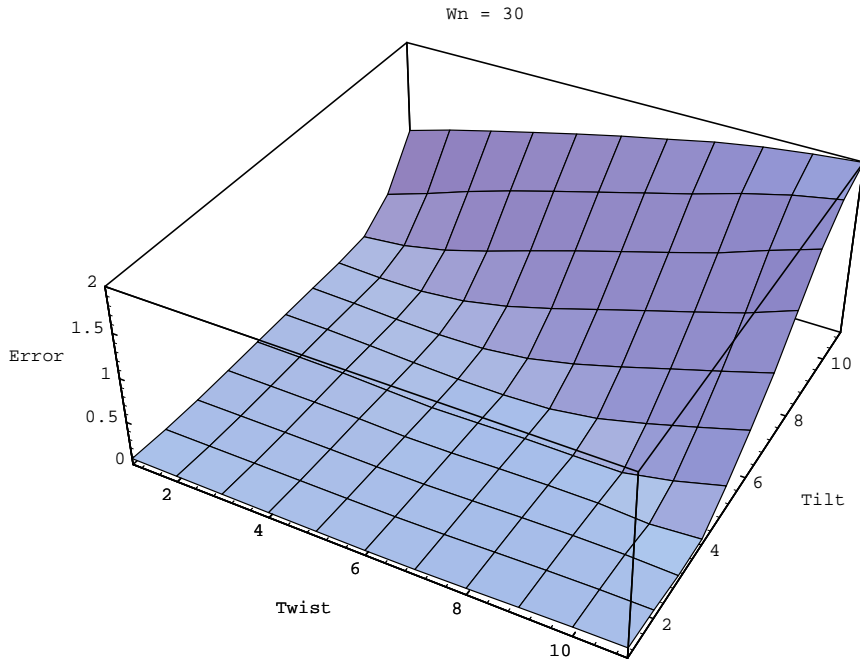


Figure 6-3: This figure shows the accuracy of a 1 1/2 twisting somersault in the presence of off-nominal conditions. The simulated performer used feed forward torques plus passive pd servos at the joints to perform the maneuver. Pd servo gains were chosen according to $\omega_n = 30 \text{ rad/s}$. The pd servos used the prescribed joint angles from the nominal maneuver as desired values. The two grid axes correspond to initial tilt and twist angles of the body, $-0.1 \text{ rad} \leq \Theta_0 \leq 0.1 \text{ rad}$, $-0.1 \text{ rad} \leq \Psi_0 \leq 0.1 \text{ rad}$. The height of the grid indicates the accuracy of the landing attitude of the simulation starting from the corresponding set of initial conditions.

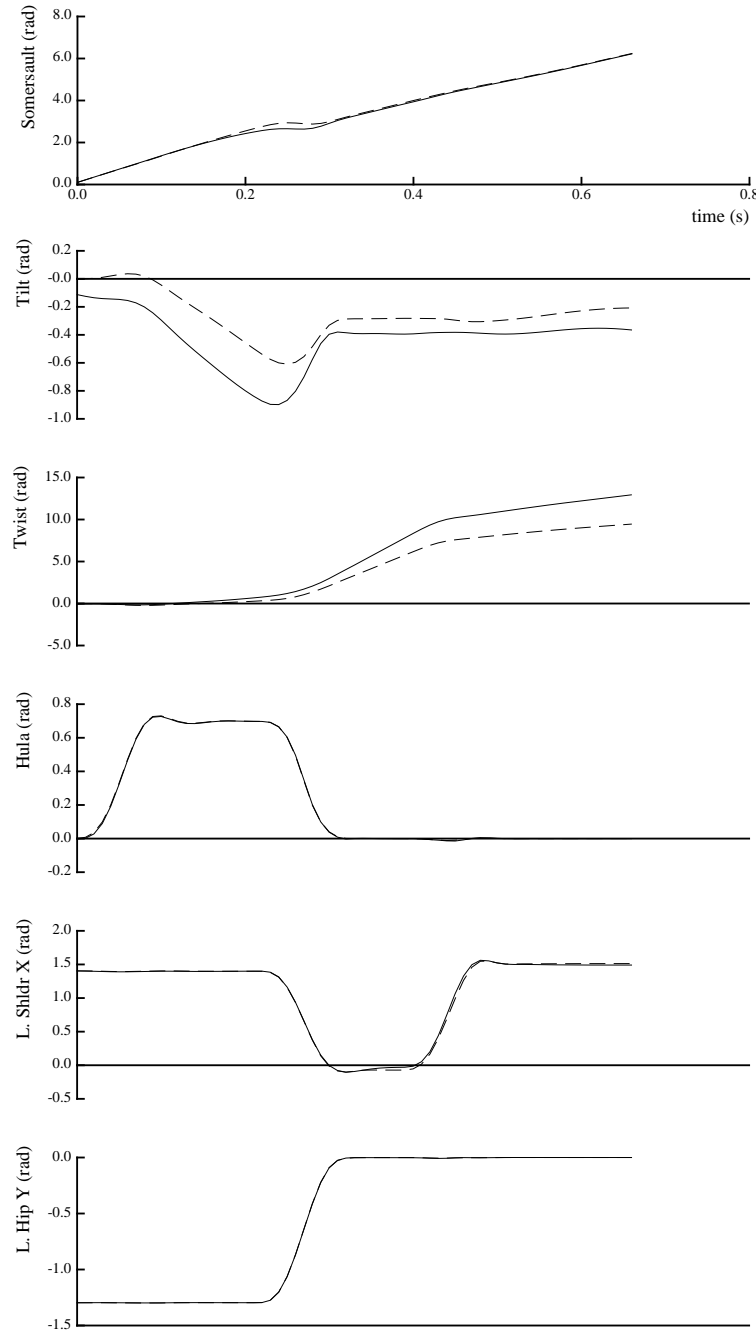


Figure 6-4: Simulation data from a 1 1/2 twisting somersault that used prescribed control motions for initial conditions $\Theta_0 = -0.1$, and $\Psi_0 = -0.1$ are shown with solid lines. The body attitude and joint angles of the nominal maneuver are shown with dashed lines. While the prescribed joint positions are accurate for the off-nominal case (bottom three graphs), the body landing attitude error is large. (The traces stop at the landing time.)

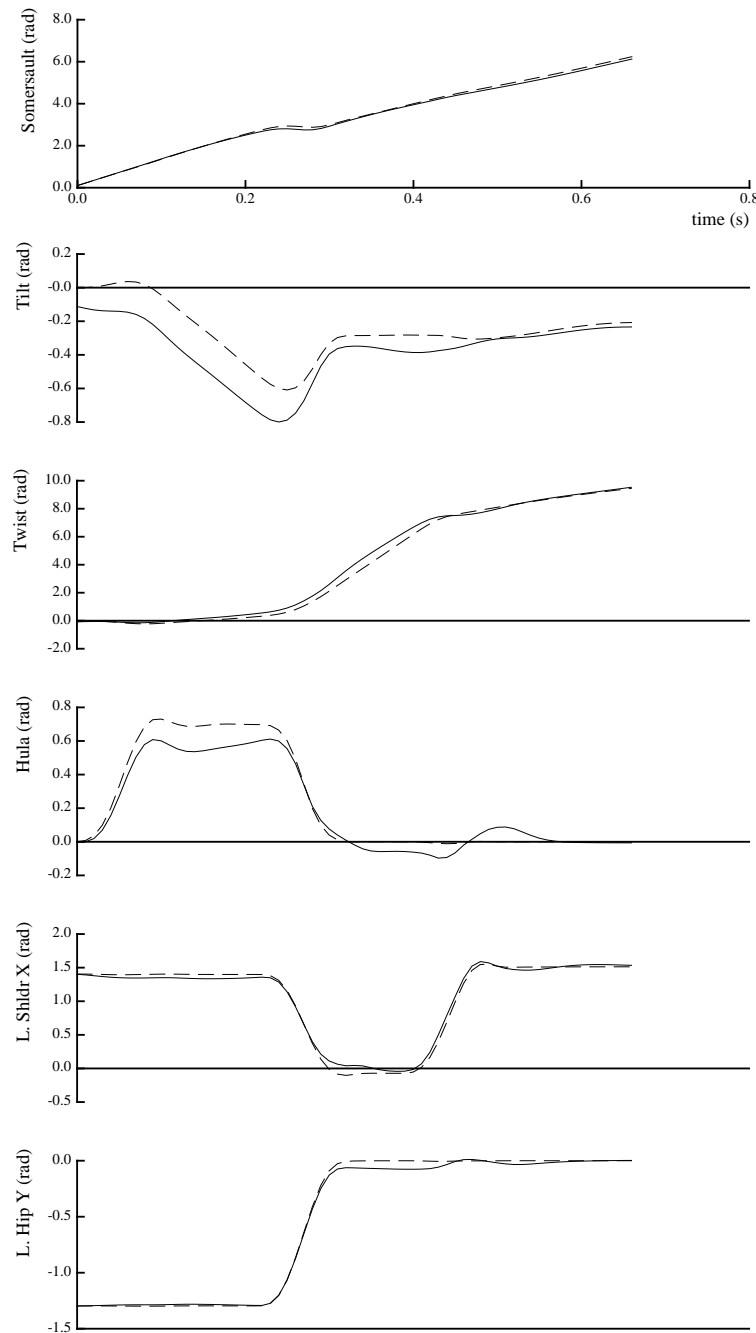


Figure 6-5: Simulation data from a 1 1/2 twisting somersault with $\omega_n = 30$, $\Theta_0 = -0.1$, and $\Psi_0 = -0.1$ are shown with solid lines. The desired values of the body attitude and joint angles are shown with dashed lines. Joint angles incur significant tracking errors but the landing attitude closely follows that of the nominal maneuver. (The traces stop at the landing time.)

the body clamped natural frequency by the maximum twist rate of the nominal maneuver, $\frac{\omega_n}{\Psi_{mx}} = \frac{30}{40.2} = 0.746$.

The body clamped natural frequency was chosen to be a simple parameter that described the natural frequency of the whole body. However, since the computation of this parameter assumed that parts of the body were inertially fixed, the actual eigenfrequencies of the system will differ from this body clamped frequency. The actual eigenfrequencies of the body for the initial configuration (pike) and the twisting configuration (wrap) of the Rudi, are shown in Table 6.3.3.

6.4 Twisting Somersault of the 3D Biped

We programmed a simulated 3D Biped robot to use the “torque twist” method to initiate a twisting somersault. To use this technique the simulated 3D Biped robot accelerated its torso in somersault and twist during the stance phase just prior to take-off. These two components of momentum should result in an angular momentum vector that is tilted with respect to the principal axes of the robot.

Figure 3-3 shows the map of rotational motion of the 3D Biped. When compared to the map for the layout somersault in the human (Figure 2-7) we see that the robot requires significantly more tilt of the principal axes (relative to the angular momentum vector) to achieve a twisting somersault. This is partly due to the fact that the robot somersault axis is the major principal axis but also due to the significantly different shape of the regions on the two maps. The qualitative difference in shape of the maps is due to the difference in rigid body inertia ratios of the robot and of the human. To put it simply the human is long and skinny and the robot is short and fat. This difference makes the twist harder to achieve (more tilt required), and it means the maneuver will not look much like that of a human.

In its current configuration, the twisting somersault mode of the 3D Biped would force the robot to lay on its side some time during flight. This body orientation is not

Table 6.1
Rudi Eigenfrequencies

| Pike | | Wrap | |
|--------------------|---------|--------------------|---------|
| ω_n rad/sec | ζ | ω_n rad/sec | ζ |
| 921.0 | 0 | 210.0 | 0 |
| 709.2 | 0 | 188.3 | 0 |
| 359.4 | 0 | 159.2 | 0 |
| 161.2 | 0 | 107.7 | 0 |
| 160.6 | 0 | 93.1 | 0 |
| 88.0 | 0 | 39.7 | 0.92 |
| 69.0 | 0 | 39.7 | 0.92 |
| 36.7 | 0.85 | 38.9 | 0.90 |
| 36.7 | 0.85 | 38.9 | 0.90 |
| 31.3 | 0.73 | 30.1 | 0.70 |
| 31.3 | 0.73 | 30.1 | 0.70 |
| 31.0 | 0 | 30.0 | 0.70 |
| 30.1 | 0.70 | 30.0 | 0.70 |
| 30.1 | 0.70 | 27.8 | 0 |
| 30.0 | 0.70 | 26.8 | 0.62 |
| 30.0 | 0.70 | 26.8 | 0.62 |
| 28.3 | 0 | 26.7 | 0 |
| 24.7 | 0 | 26.5 | 0.62 |
| 24.7 | 0 | 26.5 | 0.62 |
| 22.9 | 0.53 | 24.9 | 0.58 |
| 22.9 | 0.53 | 24.9 | 0.58 |
| 22.7 | 0 | 24.8 | 0.58 |
| 22.0 | 0 | 24.8 | 0.58 |
| 21.9 | 0 | 24.7 | 0 |
| 16.0 | 0.37 | 24.1 | 0 |
| 16.0 | 0.37 | 23.8 | 0 |

what we identify with a twisting somersault in a human. The human's long axis stays closer to the vertical during a twisting somersault. In addition, this inertial orientation of the robot is undesirable from a practical standpoint because this orientation is coincident with gimbal lock in the gyros used to measure body attitude. During laboratory experiments, the physical robot achieved this horizontal position which resulted in damage to the gyroscopes. To correct this situation we changed the robot inertia, and thus its rotational modes, to look more like that of a human.

To change the robot inertia we added weight to increase the major and intermediate principal inertias without increasing the minor principal inertia. We did this by adding weight along the '3' axis of the robot. Figure 6-6 shows the new map of rotation for the 3D Biped with a 4.0 kg weight added 0.8 m above the hips of the robot. This map looks much more like that of a human now and the twisting somersault should bear this resemblance as well. Figure 6-7 shows a sequence of computer graphic images of a simulated 3D Biped with added weight (and strong actuators) performing a front somersault with one half twist. Notice that the simulated robot lands the twisting somersault facing the opposite direction it started from. Data from the simulation is included in Figure 6-8. The simulated running robot regained balance on landing to continue stable dynamic running.

We tried this maneuver with the physical 3D Biped robot in the laboratory. The added weight and inertia were too large for the robot to achieve sufficient flight time or angular momentum to produce the maneuver.

6.5 Summary

In this chapter I presented simulation results of a $1\frac{1}{2}$ twisting front somersault performed by a model gymnast with thirteen joint degrees of freedom. The maneuver is initiated from a piked front somersault. The twisting maneuver results from a sequence of movements of the limbs and torso made during flight. We found that

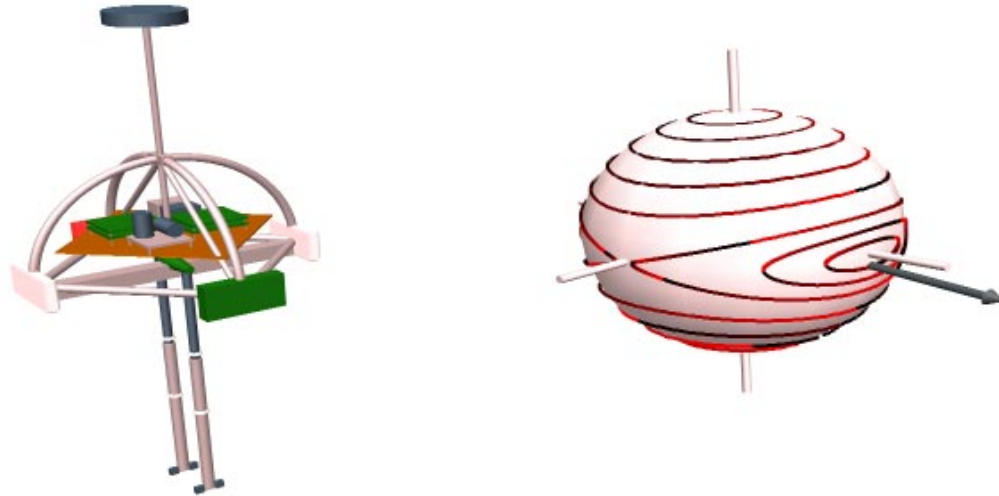


Figure 6-6: Spherical coordinate map of the tilt and twist Euler angle trajectories for the 3D Biped with 4 kg of weight added at a distance of 0.8 m above the hip.

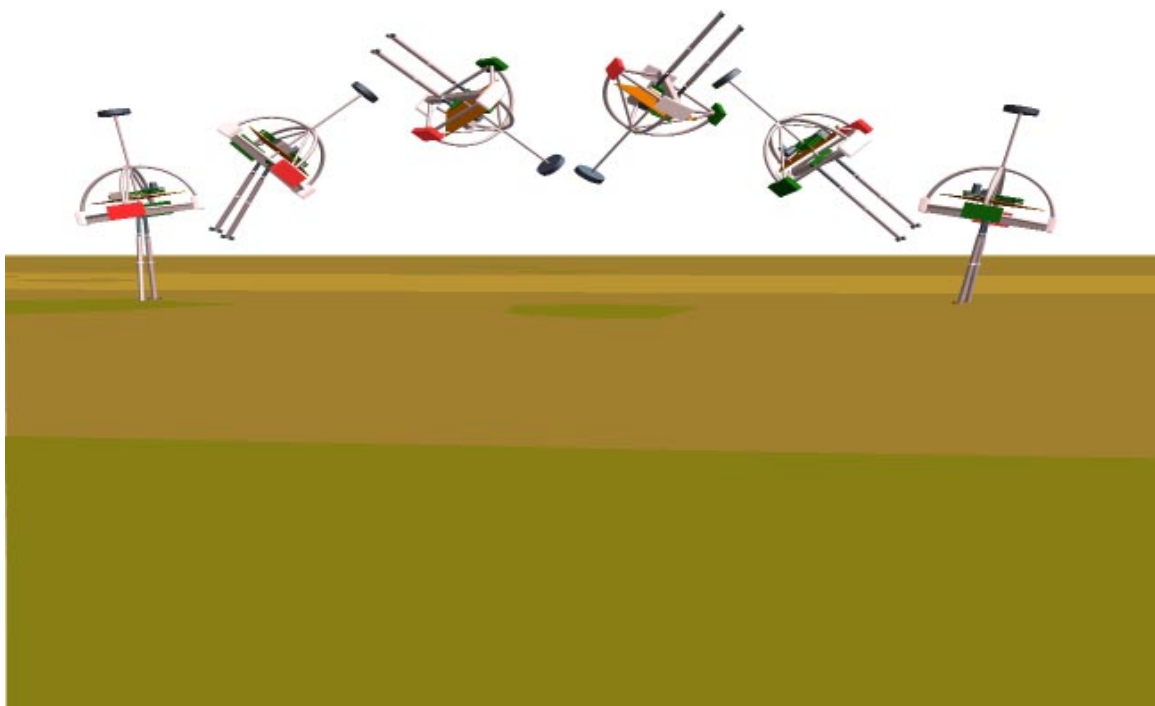


Figure 6-7: Sequence of images of the simulated 3D Biped somersault with twist.

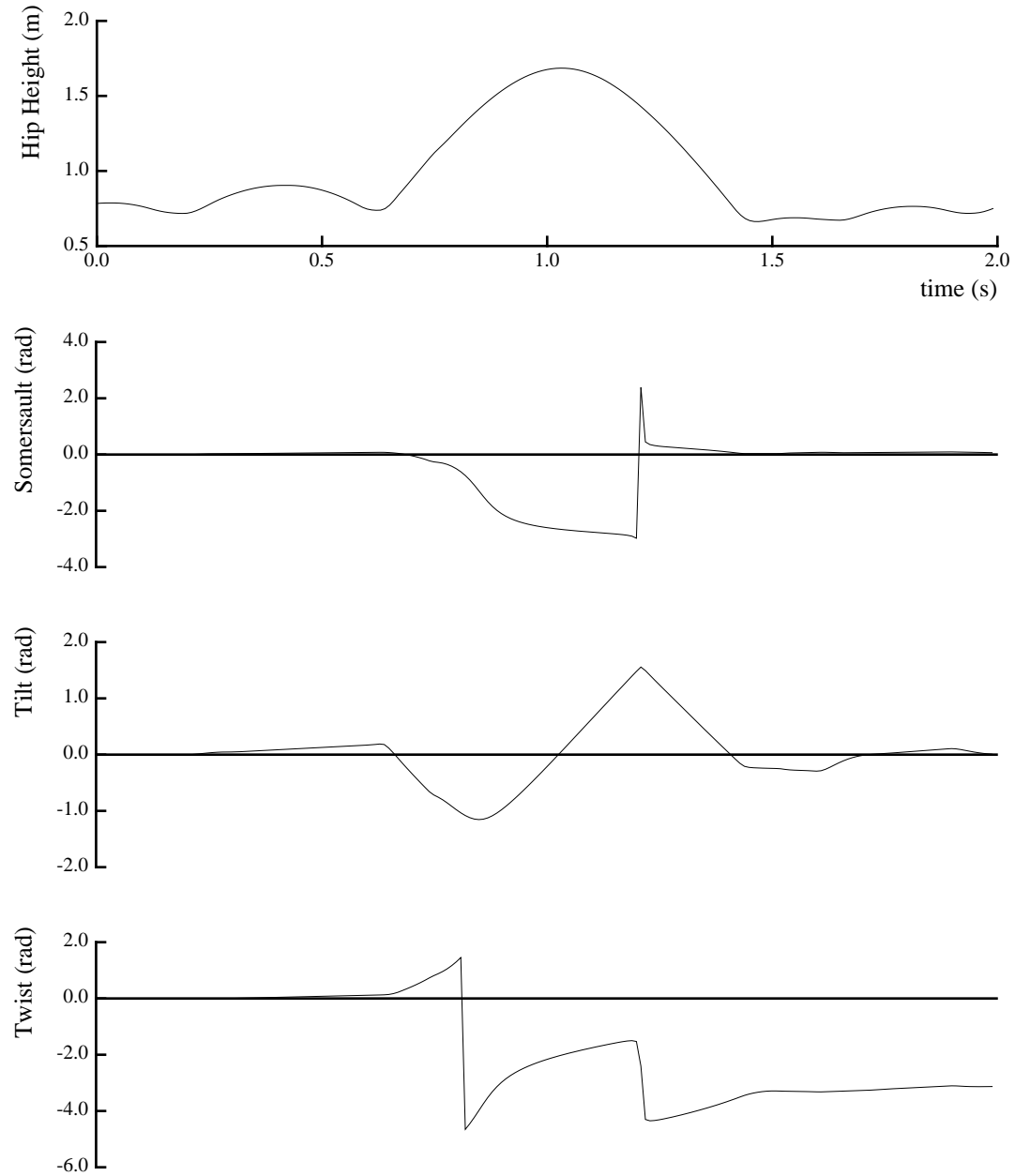


Figure 6-8: Hopping height, somersault, tilt and twist Euler angles of the 3D Biped during a simulated front somersault with $1/2$ twist. The simulated robot passes through an Euler angle singularity at approximately 1.2 sec. causing discontinuities in the data. This singularity did not affect the dynamic simulation however as a different set of attitude parameters were used.

prescribed limb movements could produce reliable 1 1/2 twisting somersaults only for a small set of off-nominal initial conditions. In contrast, a control strategy that used feed forward joint torques in a tuned passive dynamic model of the performer could produce reliable maneuvers for a much larger set of off-nominal initial conditions.

We do not yet know the significance of this result. There are many degrees of freedom of this model. Too many to easily distinguish between important and unimportant effects. Simplification of this model may reveal salient features that can be analytically confirmed. These simulation results from the rudi are potentially interesting because it suggests that a passive dynamic approach to twisting somersaults may be capable of producing reliable maneuvers as was the case with the layout somersault. It is interesting that many of the eigenfrequencies of the most reliable, tuned compliant system for the rudi were in the neighborhood of the maximum twist rate of the maneuver. This appears to be analogous to the ideal choice of arm-body oscillation in the passive layout somersault. In this case the best shoulder spring resulted in an eigenfrequency of the arm-body oscillation that was equal to the somersault rate.

In this chapter, I also described simulation experiments with 3D Biped twisting somersaults. The distribution of mass in the 3D Biped robot makes a twisting somersault particularly difficult. In order to enter a rotational mode that could produce the twist angles desired, the robot had to assume body attitudes unlike those associated with a human somersault with twist. This extreme body attitude could lead to mechanical difficulties with inertial instruments on the physical robot. We added weight to the robot so its natural rotational modes were more like those of a human. A simulated 3D Biped robot was able to perform a 1/2 twisting front somersault. The simulated robot landed the maneuver and continued running stably afterwards. The added weight made twisting somersaults of the physical 3D Biped robot impossible due at least in part to insufficient actuator power.

Chapter 7

Summary and Discussion

Inspiration for this thesis comes from the remarkable performance of aerial maneuvers by gymnasts, divers, trampolinists, and skiers. From a distance, the control of aerial maneuvers appears to be a very complex task. The shortage of control during flight and the non-linear rotational mechanics make this problem more than a little daunting. However, adversity breeds creativity and athletes and other people have been very creative in working with these difficulties to produce elegant solutions to movement control problems. It appears that we can learn something from human capability in making dynamic flying or floating machines that can reorient themselves quickly, reliably, and accurately.

This thesis is concerned with how people can incorporate known aerial movement techniques into a strategy that produces reliable performances. People can influence aerial maneuvers through the relative movement of their limbs and torso during flight. While a fixed sequence of control movements can be found to produce a desired maneuver, prescribed limb motion may provide little reliability when a maneuver is subject to the variety of conditions that would accompany any real performance. It is possible that people produce reliable maneuvers by sensing these variations and actively computing responses to compensate for them. However, the complexity of this approach warrants the search for a simpler strategy. A persistent goal of this work

has been to find control strategies that do not depend entirely on active feedback, that are simple, and that can work in laboratory machines.

The contribution of this thesis is to point out via example that passive dynamic solutions to movement control are an alternative to certain problems previously considered to require active feedback control. We focus on an open loop, passive dynamic strategy for producing gymnastic maneuvers. Open loop means that control effort (torques at joints) are simply replayed from memory during a maneuver (the motor tape model of biological control). Under identical conditions open loop control will produce identical maneuvers. Using open loop control under different initial conditions will produce different outcomes due to the inherent dynamics of the system. This may make open loop control by itself incapable of producing reliable maneuvers. However, it is possible that the passive dynamic behavior of the performer's body could automatically compensate for off-nominal conditions in a way that produces reliable maneuvers. The passive dynamic behavior of a system can be tuned through the selection of passive elements like springs (springy muscles) or by choosing nominal body configurations during the maneuver. Careful tuning of the passive dynamics of a system coupled with open loop control may provide a strategy for producing reliable gymnastic maneuvers.

This strategy is simple in the sense that it requires no computation during the maneuver. Only memory playback is required. Compensatory movements are 'computed' by the physical system as part of its natural behavior. Incorporation of this strategy could simplify gymnastic performances by reducing the amount of active control and computation required by the athlete.

To the extent possible, we have insisted upon laboratory experimentation to test our ideas. We feel that laboratory experimentation on physical machines forces one to discover the salient features of a problem that may be difficult to reveal otherwise. (Another reason is that laboratory experimentation is also a lot of fun!) However, while a laboratory experiment can be used to validate a strategy for machine control,

it can only suggest the viability of a strategy for human use.

We studied three different gymnastic maneuvers in this thesis, the tucked somersault, the layout somersault, and the 1 1/2 twisting front somersault.

7.1 Robot Tucked Somersaults

The tucked somersault is a common maneuver in athletic events. The main requirement of this maneuver is a balanced landing which in turn requires a precise body attitude. We programmed a 3D Biped robot to perform front somersaults in the laboratory. The control strategy relied implicitly upon the passive dynamic stability of the tucked somersault. We used an active feedback system to control somersault rotation rate and foot placement at landing.

A linear analysis of rigid body rotation showed that the tilt and twist attitude of the somersaulting 3D Biped robot is passively stable. However somersault attitude is unstable. This well known result led us to use active control of the somersault degree of freedom in the 3D Biped maneuver. The robot controls somersault rotation rate by tucking or untucking its legs during flight to change the rotational inertia. During flight we depend upon a stable passive dynamic response of the tilt and twist dynamics to insure small tilt and twist angles at landing. To keep the initial tilt and twist angles small we use a wide double stance of the robot during take-off and insure that the feet touch down simultaneously. Another important element of active control of the 3D Biped somersault was the placement of the feet prior to landing. This element was necessary to compensate for errors in the estimated landing time. On its best day the robot has performed successful front somersaults on seven out of ten attempts in laboratory experiments.

We do not know if active control of rotation rate in the 3D Biped robot is necessary to perform the front somersault. It is possible that open loop control plus active foot placement prior to landing could also be used to perform reliable front somersaults.

This was the case with the planar biped somersault work of Hodgins and Raibert. A strategy that we would like to experiment with in the future could provide a middle ground between the active rotation rate control used in this study and the (primarily) open loop approach used in the planar biped. This strategy would use tuned leg springs to passively influence somersault rotation rate. This technique could correct rotation rate errors by allowing the legs to extend at higher than normal rotation rates (due to higher centrifugal forces) and vice versa for slower rotation rates. This passive dynamic approach coupled with active foot placement may provide reliable front somersaults with less active feedback control.

7.2 The Layout Somersault

The layout somersault involves rotation about the middle principal axis of inertia, an unstable rotation for a rigid body. Biomechanics researchers have suggested that human athletes use active feedback control during flight to stabilize the layout somersault. We found that the layout somersault could passively be made neutrally stable.

The layout somersault is stabilized by passive arm movement in the frontal plane. The inherent tendency of the arms to tilt in response to twisting movement of the body provides a built-in correction for the layout instability. The arm accomplishes this by changing the orientation of the principal axes with respect to the angular momentum vector. This built-in correction eliminates the divergent tendency of the system as long as a carefully selected shoulder spring is used to cancel unstable centrifugal forces on the arms. These results are confirmed with linear stability analysis, non-linear dynamic simulation and laboratory experiments with a somersaulting doll. During experiments the doll can consistently perform at least three and one half stable layout somersaults.

Analysis of a simplified model of the layout somersault dynamics revealed several salient features of the movement. The simplified model revealed the simple rule

for picking stabilizing non-dimensional shoulder springs, $K_{sh} = 1.0$. This spring constant insures that the natural frequency of the arm-body oscillation is matched to the rotation rate of the body. It also is the exact spring required to cancel the destabilizing centrifugal forces on the arms. The empirically determined, best value of K_{sh} for the experimental doll was $K_{sh} = 0.82$. This value is in agreement with the theoretical results. I think that it is significant that the stabilizing shoulder spring just cancels the spring-like action of centrifugal forces. This *balance* between opposing forces allows the arm to be responsive to the gyric forces which ultimately stabilize the system.

The simple model also helped explain why arm orientation is important in stabilizing the layout somersault. The tendency of the arms to tilt in response to twist is greatest when the arms are held straight out to the side. This tendency is decreased as the arms are raised or lowered from that position. Another feature that the simple model revealed is that stabilization of the layout somersault is easier with bigger and bigger arms. This is not surprising for in the limit when the arms (held straight out to the side) are much larger than the body, the system resembles a rigid body rotating about its minimum principal axis, a well known gyroscopically stabilized configuration.

We ignored the control of somersault angle in the layout somersault. Stabilization of the somersault angle will be important for practical layout somersaults as it was for the 3D Biped tucked somersaults. However, decoupling of the tilt, twist, and asymmetric arm movement from the somersault and symmetric arm movement suggests that a somersault control strategy and a tilt-twist control strategy could be developed separately then superposed in the complete system.

7.3 Twisting Somersaults

Twisting somersaults are among the most interesting and complex of aerial maneuvers. They involve simultaneous rotation about the twist axis and the somersault

axis. Their dynamic complexity makes feedback control of these maneuvers challenging. Is it possible that open loop control can be used to reliably produce these maneuvers? Perhaps it can if the performers body acts like a tuned passive dynamic system. Our results on the open loop, passive dynamic control of twisting somersaults are of a preliminary nature. However, they point to a potentially interesting subject for future work. These results suggest that passive dynamics may help the reliable performance of twisting maneuvers as was the case for the layout somersault.

We used a thirteen joint human model to simulate the performance of a 1 1/2 twisting front somersault. The twisting maneuver was initiated from a piked front somersault using asymmetric movement of the limbs. We found that using prescribed limb motion during the maneuver produced inaccurate landing attitudes when the initial body attitude was allowed to vary. On the other hand, an open loop, passive dynamic strategy was able to produce reliable landing attitude for a relatively large set of initial conditions. In this strategy, open loop torque commands from the nominal trajectory were combined with torques from passive springs and dampers at the joints. We tuned the passive compliance of the performer's joints to find the value of compliance that produced the most reliable maneuvers. We used a single parameter to characterize the compliance of all the body joints. There was a clear choice for the best system compliance. More or less compliance at the joints led to less reliable performance. Inspection of the eigenfrequencies of the model revealed that the most reliable system had natural frequencies in the vicinity of the maximum twist rate of the maneuver. As in the layout somersault, it may be that a *balance* between the centrifugal forces of twisting and the spring forces of the joints is required to make the maneuver reliable.

While the reliability of the open loop, passive dynamic system was better than that of the prescribed motion system there is still room for improvement. There were sets of initial conditions that were 'close' to nominal for which landing attitude performance was seriously degraded. Could a different passive system improve reliability in this

region as well? Perhaps a *simple* active controller could complement the passive dynamics to produce an even more reliable system. Yeadon has discussed the need for good *timing* in certain maneuvers. Perhaps a simple active controller that changed the replay rate of a set of pre-recorded actions based on perceived errors could get the timing ‘right’ to further improve maneuver reliability.

7.4 Do Humans Use Passive Dynamics

We do not know if humans use a passive dynamic approach to stabilization of gymnastic maneuvers. This thesis can not prove or disprove the human use of such a strategy. The results of this thesis can only suggest that such a strategy is a viable one for particular maneuvers, or parts of maneuvers. What experiments could we do to learn more about how people perform these maneuvers?

It would be useful to measure the range of initial conditions from which athletes can reliably perform aerial maneuvers, and also measure their corresponding limb movements. If the variations in initial conditions and control movements were large then one may argue that dynamic compensation rather than a prescribed motion strategy was at work. One could look for correlations between different initial conditions and different control movements. Could a passive dynamic model explain any observed correlations?

Tests of the compliance of human muscle could reveal if the effective spring constants of human limbs are near the values predicted by theory to produce passively stable maneuvers. This could support a passive dynamic theory but not prove it’s use. Measurements of the electromyographic signal of the muscles may not help to decide what strategy people use. Even with accurate recordings of many performances of a maneuver it would be difficult to distinguish between a motor tape model and an active control model of muscle activation.

A difficulty in making a distinction between an active control strategy and an

open loop, passive dynamic strategy is that both approaches could produce a similar dynamic response. In fact, one may argue that if there is one clear technique to achieving a reliable maneuver then both strategies would have to use it. This possibility is illustrated by the fact that the active controller designed by Yeadon to stabilize the layout somersault used the same control effect as the passive strategy presented in this thesis. Both techniques used arm tilt to control body twist. Yeadon's technique depended upon sensing the twist rate of the body and using it to compute an appropriate arm tilt response. Whereas, in the passively stable case the arm tilt was produced from the inherent dynamics of the system. Passive dynamic control is a subset of the space of active controllers that require little if any on-line computation.

7.5 A Passive Dynamic Theory of Control Design?

Can passive dynamic control be formulated into a machine design and control theory? I did not use nor did I develop a consistent theory of passive dynamic design for controlling gymnastic maneuvers. However, beyond the educated guesses I used to find some answers, elements of linear and optimal control theory are central to the approach used to analyze the movements of this thesis. Linear analysis allows one to examine the behavior of a dynamic system in the neighborhood of a known solution. Biology provides us with many examples of movements that we know work. I have made explicit use of these known solutions to search for passive dynamic stability. Tucked and layout somersaults can be analyzed using linear methods. Linear analysis of the twisting somersault will be more difficult but may help reveal the important features of this maneuver. Searching for passive dynamic solutions to known movements could, I think, be developed into a theory. In fact, one may argue that a passive dynamic theory of control may consist of a restriction of the optimal control theory to passive dynamic elements. Extension of a passive dynamic theory to unknown move-

ment solutions will be more difficult, reflecting the complexity of non-linear systems. However, perhaps this is where the greatest pay-off from a passive dynamic theory could lie.

Why is it so easy to tell animal movement from machine movement? The richness of human and animal behavior reflects the complexity of the dynamic systems, their bodies, they are compelled to use. But this richness does not just come from complexity, it comes also from coordination. Relatively speaking, machine movement is still in its infancy. It would be a grand goal of any designer to make a machine that could move like an animal. It is an unfortunate consequence of the complexity of non-linear systems that non-linear control design techniques frequently rely upon cancellation of the dynamics in order to reach a solution. This approach risks the design of forced, uncoordinated behavior. Perhaps we should search for design techniques that embrace the inherent dynamics of a system rather than avoid them. Perhaps passive dynamic stability could act as a guiding principal in the design of graceful movement in machines. Perhaps it already serves this purpose in animal movement.

Appendix A

Appendix

A.1 Mathematica Code for Non-linear Equations of Motion

Following is the Mathematica code for deriving the non-linear equations of motion of the five d.o.f. system.

```
(* File for defining 3D equations of motion of a three link body with
links connected separately to the central body by two pin joints
allowing rotation about the x body axis. *)
(* same as man5dof.m except arm angles defined in terms of symmetric
and antisymmetric components phil = phia + phis, phir = phia - phis)

(* inertia matrices *)
ib = {{ib11,0,0},{0,ib22,0},{0,0,ib33}}; (* main body *)
il = {{il11,0,0},{0,il22,0},{0,0,il33}}; (* left limb *)
ir = {{ir11,0,0},{0,ir22,0},{0,0,ir33}}; (* right limb *)

(* body to joint vector for left arm, in arm coord. *)
bjl = {bjl1, bjl2, bjl3};

(* body to joint vector for right arm, in arm coord. *)
bjr = {bjr1, bjr2, bjr3};

(* inboard body to joint vector for left arm, in body coord. *)
ibjl = {ibjl1, ibjl2, ibjl3};

(* inboard body to joint vector for right arm, in body coord. *)
ibjr = {ibjr1, ibjr2, ibjr3};
```

```

(* transformation from body coordinates to limb left coordinates thru phi
   a pos. phi means limb left rotates positively relative to body *)
cbtol = {{1, 0, 0},
          {0, Cos[phia[t] + phis[t]], Sin[phia[t] + phis[t]]},
          {0, -Sin[phia[t] + phis[t]], Cos[phia[t] + phis[t]]}} ;

cltob = Transpose[cbtol];

(* transformation from body coordinates to limb right coordinates thru phir
   a pos. phir means limb right rotates positively relative to body *)
cbtor = {{1, 0, 0},
          {0, Cos[phia[t] - phis[t]], Sin[phia[t] - phis[t]]},
          {0, -Sin[phia[t] - phis[t]], Cos[phia[t] - phis[t]]}} ;

crtob = Transpose[cbtor];

(* inertia matrices of arms expressed in body coord *)
ilb = cltob . il . cbtol;
irb = crtob . ir . cbtor;

(* vector from net cg to body cg, in body coord *)
rhob = -(ml (ibjl - cltob.bjl) + mr (ibjr - crtob.bjr))/mt;

(* vector from net cg to left limb cg, in body coord *)
rhol = rhob + ibjl - cltob.bjl;

(* vector from net cg to right limb cg, in body coord *)
rhor = rhob + ibjr - crtob.bjr;

```

```

(* angular velocity of body in body coord.*)
wbi = {wb1[t], wb2[t], wb3[t]};

(* angular velocity of left limb w.r.t. body in body coord.*)
wlb = {phia'[t] + phis'[t], 0, 0};

(* angular velocity of limb in body coord.*)
wli = wbi + wlb;

(* angular velocity of right limb w.r.t. body in body coord.*)
wrh = {phia'[t] - phis'[t], 0, 0};

(* angular velocity of right limb in body coord.*)
wri = wbi + wrh;

(* wbi tilde matrix for cross products *)
wbitilde = {{0,-wbi[[3]],wbi[[2]]},{wbi[[3]],0,-wbi[[1]]},{-wbi[[2]],wbi[[1]],0}};

(* wli tilde matrix for cross products *)
wlitilde = {{0,-wli[[3]],wli[[2]]},{wli[[3]],0,-wli[[1]]},{-wli[[2]],wli[[1]],0}};

(* wri tilde matrix for cross products *)
writilde = {{0,-wri[[3]],wri[[2]]},{wri[[3]],0,-wri[[1]]},{-wri[[2]],wri[[1]],0}};

(* velocity of body c.g. *)
vbi = Expand[D[rhob,t] + wbitilde . rhob];

```

```

(* velocity of left limb c.g. *)
(* all components of rhol in body coord. so cross with wbi *)
vli = Expand[D[rhol,t] + wbitilde . rhol];

(* velocity of right limb c.g. *)
(* all components of rhor in body coord. so cross with wbi *)
vri = Expand[D[rhor,t] + wbitilde . rhor];

(* Matrix of Partial velocities :
columns correspond to generalized speeds
1 - wrt wb1[t]
2 - wrt wb2[t]
3 - wrt wb3[t]
4 - wrt phia'[t]
5 - wrt phis'[t]

rows correspond to body velocities
1 - vbi
2 - wbi
3 - vli
4 - wli
5 - vri
6 - wri

*)
pv = {
{D[vbi,wb1[t]],D[vbi,wb2[t]],D[vbi,wb3[t]],D[vbi,phia'[t]],D[vbi,phis'[t]]},

```

```

{D[wbi,wb1[t]],D[wbi,wb2[t]],D[wbi,wb3[t]],D[wbi,phia'[t]],D[wbi,phis'[t]]},
{D[vli,wb1[t]],D[vli,wb2[t]],D[vli,wb3[t]],D[vli,phia'[t]],D[vli,phis'[t]]},
{D[wli,wb1[t]],D[wli,wb2[t]],D[wli,wb3[t]],D[wli,phia'[t]],D[wli,phis'[t]]},
{D[vri,wb1[t]],D[vri,wb2[t]],D[vri,wb3[t]],D[vri,phia'[t]],D[vri,phis'[t]]},
{D[wri,wb1[t]],D[wri,wb2[t]],D[wri,wb3[t]],D[wri,phia'[t]],D[wri,phis'[t]]}

};

(* inertia forces and inertia torques *)
(* all vectors are expressed in body coordinates. See pp26 of notebook
   dated 6/4/93- for explanation of the following. ilb and irb are
   inertia of arms expressed in body coord therefore they are not
   constant in body coord. system. Therefore in taking total
   time derivative of ang. mom. need to take time derivative
   of ilb and wbi parts. Since everything in body coord. need
   to take cross product of ang. mom. with wbi.

*)

```

```

infb = mb wbitilde.vbi + mb D[vbi,t];
intb = D[ib,t] . wbi + ib . D[wbi,t] + wbitilde . ib . wbi;

infl = ml wbitilde.vli + ml D[vli,t];
intl = D[ilb,t] . wli + ilb . D[wli,t] + wbitilde . ilb . wli;

infr = mr wbitilde.vri + mr D[vri,t];
intr = D[irb,t] . wri + irb . D[wri,t] + wbitilde . irb . wri;

```

```
(* generalized inertia forces *)
```

```
fi1 = pv[[1,1]].infb + pv[[2,1]].intb +
      pv[[3,1]].infl + pv[[4,1]].intl +
      pv[[5,1]].infr + pv[[6,1]].intr;
```

```
fi2 = pv[[1,2]].infb + pv[[2,2]].intb +
      pv[[3,2]].infl + pv[[4,2]].intl +
      pv[[5,2]].infr + pv[[6,2]].intr;
```

```
fi3 = pv[[1,3]].infb + pv[[2,3]].intb +
      pv[[3,3]].infl + pv[[4,3]].intl +
      pv[[5,3]].infr + pv[[6,3]].intr;
```

```
fi4 = pv[[1,4]].infb + pv[[2,4]].intb +
      pv[[3,4]].infl + pv[[4,4]].intl +
      pv[[5,4]].infr + pv[[6,4]].intr;
```

```
fi5 = pv[[1,5]].infb + pv[[2,5]].intb +
      pv[[3,5]].infl + pv[[4,5]].intl +
      pv[[5,5]].infr + pv[[6,5]].intr;
```

```
(* External forces expressed in body coordinates *)
```

```
(*
```

positive acting on left limb, neg on body use wli,wbi
phi_rest is the spring rest length, should be less than
the nominal phil in order to make taul in steady rotation
cancel the centrifugal force.

*)

```
ftaul = {-ksh (phia[t] + phis[t]) - bsh(phia'[t] + phis'[t]),0,0};
ftaur = {-ksh (phia[t] - phis[t]) - bsh(phia'[t] - phis'[t]),0,0};
```

(*generalized external forces *)

```
fe1 = -pv[[2,1]].ftaul + pv[[4,1]].ftaul - pv[[2,1]].ftaur + pv[[6,1]].ftaur;
fe2 = -pv[[2,2]].ftaul + pv[[4,2]].ftaul - pv[[2,2]].ftaur + pv[[6,2]].ftaur;
fe3 = -pv[[2,3]].ftaul + pv[[4,3]].ftaul - pv[[2,3]].ftaur + pv[[6,3]].ftaur;
fe4 = -pv[[2,4]].ftaul + pv[[4,4]].ftaul - pv[[2,4]].ftaur + pv[[6,4]].ftaur;
fe5 = -pv[[2,5]].ftaul + pv[[4,5]].ftaul - pv[[2,5]].ftaur + pv[[6,5]].ftaur;
```

(* Expand necessary for later simplifications *)

```
efi1 = Expand[fi1];
efi2 = Expand[fi2];
efi3 = Expand[fi3];
efi4 = Expand[fi4];
efi5 = Expand[fi5];
```

```
efe1 = Expand[fe1];
efe2 = Expand[fe2];
efe3 = Expand[fe3];
efe4 = Expand[fe4];
efe5 = Expand[fe5];
```

A.2 Mathematica Code for Linearizing Equations of Motion

Following is the Mathematica code for analytically linearizing the non-linear equations of motion of the previous section.

```
(*  
file for linearizing man5dof_sym_antisym model for following case.  
  
here the arm movement is decomposed into symmetric and  
antisymmetric components. phil = x4 + x5, phir = x4 - x5  
x4 is the antisymmetric component  
x5 is the symmetric component  
  
vector from left limb c.g. to shoulder is {0,0,bj3} in limb coord.  
vector from right limb c.g. to shoulder is {0,0,bj3} in limb coord.  
mass of left and right limb are equal, mr = ml = m  
inertia of left and right limb are equal, Il=Ir  
vector from body c.g. to left shoulder is {0,ibj2,ibj3}in body coord  
vector from body c.g. to rt. shoulder is {0,-ibj2,ibj3}in body coord  
nominal body rotation rate is {0,W,0}  
  
left arm is nominally at phi0, right arm is nominally at -phi0,  
deviations in both arm movements are of equal sign and magnitude.
```

After the 5 dof linearized model is complete, a constraint equation of the form $x = B z$ can be applied to the system of equations. B represents the dependence of the original state x on another state vector z . z can be of lower dimension than x . Then the

transformed set of linear equations are produced as follows:

$B^T M B zddot + B^T C B zdot + B^T K B z$

This transformation can be applied in this file or in a later one that evaluates the numerical quantities.

```
*)
(* for yman model *)
(*
simplify = {bjl1->0, bjl2->0, bjl3->bj3,\n
            bjr1->0, bjr2->0, bjr3->bj3,\n
            ibjl1->0, ibjl2-> ibj2, ibjl3->ibj3,\n
            ibjr1->0, ibjr2-> -ibj2, ibjr3->ibj3,\n
            ir11->il11, ir22->il22, ir33->il33, mr->m, ml->m,\n
            mt->mb+2m};\n
*)
(* for yman model with no shoulder width and pvt at c.g.*)

simplify = {bjl1->0, bjl2->0, bjl3->bj3,\n
            bjr1->0, bjr2->0, bjr3->bj3,\n
            ibjl1->0, ibjl2-> 0, ibjl3->0,\n
            ibjr1->0, ibjr2-> 0, ibjr3->0,\n
            ir11->il11, ir22->il22, ir33->il33, mr->m, ml->m,\n
            mt->mb+2m};\n

sfi1 = efi1/.simplify;
sfi2 = efi2/.simplify;
```

```
sfi3 = efi3/.simplify;
sfi4 = efi4/.simplify;
sfi5 = efi5/.simplify;

(* Replace angular velocities and accelerations with corresponding
   euler angle expressions.
*)

S213 = {

{0,  Cos[th1[t]],  Sin[th1[t]]Cos[th2[t]]},
{0, -Sin[th1[t]],  Cos[th1[t]]Cos[th2[t]]},
{1,  0, -Sin[th2[t]]}

};

C213 = {

{ Cos[th1[t]]Cos[th3[t]] + Sin[th1[t]]Sin[th2[t]]Sin[th3[t]] ,
  Sin[th1[t]]Cos[th2[t]] ,
  -Cos[th1[t]]Sin[th3[t]] + Sin[th1[t]]Sin[th2[t]]Cos[th3[t]]} ,
{ -Sin[th1[t]]Cos[th3[t]] + Cos[th1[t]]Sin[th2[t]]Sin[th3[t]] ,
  Cos[th1[t]]Cos[th2[t]] ,
  Sin[th1[t]]Sin[th3[t]] + Cos[th1[t]]Sin[th2[t]]Cos[th3[t]]} ,
{ Cos[th2[t]]Sin[th3[t]] ,
  -Sin[th2[t]] ,
  Cos[th2[t]]Cos[th3[t]]}

};

thdot = {th1'[t], th2'[t], th3'[t]};
wba = {0,W,0};
wca = S213.thdot + C213.wba
```

```

wcadot = D[wca,t];

(* See Hughs pp 116 and my notebood 6/14/93 pp 33 to see linearization
of a steadily rotating system. This system steadily rotates
about the 2 axis with speed W.

```

the linearized states are not consistent with Hughs notation so
that the mass matrix retains its nominal form.

```

x1  tilt  angle          (th2)
x2  dev. from nominal sault angle (th3)
x3  twist angle          (th1)
x4  dev of both arms in anit-symmetric mode form Phi0
x5  dev of both arms in symmetric mode form Phi0
*)


```

```

eulerreplace = {wb1[t] -> wca[[1]], wb2[t] -> wca[[2]], wb3[t] -> wca[[3]],
wb1'[t] -> wcadot[[1]], wb2'[t] -> wcadot[[2]], wb3'[t] -> wcadot[[3]]};

linname = {phia[t] -> x4, phis[t] -> x5, \
th1[t] -> x3, th2[t] -> x1, th3[t] -> x2, \
th1'[t] -> xdot3 W, th2'[t] -> xdot1 W, th3'[t] -> xdot2 W, \
phia'[t] -> xdot4 W, phis'[t] -> xdot5 W, \
th1''[t] -> xddot3 (W W), th2''[t] -> xddot1 (W W), th3''[t] -> xddot2 (W W), \
phia''[t] -> xddot4 (W W), \
phis''[t] -> xddot5 (W W)};

lincond = {xdot1->0, xdot2->0, xdot3->0, xdot4->0, xdot5->0, \

```

```
x1->0, x2->0, x3->0, x4->0, x5->phi0};

eulfi1 = Expand[sfi1/.eulerreplace];
eulfi2 = Expand[sfi2/.eulerreplace];
eulfi3 = Expand[sfi3/.eulerreplace];
eulfi4 = Expand[sfi4/.eulerreplace];
eulfi5 = Expand[sfi5/.eulerreplace];

renfi1 = Expand[eulfi1/.linname];
renfi2 = Expand[eulfi2/.linname];
renfi3 = Expand[eulfi3/.linname];
renfi4 = Expand[eulfi4/.linname];
renfi5 = Expand[eulfi5/.linname];

renfe1 = Expand[efe1/.linname];
renfe2 = Expand[efe2/.linname];
renfe3 = Expand[efe3/.linname];
renfe4 = Expand[efe4/.linname];
renfe5 = Expand[efe5/.linname];

mm11 = Coefficient[renfi1,xddot1]/.lincond;
mm12 = Coefficient[renfi1,xddot2]/.lincond;
mm13 = Coefficient[renfi1,xddot3]/.lincond;
mm14 = Coefficient[renfi1,xddot4]/.lincond;
mm15 = Coefficient[renfi1,xddot5]/.lincond;

mm21 = Coefficient[renfi2,xddot1]/.lincond;
mm22 = Coefficient[renfi2,xddot2]/.lincond;
```

```
mm23 = Coefficient[renfi2,xddot3]/.lincond;
mm24 = Coefficient[renfi2,xddot4]/.lincond;
mm25 = Coefficient[renfi2,xddot5]/.lincond;

mm31 = Coefficient[renfi3,xddot1]/.lincond;
mm32 = Coefficient[renfi3,xddot2]/.lincond;
mm33 = Coefficient[renfi3,xddot3]/.lincond;
mm34 = Coefficient[renfi3,xddot4]/.lincond;
mm35 = Coefficient[renfi3,xddot5]/.lincond;

mm41 = Coefficient[renfi4,xddot1]/.lincond;
mm42 = Coefficient[renfi4,xddot2]/.lincond;
mm43 = Coefficient[renfi4,xddot3]/.lincond;
mm44 = Coefficient[renfi4,xddot4]/.lincond;
mm45 = Coefficient[renfi4,xddot5]/.lincond;

mm51 = Coefficient[renfi5,xddot1]/.lincond;
mm52 = Coefficient[renfi5,xddot2]/.lincond;
mm53 = Coefficient[renfi5,xddot3]/.lincond;
mm54 = Coefficient[renfi5,xddot4]/.lincond;
mm55 = Coefficient[renfi5,xddot5]/.lincond;

(* this gets the d.c. forcing part *)

dc1 = renfi1/.lincond;
dc2 = renfi2/.lincond;
dc3 = renfi3/.lincond;
dc4 = renfi4/.lincond;
```

```
dc5 = renfi5/.lincond;

c1 = renfi1/.{xddot1->0,xddot2->0,xddot3->0,xddot4->0,xddot5->0};
c2 = renfi2/.{xddot1->0,xddot2->0,xddot3->0,xddot4->0,xddot5->0};
c3 = renfi3/.{xddot1->0,xddot2->0,xddot3->0,xddot4->0,xddot5->0};
c4 = renfi4/.{xddot1->0,xddot2->0,xddot3->0,xddot4->0,xddot5->0};
c5 = renfi5/.{xddot1->0,xddot2->0,xddot3->0,xddot4->0,xddot5->0};

dcdx11 = D[c1,x1]/.lincond;
dcdx12 = D[c1,x2]/.lincond;
dcdx13 = D[c1,x3]/.lincond;
dcdx14 = D[c1,x4]/.lincond;
dcdx15 = D[c1,x5]/.lincond;

dcdx21 = D[c2,x1]/.lincond;
dcdx22 = D[c2,x2]/.lincond;
dcdx23 = D[c2,x3]/.lincond;
dcdx24 = D[c2,x4]/.lincond;
dcdx25 = D[c2,x5]/.lincond;

dcdx31 = D[c3,x1]/.lincond;
dcdx32 = D[c3,x2]/.lincond;
dcdx33 = D[c3,x3]/.lincond;
dcdx34 = D[c3,x4]/.lincond;
dcdx35 = D[c3,x5]/.lincond;

dcdx41 = D[c4,x1]/.lincond;
dcdx42 = D[c4,x2]/.lincond;
```

```
dcdx43 = D[c4,x3]/.lincond;
dcdx44 = D[c4,x4]/.lincond;
dcdx45 = D[c4,x5]/.lincond;

dcdx51 = D[c5,x1]/.lincond;
dcdx52 = D[c5,x2]/.lincond;
dcdx53 = D[c5,x3]/.lincond;
dcdx54 = D[c5,x4]/.lincond;
dcdx55 = D[c5,x5]/.lincond;

dcdxdot11 = D[c1,xdot1]/.lincond;
dcdxdot12 = D[c1,xdot2]/.lincond;
dcdxdot13 = D[c1,xdot3]/.lincond;
dcdxdot14 = D[c1,xdot4]/.lincond;
dcdxdot15 = D[c1,xdot5]/.lincond;

dcdxdot21 = D[c2,xdot1]/.lincond;
dcdxdot22 = D[c2,xdot2]/.lincond;
dcdxdot23 = D[c2,xdot3]/.lincond;
dcdxdot24 = D[c2,xdot4]/.lincond;
dcdxdot25 = D[c2,xdot5]/.lincond;

dcdxdot31 = D[c3,xdot1]/.lincond;
dcdxdot32 = D[c3,xdot2]/.lincond;
dcdxdot33 = D[c3,xdot3]/.lincond;
dcdxdot34 = D[c3,xdot4]/.lincond;
dcdxdot35 = D[c3,xdot5]/.lincond;
```

```
dcdxdot41 = D[c4,xdot1]/.lincond;
dcdxdot42 = D[c4,xdot2]/.lincond;
dcdxdot43 = D[c4,xdot3]/.lincond;
dcdxdot44 = D[c4,xdot4]/.lincond;
dcdxdot45 = D[c4,xdot5]/.lincond;

dcdxdot51 = D[c5,xdot1]/.lincond;
dcdxdot52 = D[c5,xdot2]/.lincond;
dcdxdot53 = D[c5,xdot3]/.lincond;
dcdxdot54 = D[c5,xdot4]/.lincond;
dcdxdot55 = D[c5,xdot5]/.lincond;

(* this is the linearization of the external forces *)

dtaudxdot11 = D[renfe1,xdot1]/.lincond;
dtaudxdot12 = D[renfe1,xdot2]/.lincond;
dtaudxdot13 = D[renfe1,xdot3]/.lincond;
dtaudxdot14 = D[renfe1,xdot4]/.lincond;
dtaudxdot15 = D[renfe1,xdot5]/.lincond;

dtaudxdot21 = D[renfe2,xdot1]/.lincond;
dtaudxdot22 = D[renfe2,xdot2]/.lincond;
dtaudxdot23 = D[renfe2,xdot3]/.lincond;
dtaudxdot24 = D[renfe2,xdot4]/.lincond;
dtaudxdot25 = D[renfe2,xdot5]/.lincond;
```

```
dtaudxdot31 = D[renfe3,xdot1]/.lincond;
dtaudxdot32 = D[renfe3,xdot2]/.lincond;
dtaudxdot33 = D[renfe3,xdot3]/.lincond;
dtaudxdot34 = D[renfe3,xdot4]/.lincond;
dtaudxdot35 = D[renfe3,xdot5]/.lincond;

dtaudxdot41 = D[renfe4,xdot1]/.lincond;
dtaudxdot42 = D[renfe4,xdot2]/.lincond;
dtaudxdot43 = D[renfe4,xdot3]/.lincond;
dtaudxdot44 = D[renfe4,xdot4]/.lincond;
dtaudxdot45 = D[renfe4,xdot5]/.lincond;

dtaudxdot51 = D[renfe5,xdot1]/.lincond;
dtaudxdot52 = D[renfe5,xdot2]/.lincond;
dtaudxdot53 = D[renfe5,xdot3]/.lincond;
dtaudxdot54 = D[renfe5,xdot4]/.lincond;
dtaudxdot55 = D[renfe5,xdot5]/.lincond;

dtaudx11 = D[renfe1,x1]/.lincond;
dtaudx12 = D[renfe1,x2]/.lincond;
dtaudx13 = D[renfe1,x3]/.lincond;
dtaudx14 = D[renfe1,x4]/.lincond;
dtaudx15 = D[renfe1,x5]/.lincond;

dtaudx21 = D[renfe2,x1]/.lincond;
dtaudx22 = D[renfe2,x2]/.lincond;
dtaudx23 = D[renfe2,x3]/.lincond;
```

```
dtaudx24 = D[renfe2,x4]/.lincond;
dtaudx25 = D[renfe2,x5]/.lincond;

dtaudx31 = D[renfe3,x1]/.lincond;
dtaudx32 = D[renfe3,x2]/.lincond;
dtaudx33 = D[renfe3,x3]/.lincond;
dtaudx34 = D[renfe3,x4]/.lincond;
dtaudx35 = D[renfe3,x5]/.lincond;

dtaudx41 = D[renfe4,x1]/.lincond;
dtaudx42 = D[renfe4,x2]/.lincond;
dtaudx43 = D[renfe4,x3]/.lincond;
dtaudx44 = D[renfe4,x4]/.lincond;
dtaudx45 = D[renfe4,x5]/.lincond;

dtaudx51 = D[renfe5,x1]/.lincond;
dtaudx52 = D[renfe5,x2]/.lincond;
dtaudx53 = D[renfe5,x3]/.lincond;
dtaudx54 = D[renfe5,x4]/.lincond;
dtaudx55 = D[renfe5,x5]/.lincond;
```

A.3 Parameters of the Five D.O.F. Linear Model

In this section I present the algebraic expressions for the elements of the linear dynamic model used to study passive layout stability. These elements were computed from the symbolic linearization of the full non-linear dynamic equations of the five d.o.f. system. The equations of motion and the associated matrices are repeated from Chapter 4 Equations 4.1-4.6.

$$M\ddot{x} + \Omega(G + D)\dot{x} + \Omega^2(K + K')x = 0$$

where

$$M = \begin{bmatrix} m_{11} & 0 & m_{13} & 0 & 0 \\ 0 & m_{22} & 0 & 0 & 0 \\ m_{13} & 0 & m_{33} & 0 & 0 \\ 0 & 0 & 0 & m_{44} & 0 \\ 0 & 0 & 0 & 0 & m_{55} \end{bmatrix}$$

$$G = \begin{bmatrix} 0 & g_{12} & 0 & 0 & 0 \\ -g_{12} & 0 & g_{23} & 0 & 0 \\ 0 & -g_{23} & 0 & 0 & 0 \\ 0 & 0 & 0 & 0 & g_{45} \\ 0 & 0 & 0 & -g_{45} & 0 \end{bmatrix}$$

$$D = \begin{bmatrix} 0 & 0 & 0 & 0 & 0 \\ 0 & 0 & 0 & 0 & 0 \\ 0 & 0 & 2b'_{sh}/\Omega & 0 & 0 \\ 0 & 0 & 0 & 0 & 0 \\ 0 & 0 & 0 & 0 & 2b'_{sh}/\Omega \end{bmatrix}$$

$$K = \begin{bmatrix} k_{11} & 0 & k_{13} & 0 & 0 \\ 0 & k_{22} & 0 & 0 & 0 \\ k_{31} & 0 & k_{33} & 0 & 0 \\ 0 & 0 & 0 & 0 & 0 \\ 0 & 0 & 0 & 0 & k_{55} \end{bmatrix}$$

$$K' = \begin{bmatrix} 0 & 0 & 0 & 0 & 0 \\ 0 & 0 & 0 & 0 & 0 \\ 0 & 0 & 2k_{sh}/\Omega^2 & 0 & 0 \\ 0 & 0 & 0 & 0 & 0 \\ 0 & 0 & 0 & 0 & 2k_{sh}/\Omega^2 \end{bmatrix}$$

The state vector, x , is comprised of (in order): β - the tilt angle, γ - the twist angle, ϕ_a - the asymmetric deviation of the two arms from the nominal arm angle, α - the deviation of the somersault angle from the frame steadily rotating at rate Ω , and ϕ_s - the symmetric deviation of the two arms from the nominal arm angle.

The individual elements of the above matrices are given below.

$$m_{11} = (Ib_1 + 2Il_1 + 2rb_2^2m_l + 2rb_3^2m_l + \frac{8rb_3^2m_l^3}{(2m_l+m_b)^2} + \frac{4rb_3^2m_l^2m_b}{(2m_l+m_b)^2} - \frac{8rb_3^2m_l^2}{2m_l+m_b} - 4rl_3rb_3m_l\cos(\Phi_\theta) - \frac{16rl_3rb_3m_l^3\cos(\Phi_\theta)}{(2m_l+m_b)^2} - \frac{8rl_3rb_3m_l^2m_b\cos(\Phi_\theta)}{(2m_l+m_b)^2} + \frac{16rl_3rb_3m_l^2\cos(\Phi_\theta)}{2m_l+m_b} + 2rl_3^2m_l\cos(\Phi_\theta)^2 + \frac{8rl_3^2m_l^3\cos(\Phi_\theta)^2}{(2m_l+m_b)^2} + \frac{4rl_3^2m_l^2m_b\cos(\Phi_\theta)^2}{(2m_l+m_b)^2} - \frac{8rl_3^2m_l^2\cos(\Phi_\theta)^2}{2m_l+m_b} + 4rl_3rb_2m_l\sin(\Phi_\theta) + 2rl_3^2m_l\sin(\Phi_\theta)^2)$$

$$m_{13} = (2Il_1 - 2rl_3rb_3m_l\cos(\Phi_\theta) - \frac{8rl_3rb_3m_l^3\cos(\Phi_\theta)}{(2m_l+m_b)^2} - \frac{4rl_3rb_3m_l^2m_b\cos(\Phi_\theta)}{(2m_l+m_b)^2} + \frac{8rl_3rb_3m_l^2\cos(\Phi_\theta)}{2m_l+m_b} + 2rl_3^2m_l\cos(\Phi_\theta)^2 +$$

$$\frac{8 r l_3^2 m_l^3 \cos(\Phi_\theta)^2}{(2 m_l + m_b)^2} + \frac{4 r l_3^2 m_l^2 m_b \cos(\Phi_\theta)^2}{(2 m_l + m_b)^2} - \frac{8 r l_3^2 m_l^2 \cos(\Phi_\theta)^2}{2 m_l + m_b} + \\ 2 r l_3 r b_2 m_l \sin(\Phi_\theta) + 2 r l_3^2 m_l \sin(\Phi_\theta)^2)$$

$$m_{22} = (Ib_3 + 2 r b_2^2 m_l + 2 I l_3 \cos(\Phi_\theta)^2 + 4 r l_3 r b_2 m_l \sin(\Phi_\theta) + \\ 2 I l_2 \sin(\Phi_\theta)^2 + 2 r l_3^2 m_l \sin(\Phi_\theta)^2)$$

$$m_{33} = (2 I l_1 + 2 r l_3^2 m_l \cos(\Phi_\theta)^2 + \frac{8 r l_3^2 m_l^3 \cos(\Phi_\theta)^2}{(2 m_l + m_b)^2} + \\ \frac{4 r l_3^2 m_l^2 m_b \cos(\Phi_\theta)^2}{(2 m_l + m_b)^2} - \frac{8 r l_3^2 m_l^2 \cos(\Phi_\theta)^2}{2 m_l + m_b} + 2 r l_3^2 m_l \sin(\Phi_\theta)^2)$$

$$m_{44} = (Ib_2 + 2 r b_3^2 m_l + \frac{8 r b_3^2 m_l^3}{(2 m_l + m_b)^2} + \frac{4 r b_3^2 m_l^2 m_b}{(2 m_l + m_b)^2} - \frac{8 r b_3^2 m_l^2}{2 m_l + m_b} - \\ 4 r l_3 r b_3 m_l \cos(\Phi_\theta) - \frac{16 r l_3 r b_3 m_l^3 \cos(\Phi_\theta)}{(2 m_l + m_b)^2} - \frac{8 r l_3 r b_3 m_l^2 m_b \cos(\Phi_\theta)}{(2 m_l + m_b)^2} + \\ \frac{16 r l_3 r b_3 m_l^2 \cos(\Phi_\theta)}{2 m_l + m_b} + 2 I l_2 \cos(\Phi_\theta)^2 + 2 r l_3^2 m_l \cos(\Phi_\theta)^2 + \\ \frac{8 r l_3^2 m_l^3 \cos(\Phi_\theta)^2}{(2 m_l + m_b)^2} + \frac{4 r l_3^2 m_l^2 m_b \cos(\Phi_\theta)^2}{(2 m_l + m_b)^2} - \frac{8 r l_3^2 m_l^2 \cos(\Phi_\theta)^2}{2 m_l + m_b} + \\ 2 I l_3 \sin(\Phi_\theta)^2)$$

$$m_{55} = (2 I l_1 + 2 r l_3^2 m_l \cos(\Phi_\theta)^2 + 2 r l_3^2 m_l \sin(\Phi_\theta)^2 + \frac{8 r l_3^2 m_l^3 \sin(\Phi_\theta)^2}{(2 m_l + m_b)^2} + \\ \frac{4 r l_3^2 m_l^2 m_b \sin(\Phi_\theta)^2}{(2 m_l + m_b)^2} - \frac{8 r l_3^2 m_l^2 \sin(\Phi_\theta)^2}{2 m_l + m_b})$$

$$g_{12} = (Ib_1 - Ib_2 + Ib_3 + 2 I l_1 + 4 r b_2^2 m_l - 2 I l_2 \cos(\Phi_\theta)^2 + \\ 2 I l_3 \cos(\Phi_\theta)^2 + 8 r l_3 r b_2 m_l \sin(\Phi_\theta) + 2 I l_2 \sin(\Phi_\theta)^2 - 2 I l_3 \sin(\Phi_\theta)^2 + \\ 4 r l_3^2 m_l \sin(\Phi_\theta)^2)$$

$$g_{23} = (-2 I_{l_1} + 2 I_{l_2} \cos(\Phi_\theta)^2 - 2 I_{l_3} \cos(\Phi_\theta)^2 - 4 r_{l_3} r_{b_2} m_l \sin(\Phi_\theta) - 2 I_{l_2} \sin(\Phi_\theta)^2 + 2 I_{l_3} \sin(\Phi_\theta)^2 - 4 r_{l_3}^2 m_l \sin(\Phi_\theta)^2)$$

$$g_{45} = (4 r_{l_3} r_{b_3} m_l \sin(\Phi_\theta) + \frac{16 r_{l_3} r_{b_3} m_l^3 \sin(\Phi_\theta)}{(2 m_l + m_b)^2} + \frac{8 r_{l_3} r_{b_3} m_l^2 m_b \sin(\Phi_\theta)}{(2 m_l + m_b)^2} - \frac{16 r_{l_3} r_{b_3} m_l^2 \sin(\Phi_\theta)}{2 m_l + m_b} - 4 I_{l_2} \cos(\Phi_\theta) \sin(\Phi_\theta) + 4 I_{l_3} \cos(\Phi_\theta) \sin(\Phi_\theta) - 4 r_{l_3}^2 m_l \cos(\Phi_\theta) \sin(\Phi_\theta) - \frac{16 r_{l_3}^2 m_l^3 \cos(\Phi_\theta) \sin(\Phi_\theta)}{(2 m_l + m_b)^2} - \frac{8 r_{l_3}^2 m_l^2 m_b \cos(\Phi_\theta) \sin(\Phi_\theta)}{(2 m_l + m_b)^2} + \frac{16 r_{l_3}^2 m_l^2 \cos(\Phi_\theta) \sin(\Phi_\theta)}{2 m_l + m_b})$$

$$k_{11} = (I_{b_2} - I_{b_3} - 2 r_{b_2}^2 m_l + 2 r_{b_3}^2 m_l + \frac{8 r_{b_3}^2 m_l^3}{(2 m_l + m_b)^2} + \frac{4 r_{b_3}^2 m_l^2 m_b}{(2 m_l + m_b)^2} - \frac{8 r_{b_3}^2 m_l^2}{2 m_l + m_b} - 4 r_{l_3} r_{b_3} m_l \cos(\Phi_\theta) - \frac{16 r_{l_3} r_{b_3} m_l^3 \cos(\Phi_\theta)}{(2 m_l + m_b)^2} - \frac{8 r_{l_3} r_{b_3} m_l^2 m_b \cos(\Phi_\theta)}{(2 m_l + m_b)^2} + \frac{16 r_{l_3} r_{b_3} m_l^2 \cos(\Phi_\theta)}{2 m_l + m_b} + 2 I_{l_2} \cos(\Phi_\theta)^2 - 2 I_{l_3} \cos(\Phi_\theta)^2 + 2 r_{l_3}^2 m_l \cos(\Phi_\theta)^2 + \frac{8 r_{l_3}^2 m_l^3 \cos(\Phi_\theta)^2}{(2 m_l + m_b)^2} + \frac{4 r_{l_3}^2 m_l^2 m_b \cos(\Phi_\theta)^2}{(2 m_l + m_b)^2} - \frac{8 r_{l_3}^2 m_l^2 \cos(\Phi_\theta)^2}{2 m_l + m_b} - 4 r_{l_3} r_{b_2} m_l \sin(\Phi_\theta) - 2 I_{l_2} \sin(\Phi_\theta)^2 + 2 I_{l_3} \sin(\Phi_\theta)^2 - 2 r_{l_3}^2 m_l \sin(\Phi_\theta)^2)$$

$$k_{13} = (-2 r_{l_3} r_{b_3} m_l \cos(\Phi_\theta) - \frac{8 r_{l_3} r_{b_3} m_l^3 \cos(\Phi_\theta)}{(2 m_l + m_b)^2} - \frac{4 r_{l_3} r_{b_3} m_l^2 m_b \cos(\Phi_\theta)}{(2 m_l + m_b)^2} + \frac{8 r_{l_3} r_{b_3} m_l^2 \cos(\Phi_\theta)}{2 m_l + m_b} + 2 I_{l_2} \cos(\Phi_\theta)^2 - 2 I_{l_3} \cos(\Phi_\theta)^2 + 2 r_{l_3}^2 m_l \cos(\Phi_\theta)^2 + \frac{8 r_{l_3}^2 m_l^3 \cos(\Phi_\theta)^2}{(2 m_l + m_b)^2} + \frac{4 r_{l_3}^2 m_l^2 m_b \cos(\Phi_\theta)^2}{(2 m_l + m_b)^2} - \frac{8 r_{l_3}^2 m_l^2 \cos(\Phi_\theta)^2}{2 m_l + m_b} - 2 r_{l_3} r_{b_2} m_l \sin(\Phi_\theta) - 2 I_{l_2} \sin(\Phi_\theta)^2 + 2 I_{l_3} \sin(\Phi_\theta)^2 - 2 r_{l_3}^2 m_l \sin(\Phi_\theta)^2)$$

$$k_{22} = (-Ib_1 + Ib_2 - 2Il_1 - 2rb_2^2 m_l + 2Il_2 \cos(\Phi_\theta)^2 - 4rl_3 rb_2 m_l \sin(\Phi_\theta) + 2Il_3 \sin(\Phi_\theta)^2 - 2rl_3^2 m_l \sin(\Phi_\theta)^2)$$

$$k_{33} = (-2rl_3 rb_3 m_l \cos(\Phi_\theta) - \frac{8rl_3 rb_3 m_l^3 \cos(\Phi_\theta)}{(2m_l + m_b)^2} - \frac{4rl_3 rb_3 m_l^2 m_b \cos(\Phi_\theta)}{(2m_l + m_b)^2} + \frac{8rl_3 rb_3 m_l^2 \cos(\Phi_\theta)}{2m_l + m_b} + 2Il_2 \cos(\Phi_\theta)^2 - 2Il_3 \cos(\Phi_\theta)^2 + 2rl_3^2 m_l \cos(\Phi_\theta)^2 + \frac{8rl_3^2 m_l^3 \cos(\Phi_\theta)^2}{(2m_l + m_b)^2} + \frac{4rl_3^2 m_l^2 m_b \cos(\Phi_\theta)^2}{(2m_l + m_b)^2} - \frac{8rl_3^2 m_l^2 \cos(\Phi_\theta)^2}{2m_l + m_b} - 2Il_2 \sin(\Phi_\theta)^2 + 2Il_3 \sin(\Phi_\theta)^2 - 2rl_3^2 m_l \sin(\Phi_\theta)^2)$$

$$k_{55} = (-2rl_3 rb_3 m_l \cos(\Phi_\theta) - \frac{8rl_3 rb_3 m_l^3 \cos(\Phi_\theta)}{(2m_l + m_b)^2} - \frac{4rl_3 rb_3 m_l^2 m_b \cos(\Phi_\theta)}{(2m_l + m_b)^2} + \frac{8rl_3 rb_3 m_l^2 \cos(\Phi_\theta)}{2m_l + m_b} + 2Il_2 \cos(\Phi_\theta)^2 - 2Il_3 \cos(\Phi_\theta)^2 + 2rl_3^2 m_l \cos(\Phi_\theta)^2 + \frac{8rl_3^2 m_l^3 \cos(\Phi_\theta)^2}{(2m_l + m_b)^2} + \frac{4rl_3^2 m_l^2 m_b \cos(\Phi_\theta)^2}{(2m_l + m_b)^2} - \frac{8rl_3^2 m_l^2 \cos(\Phi_\theta)^2}{2m_l + m_b} - 2Il_2 \sin(\Phi_\theta)^2 + 2Il_3 \sin(\Phi_\theta)^2 - 2rl_3^2 m_l \sin(\Phi_\theta)^2 - \frac{8rl_3^2 m_l^3 \sin(\Phi_\theta)^2}{(2m_l + m_b)^2} - \frac{4rl_3^2 m_l^2 m_b \sin(\Phi_\theta)^2}{(2m_l + m_b)^2} + \frac{8rl_3^2 m_l^2 \sin(\Phi_\theta)^2}{2m_l + m_b})$$

A.4 Analytic Solution

Solving for the torque-free motion of a rigid body tumbling in space is one of the classic problems of dynamics. Given the limited value of numerical integration as a means of studying dynamics problems before the advent of the digital computer, much effort was applied to finding an analytic solution to the governing equations of motion. The analytic solution provides the angular velocity of the body in a body fixed principle axes system and the attitude of the principle axis system with respect to an inertial coordinate system [Hughes 86]. The contribution that these analytic solutions offer today is a concise description of the minimal number of states and non-dimensional parameters that govern rigid body rotation. The analytic solutions also give rise to elegant geometric interpretations of the motion that helps provide some intuition of this otherwise complex movement.

I present the analytic solution for a tri-inertial body. A tri-inertial body is one in which each of the principal inertias is distinct. Without loss of generality for the rest of this section I will insist that, $I_1 > I_2 > I_3$. The analytic solution for rotation of a tri-inertial body uses the Jacobian elliptic functions. Elliptic functions are a generalization of the circular functions, sine and cosine, that originated from an effort to compute the circumference of an ellipse [Bowman 61]. The Euler angles describing the body attitude with respect to inertial space can also be written using elliptic functions.

Two integrals of motion are essential in the analytic solution for torque free rigid body motion. These represent conservation of angular momentum \vec{h} and conservation of kinetic energy T .

$$h^2 = I_1^2\omega_1^2 + I_2^2\omega_2^2 + I_3^2\omega_3^2 \quad (\text{A.1})$$

$$2T = I_1\omega_1^2 + I_2\omega_2^2 + I_3\omega_3^2 \quad (\text{A.2})$$

For a fixed angular momentum, the kinetic energy of rotation is bounded above and below by the kinetic energy of two pure spin solutions. The highest possible energy

state corresponds to rotation about the minor principal axis and the lowest energy state corresponds to rotation about the major principal axis. A continuum of solutions of rotational motion of a rigid body exist, each corresponding to a different energy level, between these two bounds,

$$\frac{h^2}{2I_1} \leq T \leq \frac{h^2}{2I_3}$$

The qualitative nature of the solution is divided into two regions between these bounds and separated by the solution of pure spin about the middle principal axis. The following parameter is useful in distinguishing between the two qualitatively different solutions.

$$I = \frac{h^2}{2T}$$

I has units of inertia. The bounds on I corresponding to the bounds on energy are

$$I_1 \geq I \geq I_3$$

$I = I_1$, $I = I_2$, and $I = I_3$ correspond to the pure spin solutions.

The maximum amplitude of the body fixed angular velocities can be obtained directly from the two integrals of motion.

$$\omega_{1m} = h \left[\frac{I - I_3}{II_1(I_1 - I_3)} \right]^{1/2} \quad (A.3)$$

$$\omega_{3m} = h \left[\frac{I_1 - I}{II_3(I_1 - I_3)} \right]^{1/2} \quad (A.4)$$

$$\omega_{2m} = h \left[\frac{I_1 - I}{II_2(I_1 - I_2)} \right]^{1/2} \quad (I_1 \geq I > I_2) \quad (A.5)$$

$$\omega_{2m} = \frac{h}{I_2} \quad (I = I_2) \quad (A.6)$$

$$\omega_{2m} = h \left[\frac{I - I_3}{II_2(I_2 - I_3)} \right]^{1/2} \quad (I_2 > I \geq I_3) \quad (A.7)$$

Next, the analytic solution for the angular velocity is given for the case of $I_1 \geq I > I_2$

$$\omega_1 = s_1 \omega_{1m} dn(\tau; k) \quad (\text{A.8})$$

$$\omega_2 = s_2 \omega_{2m} sn(\tau; k) \quad (\text{A.9})$$

$$\omega_3 = s_3 \omega_{3m} cn(\tau; k) \quad (\text{A.10})$$

$$\tau = h \left[\frac{(I_1 - I_2)(I - I_3)}{II_1 I_2 I_3} \right]^{1/2} (t - t_0) \quad (\text{A.11})$$

$$k = \left[\frac{(I_2 - I_3)(I_1 - I)}{(I_1 - I_2)(I - I_3)} \right]^{1/2} \quad (\text{A.12})$$

and similarly for $I_2 > I \geq I_3$

$$\omega_1 = s_1 \omega_{1m} cn(\tau; k) \quad (\text{A.13})$$

$$\omega_2 = s_2 \omega_{2m} sn(\tau; k) \quad (\text{A.14})$$

$$\omega_3 = s_3 \omega_{3m} dn(\tau; k) \quad (\text{A.15})$$

$$\tau = h \left[\frac{(I_2 - I_3)(I_1 - I)}{II_1 I_2 I_3} \right]^{1/2} (t - t_0) \quad (\text{A.16})$$

$$k = \left[\frac{(I_1 - I_2)(I - I_3)}{(I_2 - I_3)(I_1 - I)} \right]^{1/2} \quad (\text{A.17})$$

The coefficients s_1, s_2 and s_3 are all ± 1 such that $s_1 s_2 s_3 = -1$, allowing four combinations of signs. The Jacobian elliptic functions, (sn, cn and dn), depend on the scaled time, τ and the modulus k . When $k - > 0$ $sn, cn, dn - > \sin, \cos, 1$.

To complete the solution of the tumbling motion we require the attitude of the body as a function of time. Since angular momentum is conserved, the inertially fixed angular momentum vector provides the reference with which to measure body attitude. The components of angular momentum as measured in the body fixed axis

system is given by

$$\begin{bmatrix} h_1 \\ h_2 \\ h_3 \end{bmatrix} = \begin{bmatrix} I_1\omega_1 \\ I_2\omega_2 \\ I_3\omega_3 \end{bmatrix} \quad (\text{A.18})$$

Another expression for this vector can be obtained by projecting the inertially fixed angular momentum vector onto the body fixed axes using the matrix C_{bi} (2.2). Since the orientation of the inertial coordinate system is arbitrary, we choose it to be oriented such that the angular momentum vector is oriented entirely along the inertial y axis. With this assumption in mind, equating the components of these two expressions for angular momentum gives

$$\begin{bmatrix} I_1\omega_1 \\ I_2\omega_2 \\ I_3\omega_3 \end{bmatrix} = \begin{bmatrix} S_\Psi C_\Theta h \\ C_\Psi C_\Theta h \\ -S_\Theta h \end{bmatrix} \quad (\text{A.19})$$

Solutions for two of the Euler angles are available immediately as

$$\Theta = \sin^{-1} \left[\frac{I_3\omega_3}{h} \right] \quad (\text{A.20})$$

$$\Psi = \tan^{-1} \left[\frac{I_1\omega_1}{I_2\omega_2} \right] \quad (\text{A.21})$$

The solution for Φ requires significantly more work. First we use equation (2.4) to substitute for ω_i in (A.19).

$$\begin{aligned} I_1(S_\Psi C_\Theta \dot{\Phi} + C_\Psi \dot{\Theta}) &= S_\Psi C_\Theta h \\ I_2(C_\Psi C_\Theta \dot{\Phi} - S_\Psi \dot{\Theta}) &= C_\Psi C_\Theta h \\ I_3(-S_\Theta \dot{\Phi} + \dot{\Psi}) &= -S_\Theta h \end{aligned}$$

Solving for $\dot{\Phi}$ from the first two of these equations yields

$$\dot{\Phi} = \frac{h(I_2 S_\Psi^2 + I_1 C_\Psi^2)}{I_1 I_2} \quad (\text{A.22})$$

To proceed we need an expression for C_Ψ^2 and S_Ψ^2 . Using equation A.21, we obtain

$$\tan \Psi^2 = \frac{(I_1 \omega_1)^2}{(I_2 \omega_2)^2}$$

Using trigonometric identities we obtain

$$\sin^2 \Psi = \frac{(I_1 \omega_1)^2}{(I_1 \omega_1)^2 + (I_2 \omega_2)^2} \quad (\text{A.23})$$

$$\cos^2 \Psi = \frac{(I_2 \omega_2)^2}{(I_1 \omega_1)^2 + (I_2 \omega_2)^2} \quad (\text{A.24})$$

Using these in equation A.22 we obtain

$$\dot{\Phi} = h \left[\frac{I_1 \omega_1^2 + I_2 \omega_2^2}{(I_1 \omega_1)^2 + (I_2 \omega_2)^2} \right]$$

Using equation 2.15 for the denominator and equation 2.16 for the numerator, $\dot{\Phi}$ can be written as

$$\dot{\Phi} = h \left[\frac{2T - I_3 \omega_3^2}{h^2 - (I_3 \omega_3)^2} \right]$$

At this point we have to specialize the solution for one of the two qualitatively different cases. First we solve for the case $I_1 \geq I > I_2$. Substituting for ω_3 from equation A.10

$$\dot{\Phi} = h \left[\frac{2T - I_3 s_3^2 \omega_{3m}^2 cn^2}{h^2 - I_3^2 s_3^2 \omega_{3m}^2 cn^2} \right]$$

When we use the identity $sn^2 + cn^2 = 1$ we obtain,

$$\dot{\Phi} = \left[\frac{L_1 + L_2 sn^2 \tau}{L_3 + L_4 sn^2 \tau} \right] \quad (\text{A.25})$$

where

$$L_1 = h(2T - I_3 \omega_{3m}^2) \quad (\text{A.26})$$

$$L_2 = h I_3 \omega_{3m}^2 \quad (\text{A.27})$$

$$L_3 = h^2 - I_3^2 \omega_{3m}^2 \quad (A.28)$$

$$L_4 = I_3^2 \omega_{3m}^2 \quad (A.29)$$

Integrating the equation above for $\dot{\phi}$ will provide the somersault angle as a function of time. This integral can be written in terms of the Legendre elliptic integrals.

In a similar fashion we can solve for the somersault angle for the second case $I_2 > I \geq I_3$. In this case substitute ω_3 from equation A.15 into A.4 and use the following identity: $dn^2 = 1 - k^2 sn^2$. This results in the same form for $\dot{\Phi}$ with new coefficients.

$$\dot{\phi} = \left[\frac{L_1 + L_2 sn^2 \tau}{L_3 + L_4 sn^2 \tau} \right]$$

where

$$L_1 = h(2T - I_3 \omega_{3m}^2) \quad (A.30)$$

$$L_2 = h I_3 \omega_{3m}^2 k^2 \quad (A.31)$$

$$L_3 = h^2 - I_3^2 \omega_{3m}^2 \quad (A.32)$$

$$L_4 = I_3^2 \omega_{3m}^2 k^2 \quad (A.33)$$

To integrate equation A.25 we split the integrand into two parts to obtain

$$\Phi = \frac{L_1}{L_3} \int \frac{dt}{1 + n sn^2} + \frac{L_2}{L_3 n} \int_{t_0}^{tf} \frac{n sn^2 dt}{1 + n sn^2}$$

where $n = L_1/L_3$. We would like to integrate this equation with respect to the scaled time $\tau = C_\tau t$ (A.11 or A.16) since $sn = sn(\tau)$. Therefore, we compute the differential $dt = \frac{d\tau}{C_\tau}$ and substitute it into the integral

$$\alpha = \frac{L_1}{L_3 C_\tau} \int \frac{d\tau}{1 + n sn^2} + \frac{L_2}{L_3 C_\tau n} \int_{t_0}^{tf} \frac{n sn^2 d\tau}{1 + n sn^2}$$

To find the change in somersault angle in a set period of time we define the limits of

integration to be the initial time, t_0 , and the final time, t_f or equivalently τ_0 and τ_f . The change in somersault angle is then given by the following integral

$$\alpha_f - \alpha_0 = \frac{L_1}{L_3 C_\tau} \int_{\tau_0}^{\tau_f} \frac{d\tau}{1 + n \operatorname{sn}^2} + \frac{L_2}{L_3 C_\tau n} \int_{\tau_0}^{\tau_f} \frac{n \operatorname{sn}^2 d\tau}{1 + n \operatorname{sn}^2}$$

These integrals can be expressed as standard elliptic integrals

$$\int_0^\tau \frac{d\tau}{1 + n \operatorname{sn}^2(\tau)} = \Pi(k, n, \phi)$$

and

$$\int_0^\tau \frac{n \operatorname{sn}^2(\tau) d\tau}{1 + n \operatorname{sn}^2(\tau)} = \tau - \Pi(k, n, \phi)$$

where $\sin \phi = \operatorname{sn} \tau$. Therefore, breaking up the limits of integration we obtain,

$$\alpha_f - \alpha_0 = \frac{L_1}{L_3 C_\tau} \left[\int_0^{\tau_f} \frac{d\tau}{1 + n \operatorname{sn}^2} - \int_0^{\tau_0} \frac{d\tau}{1 + n \operatorname{sn}^2} \right] + \frac{L_2}{L_3 C_\tau n} \left[\int_0^{\tau_f} \frac{n \operatorname{sn}^2 d\tau}{1 + n \operatorname{sn}^2} - \int_0^{\tau_0} \frac{n \operatorname{sn}^2 d\tau}{1 + n \operatorname{sn}^2} \right]$$

which is written compactly as,

$$\alpha_f - \alpha_0 = \frac{L_1}{L_3 C_\tau} [\Pi(k, n, \phi_f) - \Pi(k, n, \phi_0)] + \frac{L_2}{L_3 C_\tau n} [(\tau_f - \Pi(k, n, \phi_f)) - (\tau_0 - \Pi(k, n, \phi_0))]$$

To compute these integrals we must solve for the initial scaled time, τ_0 , for a given initial state. To this end, the angular velocity, ω_2 , is given by the elliptic function sn

$$\omega_2(\tau) = s_2 \omega_{2m} \operatorname{sn}(\tau; k)$$

For a given value of $\omega_2 / (\omega_{2m} s_2)$ we need to compute τ . If we assume that $\tau = 0$ when ω_2 is zero and increasing then by definition $s_2 = 1$. The inverse of the Jacobian elliptic function, sn , is the Jacobian elliptic integral of the first kind.

$$\tau = \int_0^{\frac{\omega_2}{\omega_{2m} s_2}} \frac{dx}{\sqrt{(1 - x^2)(1 - k^2 x^2)}}$$

Computation of this integral allows us to compute τ_0 for a given initial ω_2 .

Bibliography

[Batterman 68] Batterman, C., 1968. *The Techniques of Springboard Diving*. The MIT Press, Cambridge, Ma.

[Bowman 61] Bowman, F. 1961. *Introduction to Elliptic Functions with Applications*. Dover Publications, New York.

[Crandall 68] Crandall, S.H., Karnopp, D.C., Kurtz, E.F., Pridmore-Brown, D.C., 1968. *Dynamics of Mechanical and Electromechanical Systems*. Robert E. Krieger Publishing Co., Malabar, Florida.

[Duncan 89] Duncan, M.J., Levison, H.F. April 1, 1989. A Highly Triaxial N-Body System Tumbling About Its Intermediate Axis *The Astrophysical Journal* 339:L17-L20.

[Frohlich 79] Frohlich, C. 1979. Do Springboard Divers Violate Angular Momentum Conservation? *American Journal of Physics* 47(7):583–592.

[Frohlich 80] Frohlich, C. 1980. The Physics of Somersaulting and Twisting. *Scientific American* 242(3):154–164.

[Hinrichs 78] Hinrichs, R.N. 1978. *Principle Axes and Moments of Rotary Motions*. Masters Thesis. University of Iowa.

[Hodgins 90] Hodgins, J., Raibert, M. H. 1990. Biped gymnastics. *International J. Robotics Research*, 9:(2) 115–132.

[Hughes 86] Hughes, P. C., 1986. *Spacecraft Attitude Dynamics*. John Wiley & Sons, Inc.

[Kane 69] Kane, T. R. and Scher, M. P., 1969. A Dynamical Explanation of the Falling Cat Phenomenon. *Int. J. Solids Structures* 5:663–670.

[Kane 85] Kane, T.R., Levinson, D.A., 1985. *Dynamics: Theory and Applications*. McGraw-Hill Publishing Co., New York.

[Lagrange] Lagrange, J. L., 1870. Recherches sur la libration de la lune. *Oeuvres VI* (Edited by M. Serret), 5-61. Gauthier-Villars, Paris.

[Marandi 89] Marandi, S.R., Modi, V.J., 1989. *Attitude Stability of Rigid Satellites via a Normalized Hamiltonian*. *Acta Astronautica* 19:(4) 287–299.

[Marey] Marey, M., 1894. Des mouvements que certains animaux executent pour retomber sur leurs pieds, lorsqu'ils sont precipites dun lieu eleve. *C.r.hebd.Seanc.Acad.Sci., Paris.* 119:714–717.

[McGeer 89] McGeer, T. 1989. Powered flight, child's play, silly wheels and walking machines, *IEEE Conference on Robotics and Automation*, Phoenix.

[Mochon 80] Mochon, S., McMahon, T. A. *Ballistic Walking*. *J. Biomech.* 13:49–57.

[Ogata] Ogata, K., 1990. *Modern Control Engineering*. Prentice-Hall, Inc. Englewood Cliffs, New Jersey.

[Poincare] Poincaré, H. 1885. Sur l'équilibre d'une mass fluide. *Acta math. VIII*, 293-299.

[Nigg 74] Nigg, B.M., 1974. Analysis of Twisting and Turning Movements. *Biomechanics IV*. London: MacMillan. 279–283.

[Raibert 84] Raibert, M. H., H. B. Brown, Jr., and M. Chepponis, 1984. Experiments in Balance with a 3D One-Legged Hopping Machine. *International J. Robotics Research*, 3:(2) 75–92.

[Santschi 63] Santschi, W.R., Dubois, J. and Omoto, C. 1963. *Moments of Inertia and Centers of Gravity of the Living Human Body*. AMRL-TDR-63-36, AD-410 451. Aerospace Medical Research Laboratories, Wright-Patterson Air Force Base, Ohio.

[Smith 67] Smith, P. G. and Kane, T. R., 1967. *The Reorientation of a Human Being in Free Fall*. Stanford University, Division of Engineering Mechanics, Technical Report No. 171.

[Strang 86] Strang, G. 1986. *Introduction to Applied Mathematics*. Wellesley-Cambridge Press, Wellesley, MA.

[Takashima 90] Takashima, S., 1990. Dynamic Modeling of a Gymnast on a High Bar. *IEEE International Workshop on Intelligent Robots and Systems, IROS 90*. 955–962.

[Wittenburg 77] Wittenburg, J. 1977. *Dynamics of Systems of Rigid Bodies*. B. G. Teubner, Stuttgart.

[Yeadon 84] Yeadon, M. R., 1984. *The Mechanics of Twisting Somersaults* Ph.D Thesis, University of Loughborough, Loughborough, United Kingdom.

[Yeadon 90] Yeadon, M. R., 1990. The Simulation of Aerial Movement I-IV. *J. Biomechanics* 23(1):59–89.

[Yeadon] Yeadon, M. R., Mikulcik, E.C., 1992. Control Strategies for Non-Twisting Somersaults. Unpublished paper.